Effect of Carbon Type on Arsenic and Trichloroethylene Removal Capacity of Iron (Hydr)oxide Nanoparticle Impregnated Granulated Activated Carbon

by

Anne Marie Cooper

A Thesis Presented in Partial Fulfillment
of the Requirements for the Degree
Master of Science

Approved November 2010 by the
Graduate Supervisory Committee:

Kiril Hristovski, Chair
Larry Olson
David Edwards

ARIZONA STATE UNIVERSITY

December 2010

ABSTRACT

This study investigates the effect of the virgin granular activated carbon (GAC) on the properties of synthesized iron (hydr)oxide nanoparticles impregnated GAC (Fe-GAC) media and its ability to remove arsenate and organic trichloroethylene (TCE) from water. Fe-GAC media were synthesized from bituminous and lignite-based virgin GAC via three variations of a permanganate/Fe(II) synthesis method. Data obtained from an array of characterization techniques indicated that differences in pore size distribution and surface chemistry of the virgin GAC favor different reaction paths for the iron (hydr)oxide nanoparticles formation. Batch equilibrium isotherm testing (120 μg-As/L; 6 mg-TCE/L, 10 mM NaHCO3 at pH = 7.2 ± 0.1 and pH = 8.2 ± 0.1) showed arsenic removal capability was increased as a result of iron (nanoparticles) impregnation, while TCE removal properties were decreased in Fe-GAC media. This tradeoff was displayed by both lignite and bituminous Fe-GAC but was most pronounced in lignite-based Fe-GAC having the highest Fe content (13.4% Fe) which showed the most favorable Freundlich adsorption and intensity parameters for arsenic of Ka = 72.6 (μg-As/g-FeGAC)(L/μg-As)1/n, 1/n = 0.6; and least favorable adsorption for TCE of Ka = 0.8 (mg-TCE/g-FeGAC)(L/mg-TCE)1/n, 1/n = 4.47. It was concluded that iron content was the main factor contributing to enhanced arsenic removal and that this was affected by base GAC properties such as pore size distribution and surface functional groups. However high Fe content can result in pore blockage; reduction in available adsorption sites for organic co-contaminants; and have a significant effect on the Fe-GACs overall adsorption capacity.

DEDICATION

I would like to dedicate my thesis to my loving and devoted husband David Hardinger, whose patience, support, and encouragement made my work possible.

ACKNOWLEDGEMENTS

This thesis never would have been written without the help of Dr. Kiril Hristovski whose ideas and enthusiasm inspired and guided my research. His focus, drive and attention to detail prevented me from going astray. I am a much better scientist today for having worked for him.

I would like to thank Dr. Paul Westerhoff for providing lab resources and Tom Colella for all his patient explanations and help with the media characterizations. I would also like to thank my fellow lab-mate Arti Jain for her help in data collection and generally keeping the lab in order. And I would especially like to thank Teresia Möller, Paul Sylvester and the people at Solmetex Inc, A Division of Lane Christiansen for providing the funding and materials that made this research possible.

TABLE OF CONTENTS

Page

CHAPTER Page

CHAPTER Page

CHAPTER Page

LIST OF TABLES

TABLE Page

TABLE Page

LIST OF FIGURES

FIGURE Page

FIGURE Page

FIGURE Page

LIST OF EQUATIONS

EQUATION Page

LIST OF ACRONYMS

ACRONYM	DEFINITION
AC	Activated Carbon
As(III)	Arsenite
As(V)	Arsenate
ATSDR	Agency for Toxic Substances and Disease Registry
BAT	Best Available Technology
BET	Brunauer Emmet Teller
CDC	Center For Disease Control
CNS	Central Nervous System
DNAPL	Dense Nonaqueous Phase Liquid
EBCT	Empty Bed Contact Time
EDX	Electron Dispersive X-Ray
FAA	Flame Atomic Adsorption
Fe-GAC	Iron Hydroxide impregnated Granular Activated Carbon
FeOOH	Iron (Hydr)oxide
FIB	Focused Ion Beam
FMO	Ferruginous Manganese Ore
GAC	Granular Activated Carbon
GFH	Granular Ferric Hydroxide
GFO	Granular Ferric Oxide
GTA	Graphite Tube Analysis

ACRONYM	DEFINITION
HAL	Health Advisory Level
HFO	Hydrous Ferric Oxide
IARC	International Agency for Research on Cancer
IIS	Iron Impregnated Sand
IOCS	Iron Oxide Coated Sand
IUPAC	International Union of Pure and Applied Chemistry
MCL	Maximum Contaminant Level
MCLG	Maximum Contaminant Level Goal
MF	Microfiltration
MTBE	Methyl Tertiary-Butyl Ether
NAPL	Non-Aqueous Phase Liquids
NF	Nanofiltration
NOM	Natural Organic Matter
PAC	Powdered Activated Carbon
PSD	Pore Size Distribution
PTA	Packed Tower Aeration
RO	Reverse Osmosis
SDWAA	Safe Drinking Water Act Amendment
SEM	Scanning Electron Microscopy
SOC	Soluble Organic Compounds
TCE	Trichloroethylene

ACRONYM	DEFINITION
UF	Ultrafiltration
USDHHS	US Department of Health and Human Services
USEPA	US Environmental Protection Agency
UVV	UV/Vis
VOC	Volatile Organic Compounds
WQARF	Water Quality Assurance Revolving Fund
XRD	X-Ray Diffraction
ZVI	Zero Valent Iron

CHAPTER ONE – INTRODUCTION

Population growth has created a worldwide demand for new drinking water sources and so access to safe drinking water is a problem now faced by developed as well as developing nations (Reitner, Falk, Groat, & Coussens, 2004). Unfortunately, many potential water sources contain levels of contaminants that are hazardous to human health as a result of natural forces and human activities (Reitner et al., 2004).

Arsenic is an example of a contaminant found in water and soil worldwide as a result of both natural and manmade processes. Arsenic levels in fresh water typically range from 1 – 10 μg-As/L but can reach 100 – 5000 μg-As/L in areas where mining activities occur (Mandal & Suzuki, 2002). Human activities such as mining, pesticide use, manufacturing waste, and fossil fuel combustion contribute to the release of arsenic in the environment. However, most cases of arsenic contamination are the result of natural processes, including the natural weathering of rocks, geochemical processes, volcanic emissions, soil erosion, and leaching (Mandal & Suzuki, 2002; Mohan & Pittman, Jr., 2007).

The health hazards posed to humans as a result of exposure to arsenic are well known and documented. Arsenic is recognized as a Group 1 human carcinogen by the International Agency for Research on Cancer (IARC, 2008). The United States Environmental Protection Agency (USEPA) has established a Maximum Contaminant Level (MCL) for arsenic in drinking water of 10 μg-As/L (United States Environmental Protection Agency [USEPA], 2006). However, arsenic levels in untreated groundwaters often exceed these recommendations,

resulting in USEPA mandated water treatment to reduce arsenic concentrations below the MCL (USEPA, 2006).

In addition to arsenic, water may contain other contaminants that have chemistries different from that of arsenic. Examples of this include organic chemicals that can often be found in water in areas that have been affected by heavy industrial activity. Trichloroethylene (TCE, CAS# 79-01-6) is an example of an organic contaminant found in US drinking water supplies as the result of discharge from metal degreasing sites and other factories (USEPA, 2009). The USEPA has established an MCL for TCE in drinking water of 5 µg-TCE/L (USEPA, 2006).

Water sources can contain a combination of contaminants with different chemistries. For example, arsenic, an inorganic contaminant, was found in combination with TCE and other non-aqueous phase liquids (NAPLs) at the Water Quality Assurance Revolving Fund (WQARF) 56th Street and Earl Drive site at levels of 86 µg-As/L and 960 µg-TCE/L (Arizona Department of Environmental Quality [ADEQ], 2002.; ADEQ, 2004). Due to their chemical differences, the combination of inorganic and organic contaminants, like arsenic and TCE, can complicate the task of their removal. In the case of the 56th Street and Earl Drive WQARF site, both contaminants are present at levels requiring their reduction to concentrations below their MCLs before the groundwater can be used as a source of drinking water.

Multiple studies have shown that iron-impregnated granular activated carbons (Fe-GAC) synthesized from lignite-based coal are effective for removing

arsenic from drinking water via adsorption (Hristovski, Westerhoff, Moller, & Sylvester, 2009; Gu, Fang, & Deng, 2005; Chen, Parette, & Cannon, 2008; Reed, Vaughan, & Jiang, 2000). In addition to arsenic removal capabilities, Fe-GAC also has the potential to remove multiple organic contaminants simultaneously, including organic solvents, found in groundwater as the result of industrial activities (Carter & Weber, Jr., 1994).

There have been multiple studies examining the effect of synthesis methods and carbon form; whether granular, powdered, or fibers, on the contaminant removal capability of the resulting synthesized media (Daus, Wennrich, & Weiss, 2004; Gu et al., 2005; Hristovski et al., 2009; Karanfil & Dastgheib, 2004; Hristovski, Ngyuen, & Westerhoff, 2009). However, the effect of the carbon base material, for example lignite or bituminous coal, on contaminant removal capability has not been fully explored.

Goal and Objective of Study

The goal of this study is to examine how the type of GAC (bituminous or lignite), affects the ability of the resulting Fe-GAC to remove arsenic and TCE from water. To achieve this goal, three task-oriented objectives were completed:

1. Fe-GAC media were synthesized from either lignite or bituminous GAC using three variations of a permanganate/iron sulfate synthesis method that was previously shown to be highly effective at impregnating GAC media with nanoscale iron (hydr)oxide particles (Hristovski et al., 2009).

2. The Fe-GAC media and synthesis process were fully characterized and compared.
3. Batch equilibrium adsorption tests were conducted and the data was fit with the Freundlich isotherm model to evaluate the Fe-GAC's ability to simultaneously remove arsenic and TCE from water.

Assumptions

This study was conducted under the following assumptions:

- The virgin GAC used is representative of other samples of the same types of materials. This is a reasonable assumption as the untreated media is commercially available from a reputable source (Norit Americas Inc.) and produced by a controlled process as defined by ISO9001:2000 (Norit Americas Inc. [Norit], 2007).
- Other types of lignite and bituminous based activated carbons will react in a way similar to those used in this experiment. This assumption is less assured as media produced by other companies may not be produced under the same level of quality control; and base lignite and bituminous carbons from different sources may differ somewhat in their properties.
- Due to their differences in chemistry, arsenic and TCE will not compete for the same adsorption sites. This is a valid assumption as it has been experimentally observed (Vaughan, Jr., Reed, Viadero, Jr., Jamil, & Berg, 1999).

- TCE is an appropriate choice for a representative organic co-contaminant because it is a contaminant commonly found in groundwater (USEPA, 2006), has chemistry similar to many other industrial solvents, and behaves in the same manner as other members of the class of compounds known as dense non-aqueous phase liquids (DNAPLs) (Russell, Matthews, & Sewell, 1992).
- Water buffered with 10 mM of $NaHCO_3$ provides a good model in which to estimate the maximum adsorption capabilities of arsenic and TCE without interferences from other contaminants. This assumption is reasonable as this type of model water was previously demonstrated to be effective at preventing other species present in the water from competing with arsenate for available adsorption sites and influencing the outcome (Hristovski et al., 2009; Driehaus, Jekel and Srith, 1998; Badruzzaman & Westerhoff, 2004).

Limitations

The scope of this study is limited to;

- Two commercially produced virgin GACs used as starting materials.
- GAC particle sizes with diameter defined by US Mesh 12 x 40.
- Three variations on the method of iron impregnation.
- Arsenic and TCE concentrations in the water model used in this study are limited to 120 μg-As/L and 6 mg-TCE/L, levels that might be reasonably anticipated in contaminated groundwater.

- Water used in this experiment is limited to pH ~ 7.2 ± 0.1 and ~8.1 ± 0.2, which are pH ranges that can be reasonably anticipated to be seen in natural waters.

CHAPTER TWO – LITERATURE REVIEW

Arsenic as a Contaminant

Arsenic is the 20th most abundant element in the earth's crust and can be found throughout the world in rocks, soil, and water (Woolson, 1975; Mohan & Pittman, Jr., 2007). Because it is an element, arsenic cannot be destroyed, however it can change its form through oxidation and other chemical reactions; change its form through biomethylation reactions with bacteria; or it can become adsorbed to soil or other matter in the environment (United States Department of Health and Human Services (Ed) [USDHS], 2007).

Table 1.

Properties of elemental arsenic.

Property	*Value*	*Reference*
Name (symbol)	Arsenic (As)	(USDHS, 2007)
Atomic Number (Weight)	33 (74.92 g)	(USDHS, 2007, p. 291)
Element Class:	Metalloid	(USDHS, 2007)
Periodic Group, Period, Block:	15(VA), 4, p	(USDHS, 2007, p. 291)
Electronic Configuration:	[Ar] $4s^2$ $3d^{10}$ $4p^3$	(Mandal & Suzuki, 2002)
Oxidation States:	+5 +3 +2 +1 -3	(Mandal & Suzuki, 2002)
Isotopes:	^{73}As ^{74}As ^{75}As	(de Laeter et al., 2003)
Stable Isotope	^{75}As (42 neutrons)	(de Laeter et al., 2003)

Arsenic is an element of great concern to human health because of its predominance in the environment and its lethality through acute and chronic exposure (Mandal & Suzuki, 2002; USDHS, 2007). Acute poisoning typically causes vomiting, abdominal or esophageal pain, and bloody diarrhea. Long term exposure through contaminated drinking water can result in skin, liver, bladder, and kidney cancer (IARC 2008). Other chronic effects include pigment and skin changes (such as hyperkeratosis), muscle weakness, neurological disorders, loss of appetite, and nausea (USDHS, 2007; USEPA, 2009). Arsenic is known to cross the placental barrier and so maternal exposure to arsenic can be passed to the next generation (IARC, 2008; USEPA, 2009).

There have been documented cases of arsenic poisoning in 21 countries throughout the world, including Taiwan, Chile, Argentina, India, China, Canada, and the United States (Mohan & Pittman, Jr., 2007). Arsenic has been detected in 1,149 of the 1,684 sites listed on the USEPA National Priorities List (NPL) (USDHS, 2007). Some of this contamination is due to human activities; such as mining, agriculture, and industrial manufacturing; which can create arsenic-laden waste streams (USEPA, 2000; Nriagu & Azcue, 1990). However, most arsenic contamination is the result of natural processes. For example, it can become airborne dust through the weathering of rocks and enter water supplies as the result of rain and runoff (Mandal & Suzuki, 2002).

Arsenic levels in soil and water can vary considerably from place to place. In soil, arsenic concentrations range from 0.1 – 40 mg/kg, with higher

concentrations found in alluvial soils and lower in sandy soils or those derived from granite (Kabata-Pendias & Pendias, 2001). Although it can bind to organic matter, in soil it is mainly present as inorganic trivalent arsenite [As(III)] or the more stable pentavalent arsenate [As(V)]. Under oxidizing conditions, As(V) is more common and is found strongly adsorbed onto clay soils, oxides and hydroxides of iron and manganese, as well as organic matter. Under reducing conditions, As(III) is the predominant form, which is more toxic, soluble and mobile than As(V) (Mandal & Suzuki, 2002). Arsenic in soil is relatively immobile as it tends to form insoluble complexes with elements that are found there such as iron, magnesium, and aluminum (USEPA, 2000). However, it can become mobilized under reducing conditions and enter ground or surface water sources as leachate or runoff (USDHS, 2007).

In unpolluted fresh water, arsenic concentration typically ranges from 1 – 10 µg/L but can easily reach 100 – 5000 µg/L in areas where mining activity has resulted in pollution (Mandal & Suzuki, 2002). Seawater typically contains 1 – 8 µg-As/L, mostly as the thermodynamically stable arsenate ion. The ratio of As(V):As(III) for oxygenated sea water varies from 0.1:1 – 10:1 (Johnson, 1972). However, most of the arsenic present in seawater is adsorbed onto particulate matter and only a small fraction remains dissolved (Johnson, 1972).

In water, as in soil, arsenic is most commonly present as As(III) under reducing conditions and As(V) under oxidizing conditions, although other states are possible (Mandal & Suzuki, 2002). Under most reducing conditions and

lower redox potentials, As(III) is mainly present as a species of arsenious acid (H_3AsO_3) which dissociates as shown in Equations 1 and 2 (Kartinen & Martin, 1995; Larsen & Hansen, 1992). The dissociation constant (pKa) is the pH at which the species is 50% dissociated.

$$H_3AsO_3 + H_2O \leftrightarrow H_3O^+ + H_2AsO_3^- \qquad pKa_1 = 9.22 \qquad (1)$$

$$H_2AsO_3^- + H_2O \leftrightarrow H_3O^+ + H_2AsO_3^{2-} \qquad pKa_2 = 12.3 \qquad (2)$$

At moderate to high oxidizing conditions, As(V) exists as a form of arsenic acid (H_3AsO_4), which dissociates as described by Equations 3 through 5 (Larsen & Hansen, 1992).

$$H_3AsO_4 + H_2O \leftrightarrow H_3O^+ + H_2AsO_4^- \qquad pKa_1 = 2.2 \qquad (3)$$

$$H_2AsO_4^- + H_2O \leftrightarrow H_3O^+ + HAsO_4^{2-} \qquad pKa_2 = 7.08 \qquad (4)$$

$$HAsO_4^{2-} + H_2O \leftrightarrow H_3O^+ + AsO_4^{3-} \qquad pKa_3 = 11.5 \qquad (5)$$

The pKa for the different arsenic species indicates that at the pH range normally seen in water (pH ≈ 6.5 to 8.5) As(III) is primarily present as non-ionized H_3AsO_3. However, in this same pH range, As(V) is primarily present as the ionized species $H_2AsO_4^-$ or $HAsO_4^{2-}$, both of which are more easily removed by methods relying on ionized reactions (like ion-exchange or adsorption) (Kartinen & Martin, 1995).

In groundwater aquifers, arsenic is typically only present as inorganic As(V) and As(III), however methylated forms may be present in lake and pond

water as the result of the biomethylation activity of microorganisms (USDHS, 2007).

The many different forms of arsenic present in the environment differ as to their degree of toxicity depending on the oxidation state; physical state (gas, liquid, or solid); particle size; absorption and elimination rate; and the pre-existing health of the person exposed. It is generally recognized that soluble inorganic forms of arsenic are more toxic than organic forms, and of these inorganic forms, As(III) is more toxic than As(V) (USDHS, 2007). However, in the natural environment, one species can be readily converted into another.

Although people are exposed to arsenic through air, food, and water; drinking water is the most common form of exposure to the general population (USEPA 2006). Due to its known toxicity and carcinogenicity, in January 2001 the USEPA reduced the maximum contaminant level (MCL) of arsenic in drinking water from 50 µg-As/L to 10 µg-As/L to limit public exposure (USEPA, 2006). Recent arsenic risk assessments by the Natural Resources Defense Council and others recommend that this level be further lowered to 1 µg-As/L (Subcommittee on Arsenic in Drinking Water, National Research Council [NRC], 1999). These new requirements could necessitate a reexamination of arsenic levels in existing water supplies and new treatment technologies may be needed in order to comply with the lower recommended levels (USEPA, 2000; USEPA, 2000).

Trichloroethylene as a Contaminant

Trichloroethylene is one of a number of chlorinated aliphatic organic solvents that, due to their physical properties, chemistries, and their prevalence in industry, have become problematic sources of industrial pollution. TCE is a common environmental contaminant found at US Superfund sites and Department of Defense facilities (USDHHS, 1997) and it is among the three most commonly detected volatile organic compounds (VOC) in US groundwater (Russell et al., 1992). It has been identified as a contaminant in over 60% of the sites proposed for inclusion on the National Priorities List (NPL) (USDHHS, 1997; ATSDR, 2005).

Due to its versatile solvent properties, TCE most commonly finds industrial use as an ingredient in commercial cleaning solutions or as a universal degreasing agent (USDHHS, 1997). However, prior to 1977, it had many other uses from which it has since been banned, including use as a general anesthetic, grain fumigant, disinfectant, pet food additive, and in coffee decaffeination and spice extraction (ATSDR, 2005; USDHHS, 1997). Today it is primarily used as an industrial degreaser, although it also can be found in paint removers/strippers, rug cleaners, adhesives and spot removers (USEPA, 2006).

TCE contamination presents a danger to human health as it is a central nervous system (CNS) depressant and a suspected hepatotoxin in humans. It is a known animal carcinogen and reasonably anticipated to be a human carcinogen (USEPA, 2009). TCE was designated as a priority pollutant by the USEPA and is

regulated by the Safe Drinking Water Act Amendment of 1987 (SDWAA) (USEPA, 1987). The USEPA lists the MCL for TCE as 0.005 mg/L with a goal (MCLG) of zero. There is no Health Advisory Level (HAL) of TCE for children (ATSDR, 2005). In addition to its inherent health risks, TCE can decompose to chemicals posing additional danger to human health such as dichloroacetylene, which is a neurotoxin; phosgene, which is a pulmonary irritant; or vinyl chloride which is a carcinogen (USEPA, 2006).

Table 2

Properties of trichloroethylene

Physical Properties	*Value*	*Source*
Chemical Formula	C_2HCl_3	(USEPA, 2006)
Appearance/color/odor	clear, colorless/ blue/ sweet	(USEPA, 2006)
Molecular Weight	131.4	(Russell et al., 1992)
Density	1.46 at 20 °C	(USEPA, 2006)
Water solubility	1.28 g/L at 25 °C	(Russell et al., 1992)
Boiling point	86.7 °C	(Russell et al., 1992)
Vapor pressure	57.8 mm-Hg at 20 °C	(USEPA, 2006)
Henry's Law Coefficient	0.00892 atm-m^3/mole	(Russell et al., 1992)
Octanol/H_2O (Log K_{ow})	2.29	(Mehran et. al., 1987)
Soil Sorption (Log K_{oc})	2.0 for many soils	(Mehran et. al., 1987)

Occupational exposures to TCE may occur in chemical manufacturing and industries where products containing TCE are used, for example, as degreasers or paint strippers (ATSDR, 2001). However, most human exposure to TCE is due to its presence in drinking water as a result of leaking storage tanks or transfer lines; leaching from landfills and hazardous waste sites; or accidental discharge into surface waters (ATSDR, 2005; Russell et al., 1992; USEPA, 2009).

TCE has a flat planar molecular shape with three chlorine atoms attached to the two double-bonded carbons. The result is a molecule that will readily accept electrons under a reducing atmosphere. Under ambient conditions, TCE reduction may be possible by any organic compound with an oxidation potential that is low enough to permit the room temperature transfer of electrons (Russell et al., 1992). However, steric hindrance as a result of the three large chlorine atoms prevents large nucleophillic groups from approaching and reacting with the electrophillic double bond (Russell et al., 1992). Electrons (or their equivalent) resulting from biological reactions, or from transition metals present in the soil may be the major factor in reduction reactions occurring in the environment (Russel et.al., 1992).

Natural dehalohydrolysis of TCE is possible by either hydrolysis in the aqueous phase or nucleophillic substitution and elimination at the unsaturated carbons of the double bond (Russell et al., 1992; Szecsody, Fruchter, Williams, Vermeul, & Sklarew, 2004). However, neither of these reactions is seen as a likely method of remediation. Hydrolysis is not considered a significant

degradation mechanism, and the products of nucleophillic substitution include dichloroethylene and vinyl chloride, both of which are more toxic to the environment and more resistant to further degradation than TCE (USEPA, 2003; Russell et al., 1992, Szescody et. al., 2004).

The relatively low boiling point, high vapor pressure, and high Henrys Law Constant of TCE indicate that TCE readily evaporates (Table 2), and most TCE released to the environment volatilizes and enters the atmosphere (USEPA, 2006; USDHS, 2007). Once in the atmosphere, TCE has a relatively limited half-life of 3 to 8 days during the summer or up to two weeks in the cooler winter months before it is destroyed by photo-oxidation (USDHHS, 1997).

The fraction of discharged TCE that does not evaporate has caused widespread contamination of soil and groundwater (Russell et al., 1992). TCE is one of a group of compounds referred to as dense non-aqueous phase liquids (DNAPLs), which have density greater than that of water, low water solubility and are relatively mobile in the subsurface (Russell et al., 1992; Fitts, 2002). Like other DNAPLs, a TCE spill that is sufficiently large or deep that evaporation is not a factor, moves downward through the vadose zone into the saturated zone, leaving behind a stream of contamination (Bedient, Rifai, & Newell, 1999). TCE will continue to move downward into the ground until a low permeability layer is reached where it could form a pool or, depending on the local geology and water flow, could move laterally through the subsurface (Bedient et al., 1999). As water moves through and around the DNAPL pool, some of the TCE is solubilized and

spread throughout the aquifer. Therefore, a small pool of TCE can serve as a source of contamination for a much larger volume of water (Russell et al., 1992).

Treatment Technologies for TCE Removal

Due to its limited solubility in water, TCE readily volatilizes, attaches to organic material, or otherwise tries to escape the aqueous phase (Karanfil & Dastgheib, 2004). Treatment technologies used for removing TCE from water take advantage of these properties. Best Available Technology (BAT) listed by the USEPA for removal of TCE and other VOCs from groundwater include packed tower aeration (PTA) and adsorption with GAC (USEPA, 2009; USEPA, 2003). Small system compliance technologies listed include PTA, diffused aeration, multi-stage bubble aerators, tray aeration, shallow tray aeration, and adsorption by GAC (USEPA, 2003). According to a USEPA report, "GAC is capable of 99% removal under all anticipated conditions" (USEPA, 2003).

Treatment Technologies for Arsenic Removal

Water treatment technologies commonly used for arsenic removal include precipitation processes, ion exchange, membrane processes, and adsorption (USEPA, 2000). None of these methods specifically removes only arsenic and removal efficiencies can be affected by competing species which are often present at higher concentrations than arsenic. In addition to this problem, arsenic is often

present as a range of chemical species which may be more or less amenable to a particular treatment technology (Farrell, 2002).

Precipitation processes for the removal of arsenic. Arsenic removal via precipitation involves converting the dissolved arsenic species to an insoluble form that can be removed via sedimentation or filtration (Wang, Hung, & Shammas, 2004). Precipitation processes used for arsenic removal involve one or more of the following conventional treatment steps, (1) oxidation to adjust the valence of the species and reduce solubility; (2) coagulation/flocculation to increase particle size; and (3) sedimentation/filtration to physically remove the precipitated particles (Wang et al., 2004). These treatments are generally more effective at removing the more stable As(V) species, however removal efficiency of As(III) can be increased by oxidizing it to As(V) (USEPA, 2000; Farrell, 2002).

Coprecipitation is another method of arsenic removal and involves the addition of ferric (or aluminum) salts to the influent, resulting in the formation of ferric (hydr)oxides (USEPA, 2000). Arsenate species are adsorbed to the ferric hydroxide surface and coprecipitated with the formed particles (USEPA, 2000; Wang et al., 2004). The formation of the As(V)-$Fe(OH)_3$ chemical bond makes this method less susceptible to competition from other ions than other treatment methods (Farrell, 2002). For example, when used in combination with filtration (to remove colloidally suspended arsenic), $FeCl_3$ has been shown to be capable of reducing As(V) levels below 2 ppb (Farrell, 2002). This method is less effective

at removing arsenite species as its adsorption is more affected by competition and requires an oxidation pretreatment step (USEPA, 2000).

When precipitates take the form of very fine particles that remain suspended and will not settle a separate coagulation/flocculation step may be required (Farrell, 2002). Coagulation is the process of aggregating finely divided suspended solid particles (as in colloids) into larger particles so that they can be removed from solution via gravity (Wang et al., 2004). Coagulants act on the surface properties of particles allowing them to aggregate or become enmeshed by destabilizing the electric double layer that keeps them separated and suspended (USEPA, 2000). The most commonly used coagulants include alum and ferric sulfate; although slaked/hydrated lime, ferric (hydr)oxide, chloride and sulfite have also been shown to be effective (Meng, Korfiatis, Christodoulatos, & Bang, 2001; Meng, Bang, & Korfiatis, 2000). Through flocculation, coagulated particles are further aggregated into larger particles, typically via the adsorption of large polymeric molecules which then form "bridges" between the particle groups (Wang et al., 2004).

Both pH and presence of other dissolved species influence coagulant effectiveness and must be considered during selection. For example, alum and ferric sulfate are equally effective at removing As(V) at pH below 7.6. However, when the pH is greater than 7.6; when As(III) is present; or when dissolved residues are undesirable ferric sulfate is the more effective option (Edwards, 1994; USEPA, 2000). For aluminum coagulants, performance is optimum at pH

6 – 7 and decreases sharply from 90 – 20% arsenic removal efficiency for pH 7 – 9, especially if chlorine is present. If agents like lime are used to remove arsenic, then pH must be greater than 11 – 12 (Kartinen & Martin, 1995). As with other treatments, removal efficiency is greater for As(V) than As(III) and the use of a pretreatment, like the addition of chlorine or MnO_2, to oxidize As(III) is recommended (USEPA, 2000; Driehaus, Srith, & Jekel, 1994).

In coagulation/filtration processes, arsenic was readily adsorbed onto the surface of insoluble FeOOH that was generated in situ by liquid $FeCl_3$ and the oxidizing agent sodium hypochlorite. However, worker safety issues related to the handling and storage of ferric oxide and oxidant solutions were among the sited disadvantages of this treatment (Frazer, 2005).

The advantages of precipitation processes include low capital cost and simple operation (Ng, Ujang, & Le-Clech, 2004) amd precipitation has been successfully used in both smaller and larger treatment systems (USEPA, 2000). However, disadvantages include higher operating and chemical costs, and the formation of by-products (Ng et al., 2004). Precipitated particles must be allowed to settle before they can be removed via sedimentation or filtration, requiring large containment and settling beds; as well as the handling and final disposal of the contaminant laden sludge, which can be expensive (Frazer, 2005). Therefore, arsenic removal via chemical precipitation is better suited for larger treatment facilities which may already be employing these methods to remove other

contaminants, and is less suitable for small-scale or point-of-use applications (USEPA, 2000).

Membrane processes for arsenic removal. Membrane processes use selective barrier membranes that block some constituent species while allowing others to pass through them. Movement across the barrier is driven by a potential difference in pressure, temperature, concentration, or electrical potential on the two sides of the membrane. Only pressure or electrical potential driven systems are commonly used for arsenic removal (USEPA, 2000; Crittenden, Trussell, Hand, Howe, & Tchobanoglous, 2005).

Pressure driven systems are classified by pore size and, from largest to smallest, include microfiltration (MF), ultrafiltration (UF), nanofiltration (NF), and reverse osmosis (RO). Processes with smaller pore sizes (like NF and RO) typically operate at higher pressures and remove contaminants through chemical diffusion; whereas larger pore size processes (MF and UF) operate at lower pressures and remove constituents through physical sieving. While higher pressure processes like NF and RO tend to remove a broader range of contaminants, they also require higher energy inputs than their lower pressure counterparts (USEPA, 2000).

MF membranes have larger pores on the scale of ~0.1 μm and, by themselves, are not efficient for arsenic removal unless it is predominantly present as larger sized particulates (Crittenden et al., 2005). However they have been used successfully in combination with precipitation processes (Ng et al., 2004).

UF membrane systems are smaller in pore size (~0.01 μm) and, depending on particulate size, are generally capable of removing some colloidal and particulate arsenic (Crittenden et al., 2005). Studies have shown that electrical repulsion assisted UF may be capable of arsenic removal not possible by pore size exclusion alone; however, these results are mixed (Ng et al., 2004; USEPA, 2000). The tendency for membrane fouling is lower for either of these systems than for NF and RO (Ng et al., 2004).

NF membranes have a sufficiently small pore size (~0.001 μm pores) that they are capable of removing significant portions of dissolved As(V) and As(III) from water through size exclusion (Crittenden et al., 2005; USEPA, 2000). They also remove divalent ions (e.g. Mg, Ca) but not monovalent salts (Na, K) (Sato, Kang, Kamei, & Magara, 2002). Nanofiltration is a reliable arsenic removal process for systems where up to 90% arsenic is present as dissolved species (Sato et al., 2002). However, due to their small pore size, NF membranes are prone to fouling and extensive pretreatment of the influent for particles and other constituents is required to prevent expensive filter fouling requiring filter replacement (Ng et al., 2004).

RO is a membrane process that has been traditionally used for desalinization of salt water but can also be effective at removing arsenic. Purified water passes through the membrane while the rest, along with salts and contaminants, is discharged as concentrated brine (USEPA, 2000). Pressure is much greater in RO than in other membrane systems. System performance is

affected by a number of factors including influent turbidity; the presence of iron, silica, manganese or scale producing compounds (USEPA, 2000); and dissolved chlorine, which has a corrosive effect on the membrane (Ng et al., 2004). To avoid these difficulties, the influent water must be pretreated to remove particles and undesirable dissolved constituents (Ng et al., 2004). Reverse osmosis removes many other ions in addition to arsenic and can generate large volumes of brine that require disposal (Farrell, 2002; USEPA, 2000). To avoid this, RO can be used in combination with co-precipitation and microfiltration, however the treatment costs and complexity are increased (USEPA, 2000).

Membrane processes can be adapted for use in small-scale applications and have the advantage of high removal efficiencies that are relatively unaffected by the chemical composition and pH of the incoming water stream (USEPA, 2000). Arsenic removal efficiencies of up to 100% are reported for reverse osmosis and nanofiltration (Sato et al., 2002; Ng et al., 2004). However, disadvantages including high operating costs, the high cost of membrane replacement, the need for pretreatments of the influent to prevent membrane fouling, and handling and disposal of the toxic laden waste can make these systems expensive and impractical (USEPA, 2000; Ng et al., 2004).

Ion exchange for arsenic removal. Ion exchange is a reversible physical/chemical reaction in which an ion on the surface of a solid phase is exchanged for an ion dissolved in the liquid phase. The solid phase is typically a synthetic resin selected to preferentially adsorb the particular contaminant ion

(Korngold, Belayev, & Aronov, 2001). For arsenic removal, chloride-form strong-base resins are generally used (USEPA, 2000). Feed-water is continuously passed through a bed of the ion exchange resin until all of the exchange sites have been filled (USEPA, 2000). The exchange resin is then rinsed with a regenerant solution (typically concentrated NaCl solution for chloride-form resins) to replenish the exchanged ions (Korngold et. al., 2001).

As with other treatment methods, factors including pH, competition from background species, resin selection, and influent concentration can affect performance efficiency. Arsenic removal using strong-base resins is usually effective and not pH sensitive in the range of 5.5 – 9.0 (USEPA, 2000). Outside of this range removal efficiency decreases rapidly. As waters naturally contaminated with arsenic usually exhibit high pH, adjustment is not usually necessary (Farrell, 2000).

Although strong-base anion resins have a relatively high affinity for arsenic (as $HAsO_4^{2-}$), total dissolved solids (TDS) and sulfate levels compete with arsenate and can affect efficiency (USEPA, 2000). When another ion in the influent is preferred over arsenic (e.g. sulfate), adsorbed arsenic can be displaced by the preferred ion resulting in a higher concentration of arsenic in the treated water than in the influent and systems must be monitored to prevent this occurrence (USEPA, 2000).

Other problems can result from the use of chloride-form resins. Adsorbed arsenic ions displace chloride ions, increasing the chloride concentration in the

treated water stream, which increases the potential for corrosion of iron pipes used in plumbing. Pipe corrosion can result in "red water" and require additional post-column treatments to eliminate this effect (USEPA, 2000). As with other arsenic removal methods, pretreatment may be necessary to prevent fouling of the ion exchange resin (USEPA, 2000).

Adsorption for Arsenic and TCE Removal

Adsorption is a popular water treatment technology that is commonly used to improve the taste, color, and odor of drinking water supplies, as well as removing soluble organic compounds, disinfection byproducts, heavy metals, and other dissolved contaminants (Crittenden et al., 2005). The use of adsorption processes in treating drinking water sources increased in popularity during the 1970's in response to public health concerns over drinking water supplies contaminated by industrial waste, agricultural runoff, and municipal discharges (Crittenden et al., 2005). It has remained a common treatment technology to this day and has the potential of removing both inorganic contaminants, like arsenic, and organic solvents, like TCE (Figure 1).

Adsorption is a mass transfer process in which dissolved contaminant species (adsorbates) are removed from the liquid phase and accumulated onto a solid phase (the adsorbent) through either physical attraction (physical adsorption) or chemical reaction (chemisorption) (Crittenden et al, 2005). While similar to ion exchange in that the dissolved species is removed from solution by attaching

itself to the solid phase, it differs in that the functional groups on the adsorbent surface are not necessarily displaced during bond formation.

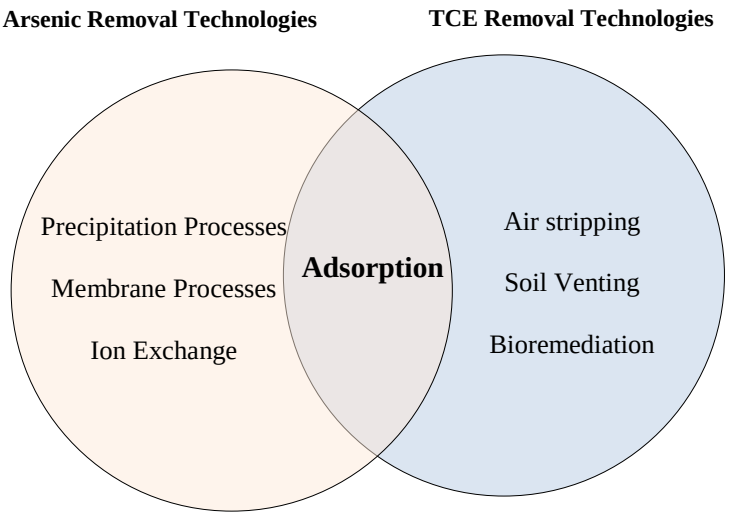

Figure 1: Conventional water treatment technologies for arsenic and TCE removal

For a gas molecule, adsorption occurs when the interaction potential energy is equal to the work required to bring the molecule to the adsorbed state. The total interaction potential is equal to the sum of the adsorbate-adsorbate and adsorbate-adsorbent interaction potentials (Yang, 2003). Adsorption from a liquid solution is more complicated as both the solvent and solute will be adsorbed to some extent (Karanfil & Dastgheib, 2004). Three types of forces contribute to adsorbate-adsorbent interactions (1) attraction/repulsion forces, (2) electrostatic forces; and (3) chemical bonding (chemisorption) (Yang, 2003). The first two of these, attraction/repulsion and electrostatic forces, are involved in physical adsorption.

In physical adsorption, adsorbate: adsorbent attraction occurs through nonspecific binding mechanisms, like London-Van der Waals Forces (Crittenden et al., 2005). It is defined as only including physical forces that exclude covalent bonding or Coulombic attraction between adsorbates and adsorbents (Crittenden et. al., 2005, Yang, 2003). These forces include the nonspecific attraction and repulsion forces operating in all adsorption systems, and electrostatic forces which arise as a result of charges on the adsorbate species and adsorbent surfaces (Yang, 2003).

Physical adsorption is an exothermic reaction and happens quickly, with heats of adsorption typically in the range of 4 – 40 kJ/mole (Crittenden et. al., 2005). It is less specific as to which species are adsorbed to the surface; has weaker forces and bond energies; and operates over greater distances than does chemisorption (Yang, 2003; Crittenden et. al., 2005). Adsorbate accumulation on the adsorbent surfaces may be multiple layers deep (Crittenden et. al., 2005).

In physical adsorption, a reversible equilibrium exists between the adsorbed and dissolved solute phases, and desorption can occur in response to changes in solution concentration or temperature (Crittenden et al., 2005). This reversibility can be used to regenerate spent media, enabling its reuse and making this a practical mechanism for use in water treatment systems.

Chemisorption occurs as the result of a chemical reaction between the solute and adsorbent surface resulting in the transfer of electrons and the formation of atomic inner-sphere complexes resulting in the formation of a

covalent or ionic chemical bond between the adsorbate and species on the adsorbent surface. It is an exothermic process with heat of adsorption typically exceeding 200 kJ/mol (Crittenden et al., 2005). The resulting bond has higher energy and shorter bond distance than that resulting from physical adsorption and is restricted to the specific atoms involved, limiting adsorbate accumulation on the adsorbent surface to a monolayer (Crittenden et. al., 2005; Yang, 2003).

Chemical adsorption is restricted to charged surface functional groups that can attract or repel oppositely charged dissolved species in accordance with Coulomb's law (Crittenden et. al., 2005). Ionic functional groups are also attracted to dipoles, however these would rather attract more polar molecules, like water, which will be prevalent in greater numbers than a dissolved polar solute (Crittenden et. al., 2005).

While not impossible, reversing chemisorption is difficult due to the chemical bond formed between the adsorbate and the adsorbent surface. Regeneration of the spent media is typically not practical as desorption, if possible, would require chemically changing the adsorbate. For this reason, this type of adsorption is regarded as less practical for use in water treatment systems (Crittenden et al., 2005).

Factors affecting adsorption efficiency. Generally speaking, adsorption efficiency is influenced by characteristics of the adsorbent, the adsorbate, and the solution matrix. These include specific surface area, pore size distribution and structure, and surface chemistry of the adsorbent; solubility, chain length,

molecular weight, polarity, and degree of ionization of the adsorbate; and pH, compatibility, solvent strength and the presence of other species in the solution matrix (Wang et al., 2004; Yang, 2003). When removing a single organic contaminant from water, adsorption efficiency is influenced by interactions between the (1) contaminant-H2O, (2) contaminant-adsorbent, and (3) adsorbent-H_2O (Karanfil & Dastgheib, 2004). For an inorganic contaminant, the situation may be further complicated by competition from other species present in the water matrix, as well as the degree of ionization and oxidation state of the target species (Wang et al., 2004; Norit Americas Inc. [Norit], 2007).

Adsorbent properties affecting adsorption efficiency. Surface area is one of the primary properties of the adsorbent determining adsorption efficiency. Adsorption efficiency is directly proportional to an adsorbent's available surface area (Crittenden et al., 2005; Wang et al., 2004). This is understandable as the greater the amount of surface area available to an adsorbate, the greater the number of available adsorption sites and the opportunity for adsorption to occur. For nonporous adsorbents, high surface area is the result of small particle size (< 10 µm) achieved through grinding or precipitation, and it increases as the particle size decreases (Wang et al., 2004). For porous adsorbents, surface area is the result of the media's high porosity and is relatively independent of particle size (Wang et al., 2004).

High surface area does not necessarily translate to high adsorption capacity as some of the surface area may be inaccessible to the targeted adsorbate

species. Pore size distribution may be a more important factor (Lu & Sorial, 2004). The International Union of Pure and Applied Chemistry (IUPAC) classifies pores with diameters < 2 nm as micropores, 2 – 50 nm as mesopores, and > 50 nm as macropores (Yang, 2003). In a highly microporous adsorbent, a large contaminant molecule may be excluded from entering the smaller micropores making most of the adsorbent surface area inaccessible to the targeted species (Karanfil & Dastgheib, 2004; Summers & Roberts, 1988). This type of size exclusion is more significant for large organic molecules, like natural organic materials (NOMs), than for small solvent molecules, like TCE (Summers & Roberts, 1988; Karanfil & Dastgheib, 2004). Pore blockage is also more likely to occur in a microporous adsorbent, as the entrances to the smaller pores may be made inaccessible by species adsorbed to sites in the larger pores (Yang, 2003).

When size exclusion is not a factor, sorption energy should be greater in micropores than in the larger macro or mesopores, because as pore width approaches the size of the target molecule, the possibility of multiple contact points increases and surface forces begin to overlap (Dubinin, 1989). Therefore, for small flat low molecular weight organic molecules, microporosity should result in increased adsorption energies and improved adsorption capacity, provided passage through the larger pores remains unimpeded (Dubinin, 1989; Karanfil & Dastgheib, 2004; Yang, 2003).

In addition to affecting adsorption energies, porosity affects mass transport kinetics through the adsorptive media. Despite occurring via different adsorptive

mechanisms, the mass transport processes governing the rate of adsorption by a porous media are the same for both metal oxide adsorption of inorganic contaminants, and the adsorption of organic contaminants by activated carbons (AC) (Badruzzaman & Westerhoff, 2004). Mass transport through the media consists of four stages;

1. Diffusion through the bulk liquid, which happens quickly (Sontheimer, Crittenden, & Summers, 1988).
2. Diffusion through the stagnant film surrounding the adsorbent particle (film diffusion), which is dependent on the concentration gradient across the adsorbent surface, the adsorbent particle size, and the packed-bed hydraulics (Sontheimer et al., 1988).
3. Intraparticle diffusion, consisting of diffusion across the particle surface (surface diffusion) and diffusion within the particle pores (pore diffusion) (Axe & Trivedi, 2002).
4. Surface adsorption, which happens quickly (Sontheimer et al., 1988).

Of these stages, intraparticle diffusion (Stage 3) is the rate limiting step (Sontheimer et al., 1988; Badruzzaman & Westerhoff, 2004; Hristovski, Westerhoff, Crittenden, & Olson, 2008). In their study of arsenic adsorption by porous granular ferric hydroxide (GFH) Badruzzaman and Westerhoff (2004), recommended that when designing arsenic treatment systems, internal diffusion should be considered as the rate limiting step and suggested that materials for arsenic adsorption should be designed with a higher proportion of macropores in

order to increase adsorption kinetics and capacity (Badruzzaman & Westerhoff, 2004).

In addition to available surface area, adsorption is controlled by the existence of specific functional groups on the adsorbent surface (Karanfil & Kilduff, 1999; Karanfil, Kitis, Kilduff, & Wigton, 1999). For uncharged adsorbents, nonspecific attraction and repulsion interactions dominate. For charged adsorbents; like metal oxides, zeolites, or ionic solids; electrostatic interactions due to electrical fields created by charges on the adsorbent surfaces often dominate (Yang, 2003).

For physical adsorption, governed by Van der Waals forces, the attraction between a given site on the adsorbent surface and a targeted adsorbate increases with increasing polarizability of the surface species (Yang, 2003). For example, alkali and alkaline-earth elements have very high polarizabilities (e.g. 24.08 and 22.8 x 10^{-24} α cm^3 for Na and Ca) and, when present on the adsorbent surface, result in high interaction potentials (Yang, 2003). However, when these same elements are present as cations, polarizability and attraction/repulsion energies (and therefore interaction potentials) are greatly reduced (e.g. 0.180 and 0.471α x 10^{-24} cm^3 for Na^+ and Ca^{2+}) (Yang, 2003).

For charged adsorbents, like zeolites or molecular sieves, both the charge and radii of the interacting species on the adsorbent surface are important, as electrostatic force is proportional to the charge (or its square), and inversely proportional to the distance between the centers of the interacting species (Yang,

2003). For uncharged adsorbents, the presence of ionic functional groups on the surface of the (otherwise nonpolar) adsorbent can be an important consideration. For example, the presence of oxygen-containing functional groups on the adsorbent surface can attract water molecules or other charged species, reducing adsorptive capacity for nonpolar organic compounds (Crittenden et. al., 2005).

Adsorbate properties affecting adsorption efficiency. Adsorption efficiency is also influenced by properties of the adsorbate, including its solubility, chain length, molecular weight, polarity, and degree of ionization. Generally speaking, adsorption efficiency is inversely proportional to adsorbate solubility (Yang, 2003). High solubility is an indication of strong solute-solvent affinity, requiring higher energy to break the solute-solvent bond; and any factors affecting an adsorbate's solubility will also affect its ability to be removed via adsorption (Wang et al., 2004).

In the absence of ionic functional groups, solubility is generally inversely related to molecular size. Therefore, adsorption efficiency is generally higher for larger solutes provided their size does not prohibit them from entering the pores of the adsorbent (Yang, 2003; Wang et al., 2004). In an aqueous solution, solubility decreases (and therefore adsorption efficiency increases) with increasing molecular weight of the adsorbate (Wang et al., 2004). Solubility of an organic molecule in an aqueous solution decreases with increasing chain length so that adsorption efficiency is greater for longer chain organic molecules (Yang,

2003). Polar solutes prefer polar solvents and, in an aqueous solution, adsorption efficiency is typically greater for nonpolar adsorbates (Wang et al., 2004).

While solubility is a direct indication of adsorption strength, all other factors are different for different classes of compounds and depend on the specific system involved. For example, polar species are very difficult to remove from a highly polar solvent, like water, as polar functional groups on an adsorbent surface are more likely to attract water molecules, which are present at higher concentration than dissolved species (Crittenden et.al., 2005). Neutral species are strongly held to nonpolar surfaces, like those of AC, and so their adsorption is generally much stronger than that of an acid or base, which is highly pH dependent.

For organic contaminants, the adsorbate-adsorbent interaction force is related to the polarizability and therefore to the size and type of the organic contaminant (Yang, 2003; Crittenden et. al., 2005). Therefore, adsorbability of a neutral organic contaminant increases with increasing polarizability and molecular size (Yang, 2003). The most important mechanism determining adsorbability of an ionic species is electrostatic attraction which depends on ionic strength and is also highly pH dependent (Crittenden et. al., 2005).

Water matrix properties affecting adsorption efficiency: Effect of pH

Water matrix properties, including pH, electrolyte content, and competition from other dissolved species affect solution chemistry and therefore affect adsorption efficiency. Solution pH affects both the charge on the adsorbent surface and the

ionization of the adsorbate; and has been identified as a primary factor governing adsorption for ionized species, like arsenic and other heavy metals (Stumm & Morgan, 1981). The specific effect of pH on removal efficiency depends on the targeted species involved. For example, in their study of heavy metal adsorption onto Fe-AC, Reed et.al. (2000) observed that in a ligand-free system, removal of cationic heavy metals, like Pb(II) and Hg(II), increased with increasing pH. The opposite was true for removal of anionic heavy metals like As(V) or $Cr_2O_7^{2-}$. For As(III), removal was unaffected by pH for pH $\leq$ 5, increased to a maximum at pH = 7, and then decreased as pH increased above 7 (Reed et al., 2000).

The amount of an ionized metal contaminant removed from solution increases from zero to 100% over a fairly narrow pH range referred to as the "pH adsorption edge", and is specific to the species involved. Solution pH must be carefully controlled to stay within this range in order to achieve maximum removal of the targeted species (Coughlin & Stone, 1995; Reed et. al., 2000). For example, Coughlin and Stone (1995) observed that adsorption of divalent heavy metals on goethite (FeOOH) increases from zero to 100% over a narrow range of ~1.5 pH units. The pH adsorption edge was from 6 to 7.5 for Mn(II); 5 to 6.5 for Co(II) or Ni(II); 4 to 5 for Cu(II); and 4 to 5.5 for Pb(II) (Coughlin & Stone, 1995).

The specific pH range for maximum adsorption is dependent on the adsorbent, as well as the targeted adsorbate. For example Payne and Abdel-Fattah (2005), found that As(V) was adsorbed most effectively over the pH range 7 to 11

by Fe-GAC, 4 to 5 by Fe-treated chabazite (a zeolite), and 4 to 11 for Fe-treated clinoptilite. The stability of the adsorbent media can also be affected by solution pH. In their study of adsorption of As(V) by nanocrystalline akaganeite [β-FeO(OH)], Deliyanni et al. (2003), observed an increase in the concentration of ferric ions (from the adsorbent) in the aqueous phase when the media was suspended in solution at pH < 4 for 24 hours. However, the concentration of ferric ions was nearly zero at pH above 4 indicating the media was stable in the less acidic range (Deliyanni, Bakoyannakis, Zouboulis, & Matis, 2003).

Removal of an acid or base is highly pH dependent as both the charge on the adsorbent surface and the polarizability of the adsorbate will be affected. The ideal pH for removal depends on the dissociation constant for the particular acid or base involved, as well as the type of adsorbent (Hingston, Atkinson, Posner, & Quirk, 1964; Crittenden et. al., 2005). For a weak acid, adsorption should be greatest at or near its pKa, where there is the greatest probability of the acid and conjugate base existing in nearly equal proportions (Hingston et al., 1964). For example Mattigood et al. (1985), observed that maximum adsorption of boron by kaolinite occured between pH 8.5 and 9.0, which is close to the pKa of boric acid (Mattigood, Frampton & Lim, 1985).

Solution pH can also affect the removal of organic contaminants, especially tautomeric compounds like phenol, which can be present in both acidic and basic form. Snoeyink et al. (1969), observed that adsorption of phenol by activated carbon was decreased at both high (pH = 10.0) and low pH (pH = 2.0).

This was explained by the dissociation of phenol into the phenolate anion and proton. The pKa value of phenol is 9.89. At pH > pKa, phenol is predominantly present as the phenolate anion, which is more attracted to water molecules than the carbon surface. At pH < pKa, the presence of protons creates competition for available carbonyl adsorption sites, resulting in lower adsorption (Snoeyink, Weber, & Mark, Jr., 1969).

The relationship between solution pH and metal adsorption is employed in the regeneration of spent adsorbent media. For example, acid rinses are used to desorb cationic heavy metals from GAC by lowering the pH and redissolving the adsorbed metals. This is followed by a base rinse to neutralize any acid remaining in the column and increase the carbon pH to a level that will restore its metal removal capacity and enable its reuse (Reed & Arunachalam, 1994).

Effect of electrolyte on adsorption efficiency. Adsorption is also affected by the charge, specific species, and concentration of background electrolyte. Ions from the background electrolyte can compete for available adsorption sites (Liu, Zhang, McWilliams, Talley, & Neal, 2008), or suppress charges present on the adsorbent surface (Matis, Zouboulis, & Valtadorou, 1999). It has been proposed that differences in response to ionic strength of electrolyte are due to differences in the complexes formed between the adsorbate and adsorbent surface. Hayes et al. (1987) proposed that weakly-bonding outer sphere (ion-pair) complexes are more greatly affected by electrolyte strength than are stronger-bonding inner-sphere surface complexes (Hayes, Papelis, & Leckie, 1987).

These effects have been experimentally observed. For example adsorption of As(V) onto akageneite (β-FeOOH) increased as the ionic strength of the electrolyte KNO_3 was increased from zero to 0.1 M. The increase was accompanied by a shift in the pH adsorption edge towards the alkaline region, and improved As(V) removal capacity at higher pH (7 to 12) (Deliyani et al., 2003). The improvement was attributed to the suppression of negative charges on the adsorbent surface which enhanced attraction between the surface sites and the As(V) oxyanions (Deliyani et al., 2003). Results were similar for adsorption of As(V) by goethite particles [α-FeO(OH)], where adsorption increased with increasing strength of KNO_3 at high pH. This is not always the case, in both studies As(V) removal was unaffected by changes in electrolyte strength at the lower pH range of 4.5 to 7 (Deliyani et al., 2003; Matis et al., 1999).

The effect of ionic strength may be different for different electrolytes and at different pH. For example, at low pH (4 to 6) adsorption of As(V) by TiO_2 was unaffected by ionic strength of $NaClO_4$ but decreased with increasing ionic strength of NaCl (Liu et al., 2008). At higher pH (7 to 12) adsorption increased with increasing ionic strength in both electrolytes (Liu et al., 2008). The same study observed that at low ionic strength (0.001 to 0.01 M) As(V) adsorption was approximately the same at the same pH in both electrolytes. However at higher ionic strength (0.1M), As(V) adsorption was higher at the same pH in $NaClO_4$ than in NaCl (Liu et al., 2008).

Effect of background ions on adsorption efficiency. Adsorption is also affected by the presence of other organic or ionic species in the water matrix, which can compete with the targeted adsorbate for available adsorption sites. The amount of competition depends on the concentration and type of ions, the number of adsorption sites, and the surface's affinity for the targeted species. Christophi and Axe (2000), observed that adsorption capacity for heavy metals on goethite increased with increasing metal electronegativity. Specifically, they observed that metal adsorption increased from Cu > Pb > Cd (Christophi & Axe, 2000). These results were consistent with an earlier study which reported adsorption capacity on goethite increased from Cu > Pb > Zn > Cd > Co > Ni > Mn (Schwertmann & Taylor, 1989).

The preferential adsorption of one species can result in the displacement of another species already adsorbed. For example, Christophi and Axe (2000) observed that Cd adsorbed onto goethite was displaced by either Cu or Pb (Christophi & Axe, 2000). In Cu-Pb competitive adsorption, nearly 60% of Pb was displaced by Cu (Christophi & Axe, 2000).

Background ions do not always have a negative effect on adsorption efficiency. Adsorption of Cu(II) onto TiO_2 was unaffected by the presence of the background anions ClO_4^-, Cl^-, NO_2^-, NO_3^-, SO_3^{2-}, and PO_4^{3-} (Yang, Lee, & Davis, 2006). However, in this same study the presence of the multivalent ions SO_3^{2-} and PO_4^{3-} reduced adsorption of EDTA and EDTA-Cu complex. The

interference was greater for adsorption of EDTA-Cu(II) than for EDTA alone, especially at lower pH (Yang et al., 2006).

The presence of background ions can also enhance removal of an adsorbate by forming a stable ion-pair species which is more attracted to sites on the adsorbent surface. For example, the adsorption of boron by kaolinite was improved in $Ca(ClO_4)_2$ due to the formation and adsorption of the stable $CaB(OH)_4^+$ ion-pair species (Mattigood et al., 1985).

Types of Adsorbents

There are many different types of adsorbent media and systems available, varying in cost, complexity, efficiency, and the contaminant removed. All of the factors previously discussed must be considered in selecting an adsorbent, and the adsorbent should be tested to insure it is suitable for the particular situation (United States Army Corp of Engineers [ACE], 2001).

Conventionally, commercial adsorbents were grouped into four categories; (1) zeolites (aluminosilicates with varying ratios of Al:Si); (2) synthetic polymeric adsorbents; (3) activated alumina; and (4) activated carbons. Of these, zeolites are charged and unsuitable for removing soluble organic compounds (SOC); whereas synthetic polymeric adsorbents typically have pores in the micropore range, making them unsuitable for removing NOMs (ACE, 2001). Activated carbons have a wide range of available pore and particle sizes which allow them

to be effective at adsorbing both SOCs and NOMs (Crittenden et. al., 2005; ACE, 2001).

Activated alumina is usually categorized as an adsorbent although it removes arsenic via the exchange of arsenate ions with alumina surface hydroxides, which is an ion exchange mechanism (USEPA, 2000). When the alumina surface sites become filled, the media is regenerated by flushing with a strong base (like NaOH), rinsing with water and then neutralizing with a strong acid (like H_2SO_4), however typically it is only restored to 50 – 70% of its original exchange capacity (Farrell, 2002). As with other adsorptive treatments, activated alumina is well suited for use in small scale systems and does not have many of the drawbacks of using chloride-form ion exchange resins (USEPA, 2000). However, like most other treatments, activated alumina is more effective at removing As(V) than As(III) and pH can have a significant effect on arsenic removal (Farrell, 2002). It is ineffective for removing uncharged As(III) and As(V) species (USEPA, 2000).

Recent advances in adsorbent technology have expanded media choice to include metal oxides/hydroxides, which are well suited to removing inorganic heavy metals like arsenic; and surface modified hybrid media including Fe-GAC, which can be tailored to simultaneously remove multiple contaminants.

GAC as an adsorbent. Activated carbon has been used as an adsorptive media for centuries, dating back to the ancient Hindu use of charcoal for water filtration (Mohan & Pittman, Jr., 2007). The modern activated carbon industry

was established in the 1900's as a replacement for bone char used in sugar refining (Yang, 2003). AC was first used for water treatment in the United States in the 1930's and has been in use for this purpose ever since (Mohan & Pittman, Jr., 2007). Activated carbons have been prepared from many different carbon-containing base materials including coconut shells, wood char, lignin, sawdust, fertilizer, carbon black, rice hulls, wood, peat, petroleum coke, waste rubber tires and coal (Yang, 2003; Pollard, Fowler, Sollars, & Perry, 1992). Anthracite, lignite, and bituminous coals have been major sources of starting materials (Yang, 2003).

Activated carbons are versatile adsorbents due to their large internal surface area available for adsorption and their complex pore structure. The structure of ACs can be modeled as a "twisted network of defective hexagonal carbon layer planes cross-linked by aliphatic bridging groups" (Yang, 2003). Non-carbon atoms (e.g. O, N, S, Si) are also incorporated into the network or bound to the plane edges, and act in much the same way as functional groups found on aromatic rings. These atoms give carbon its catalytic properties, and are important for adsorption from aqueous solutions (Yang, 2003; Albers et. al., 1994).

Both pore structure and surface functionality of AC can be tailored for specific applications by controlling variables in the activation process, such as precursors, carbonization temperatures, and conditions during the activation step (Dastgheib, Karanfil, & Cheng, 2004; Yang, 2003). Activation methods fall into

two categories: (1) gas or steam activation and (2) chemical activation (Yang, 2003; Norit Americas Inc, 2007).

Gas activation involves carbonization at 400 – 500 °C to remove volatile material, followed by partial gasification at 800 – 1000 °C to develop porosity and increase surface area. In the gasification step, a mild oxidizing gas, like CO_2 or steam, is used to insure uniform pore development. Carbon produced by gas-activation is typically used for gas and vapor adsorption applications (Yang, 2003).

Chemical activation is typically used for lignin-based materials, such as wood or sawdust. In this process, inorganic activator chemicals are used to degrade and dehydrate cellulose in the base material and prevent shrinkage in the carbonization process. Phosphoric acid, zinc chloride, potassium sulfide and potassium thiocyanate are examples of activator chemicals. Following carbonization, the material is washed in acid or water to remove any remaining activators (Yang, 2003). Pore diameters $\geq$ 30 Å are desirable for liquid phase applications whereas smaller pore sizes are desirable for gas-phase applications. A carbon with a higher distribution of meso and macropores will be more effective at removing larger organic or polymeric molecules (Dastgheib et. al., 2004). Removal of smaller flat molecules, like TCE, is enhanced by an abundance of micropores (Karanfil & Dastgheib, 2004).

Pore size is not the only factor in determining what type of molecules will adsorb to carbon surfaces. As discussed previously, surface functional groups

also play a role in determining the type of species that can be adsorbed. Chemical reactions (oxidation in particular), which are controlled by temperature and activation conditions, are used to determine the types of surface functional groups formed and tailor surface functionality to a particular application (Yang, 2003). For example, an activation temperature of 400 °C results in the formation of phenolic and lactone groups, whereas activation at high temperature (up to 1000 °C) in the presence of oxygen results in the formation of acidic surface oxides (Wang et al., 2004). In aqueous solutions, acidic surface groups show cation exchange properties, however when the carbon is degassed under vacuum (or an inert atmosphere) at high temperatures (e.g. 950 °C) it becomes basic and exhibits anion exchange properties (Yang, 2003).

Acidic properties are the result of the formation of oxygen containing groups; for example hydroxyls, lactones, carboxyls or anhydrides (Ishikazi & Marty, 1981). Basic sites are the result of the formation of pyrone or chromene groups, or from the pi-basicity of the aromatic rings in the carbon network (Yang, 2003). The formation of both of these types of polar functional groups can interfere with the ability of GAC to adsorb hydrophobic organic molecules from water (Ishikazi & Marty, 1981). For example, Karanfil and Kilduff (1999) observed that increasing the surface acidity of activated carbons increased the surface polarity and reduced the adsorptive capacity of the media for hydrophobic organic compounds like TCE (Karanfil & Kilduff, 1999).

As surface polarity increases, the carbon surface becomes more hydrophilic and attractive to water molecules. The adsorbed water molecules occupy sites on the carbon surface thereby reducing the number of sites available for adsorption of dissolved organic molecules (Karanfil, Kitis, Kilduff, & Wigton, 1999). This can interfere with adsorption of both hydrophobic solvents (like TCE) and hydrophilic chemicals (like methyl tertiary-butyl ether [MTBE]). As was observed by Quinlivan et. al. (2005), the adsorption of the more hydrophobic TCE or hydrophilic MTBE was higher for more hydrophobic carbons than for their more hydrophilic counterparts. This was attributed to the greater number of water molecules adsorbed to the surface of the latter, which interfered with the adsorption of both organic species (Quinlivan, Li, & Knappe, 2005).

Although they attract and adsorb nonpolar or weakly polar molecules preferentially to water, ACs are not truly hydrophobic, as can be seen by the adsorption of water vapor (Yang, 2003). At low vapor pressures, adsorption of water molecules onto the carbon surfaces is initially low (due to low Van der Waals interactions). However, once a few water molecules are adsorbed and adsorbate-adsorbate interactions take over, it increases rapidly, leading to the eventual saturation of the carbon. Nevertheless, the relative hydrophobicity of carbon is useful in that hydrophobic interactions drive the adsorption of organic molecules from water (Yang, 2003).

The ability of AC to remove inorganic heavy metal contaminants has been the subject of much research (Chen & Lin, 2001; Chuang et al., 2005; Pattanayak,

Mondal, Matthew, & Lalvani, 2000; Pokonova, 1997; Reed & Nonavinakere, 1992). While it has shown some ability, when used alone without modification (such as metal oxide impregnation) it is generally substantially less effective than many other adsorbents (Bayer & Finkel, 2005; Chen et al., 2008; Daus et al., 2004; Frazer, 2005; Gu et al., 2005; Hristovski, Westerhoff, Crittenden, & Olson, 2008; Hristovski et al., 2009; Vaughan, Jr. & Reed, 2005). The primary reason for this is the nonpolar nature of its surfaces, which would prefer to attract nonpolar organic compounds or even water molecules over an ionic solute.

Metal (hydr)oxides as adsorbents. In nature, many different soil materials participate in the adsorption and retention of arsenic including clays, carbonates, organic materials, and the oxides and hydroxides of Al, Fe, and Mn; depending on the many factors discussed earlier (Sadiq, 1997; Livesey & Huang, 1981). It is reasonable to propose that the same materials involved in binding heavy metals (like arsenic) to soil in nature could be employed to remove them from drinking water supplies.

For example, at lower pH, the normally negatively charged surfaces of clay develop a positive charge and become attractive to arsenic oxyanions. Under acidic conditions, aluminum oxides/hydroxides, manganese oxides, and biogenic materials are also important for arsenic adsorption. In soils with high calcium content, carbonates play a role (Sadiq, 1997). However, multiple studies have shown that, in both acidic and alkaline conditions, iron oxides and hydroxides are the soil components most commonly involved in arsenic adsorption (Sadiq, 1997;

Livesey & Huang, 1981; Carlson, Bigham, Schwertmann, Kyek, & Wagner, 2002).

Livesey and Huang (1981) found that in saline soils, arsenic adsorption was linearly related to hydroxyl-Al and hydroxyl-Fe content (Livesey & Huang, 1981). They also noted that, while the presence of phosphate reduced adsorption, the presence of chlorides, nitrates or sulfates had no effect (Livesey & Huang, 1981). In another study, a naturally occurring iron hydroxide with structure similar to that of akagenite (β-FeOOH) was found to be important in removing arsenic from acid mine tailings. Natural ferrihydrite samples with higher Cu, Zn, and Si content also played a role but showed lower adsorption capacity, especially at higher pH (Carlson et al., 2002).

Arsenic adsorption onto the surface of iron hydroxide occurs through the formation of inner sphere surface complexes via ligand exchange with the hydroxide at the mineral surface (Sherman & Randall, 2003; Ona-Nguema, Morin, Juillot, Calas, & Brown, 2005). Sherman & Randall (2001) determined that in particular, the adsorption of arsenate (as as AsO_4^{x-} where $x \leq 3$) onto iron oxide/hydroxide surfaces (as goethite, lepidocrocite and hematite) occurs through the formation of "inner-sphere surface complexes resulting from bidentate corner sharing between AsO_4 and FeO_6 polyhedra" (Sherman & Randall, 2003). Other mechanisms have also been proposed. Jain et. al.(1999) proposed that with increasing pH, the monodentate bonding mechanism might play an increasing role in the adsorption of arsenate onto ferrihydrite (Jain, Raven, & Loeppert, 1999).

However, the later study by Sherman found no evidence to support this theory (Sherman & Randall, 2003).

Many different metal oxides and hydroxides have been investigated for use as possible arsenic adsorbents including

- Titanate nanofibers (Hristovski, Westerhoff, & Crittenden, 2008),
- Commercially available TiO_2 (Liu et al., 2008),
- Metal oxide nanopowders including TiO_2, ZrO_2, Fe_2O_3 and NiO (Hristovski, Baumgardner, & Westerhoff, 2007),
- Granular ferric hydroxide (GFH) (Badruzzaman & Westerhoff, 2004),
- Manganese greensand (MGS) (Thirunavukkarasu, Viraraghavan, Subramanian, & Tanjore, 2002; Subramanian, Viraraghavan, Phommavong, & Tanjore, 1997),
- Red mud from a bauxite mine (Altundogan, Altundogan, Tuemen, & Bildik, 2000),
- Iron oxide coated sand from a Dutch water treatment plant (Petrusevski et al., 2008),
- Iron impregnated sand (IIS) made by mixing sand with a solution of $Fe(NO_3)_3$ and heating till evaporated (Vaishya & Gupta, 2003),
- Porous resin coated with hydrous zinc oxide (Suzuki, Bomani, Matsunaga, & Yokoyama, 2000),
- Cu(II) coated AC (Lorenzen, van Deventer, & Landi, 1995),
- Ce(IV) doped iron oxide (Zhang, Yang, & Huang, 2003),

- Akaganeite [β-FeO(OH)] nanocrystals (Deliyanni et al., 2003),
- Synthetic goethite (α-FeOOH) particles (Matis et al., 1999),

As in nature, iron oxides and hydroxides have been among those showing the most potential for arsenic removal. For example, in a comparison of iron oxide coated sand (IOCS), MGS, and Fe(III) coated ion exchange media, the Fe(III) coated ion-exchange media performed best at arsenic removal, followed by IOCS (Thirunavukkarasu et al., 2002).

Multiple studies have explored the use of iron oxides and hydroxides for arsenic removal, their effectiveness often depending on other factors such as pH and the presence of other ions. For example, 98.5 – 99.8% removal was reported for ferruginous manganese ore (FMO) at optimal conditions. The presence of Ni^{2+}, Co^{2+}, and Mg^{2+} enhanced adsorption efficiency (Chakravarty, Dureja, Bhattacharyya, Maity, & Bhattacharjee, 2002). Hydrous ferric oxide (HFO) effectively removed both As(III) and As(V) over pH 4 – 9. Here it was observed that adsorption efficiency was improved by the presence of Ca^{2+} and reduced by the presence of sulfate. Carbonate had only a slight effect (Wilkie & Hering, 1996).

The relationship between arsenic species adsorbed (as arsenate or arsenite) onto ferrihydrite and pH was observed by Raven, Jain and Loeppert (1998). In their study, they observed that at lower pH the ratio of adsorbed As(V):As(III) was greater. At higher pH the reverse was true, the ratio of As(III):As(V) was

greater. The adsorption envelope crossed at roughly pH 6 – 7.5 (Raven, Jain, & Loeppert, 1998).

Granular ferric oxide (GFO) is effective at removing both arsenate and arsenite at low pH range (pH < 7), although the presence of phosphates or sulfates interferes with its adsorption capacity (Frazer, 2005). However, GFO lacks mechanical strength and quickly breaks up into fine particles. When larger particles were used in an attempt to alleviate the problem, arsenic removal was decreased by 50% (Gu et al., 2005).

The corrosion products of zero valent iron (ZVI) are effective at arsenic removal. However, when used alone in packed-bed adsorbers, granular ZVI exhibits a tendency to clog.. Chen et. al. (2008) found that the addition of Fe-GAC to ZVI improved performance and reduced system clogging. A 70:30 Fe-GAC: ZVI mixture was the most effective for arsenic removal. They proposed that, in addition to providing structural stability, the Fe-GAC served as a "sink" for arsenic before the ZVI was sufficiently corroded to be effective. When ZVI and GAC were blended in the first two-thirds of the column, the GAC acted as an "iron-polisher" and any solubillized iron remained captured in the last third of the column (Chen et al., 2008).

Metal (hydr)oxide impregnated hybrid adsorbent media. As can be seen from the previous examples, iron (hydr)oxides are effective at arsenic removal however, due to corrosion, have a tendency to break down and clog packed-bed systems (Chen et al., 2008). What is needed is a high efficiency

granular media that will remain mechanically stable and not break down due to the formation of corrosion products. One way to achieve this is a hybrid media where the iron oxide/hydroxide has been deposited onto a stronger matrix. Examples of surface modified hybrid media include FeOOH coated polystyrenes and poly HIPE (Katsoyiannis & Zouboulis, 2002); iron coated pottery granules (Dong, Zini, Cowen, & Ming, 2009); Fe(III) impregnated GAC (Mondal, Majumder, & Mohanty, 2006; Mondal, Balomajumder, & Mohanty, 2007); Cu(II) coated GAC (Lorenzen et al., 1995); FeOOH coated ion-exchange media (Hristovski et al., 2008); Fe(III) coated ion-exchange media and IOCS (Thirunavukkarasu et al., 2002); and Fe-modified AC, chabazite, and clinoptilite (Payne & Abdel-Fattah, 2005).

For example, > 95% arsenic removal efficiency was reported for FeOOH coated polystyrenes and poly HIPE at pH 7.0. Removal efficiency depended on empty bed contact time (EBCT), pH and the presence of competitive ions (Katsoyiannis & Zouboulis, 2002). Iron coated pottery granules exhibited arsenic adsorption capacities similar to those of nanoscale ZVI and higher than those of nanoscale TiO_2 (Dong et al., 2009). Adsorption was through the formation of a stable Fe-Si complex on the media surfaces (Dong et al., 2009). Fe-GAC synthesized by mixing $FeCl_3$ with GAC showed 95.5 – 98% arsenic removal efficiency (Mondal et al., 2006).

Colorado-based ADA Technologies developed a hybrid media consisting of nanoscale particles of the iron oxide akageneite coated onto an inert silicate

substrate to remove arsenic from water (Frazer, 2005). The akageneite particles formed stable bonds with arsenic and exhibited the same adsorption capacity as GFO. The resulting media was able to reduce arsenic concentration from 1000 µg-As/L to 10 µg-As/L (arsenic adsorption capacity of 2 mg As/g adsorbent). However removal efficiency was decreased at the lower arsenic levels more likely to be seen in real world applications (Frazer, 2005).

Methods of iron (hydr)oxide impregnation. GAC has many properties that make it desirable as a support matrix for a hybrid media including high surface area, pore size distribution which can be tailored to suit the particular application, and organic co-contaminant removal capability. There have been many methods employed to create hybrid media by impregnating GAC with iron, including the following;

- Impregnation with ferrous chloride followed by chemical oxidation with sodium hypochlorite to attain1 – 7% Fe in the final product (Gu et al., 2005);
- Citric acid and iron mixture for 1.26% Fe (Chen et al., 2008);
- Nitric acid: acetic anhydride:$KMnO_4$ oxidation followed by $FeCl_3$ for 6.1% Fe (Chen et al., 2008);
- The "evaporation method" of heating a mixture of $Fe(NO)_3$ and GAC until dry that achieved 11.7% Fe (Chen et al., 2008);
- Mixing GAC with a Fe(III)/alcohol solution resulting in 12.5% Fe (Hristovski et al., 2009);

- Pretreatment with $KMnO_4$ followed by impregnation with $FeSO_4$ solution for a maximum of 16.4% Fe in the final dried product (Hristovski et al., 2009; U.S. Patent No.20,050,156,136, 200).

The current experiment follows the method developed by Hristovski et.al. (2009) in their study, which compared the effects of two different methods of impregnating GAC with iron. They determined that the synthesis method used affects the shape and distribution of iron in Fe-GAC, and also its capacity to adsorb As(V) from groundwater (Hristovski et al., 2009). In one method, Fe^{3+} was directly precipitated onto the GAC from a $FeCl_3$-alcohol solution. The other method used was the two-step $KMnO_4$-Fe^{2+} process used for Steps 2 and 3 of the current experiment. Solution concentration and reaction time was varied for both methods (Hristovski et al., 2009).

The $FeCl_3$-alcohol method resulted in iron deposited as spherical shaped nanoparticles distributed throughout the GAC. While arsenic removal capacity increased with increasing iron content, it was observed that iron content did not significantly increase with increased Fe^{3+} concentration or reaction time (Hristovski et al., 2009).

The $KMnO_4$-Fe^{2+} method produced "teeth-like" iron nanoparticles distributed primarily in the outer layers where permanganate had reacted with the GAC. It was determined that for 0.5 N $KMnO_4$ solution, much of the MnO_4^- remained unreacted, indicating that this concentration is in excess. Reaction times exceeding 15 minutes did not increase (and may have decreased) the iron

content of the end product. These observations were considered when deciding on the reaction conditions of 0.2 N $KMnO_4$ and 15 minutes used in the present experiment (Hristovski et al., 2009; U.S. Patent No.20,050,156,136, 200).

Fe-GAC produced by the $KMnO_4$-Fe^{2+} method was an order of magnitude more effective at removing As(V) from water than Fe-GAC synthesized using the $FeCl_3$-alcohol method. Nanoscale structure of the deposited iron particles was confirmed by focused ion beam (FIB) and scanning electron microscopy (SEM). The study concluded that an understanding of the factors controlling metal hydroxide nanoparticle formation is essential in order to optimize their deposition onto support surface (Hristovski et al., 2009).

Evaluating Adsorption Capacity

A method of evaluating media performance using a combination of materials characterization followed by adsorption isotherm testing was described by Hristovski, Westerhoff, and Crittenden (2008) in their evaluation of the arsenic removal capability of titanate nanofibers. In their experiment the synthesized titanate nanofibers were first characterized using a combination of techniques typically used in materials science investigations including x-ray diffraction (XRD), electron microscopy, surface area, zeta-potential measurement, and determination of particle size and shape. This was followed by equilibrium batch adsorption isotherm testing to evaluate contaminant removal efficiency. Although their study concluded that the titanate nanofibers under evaluation were less

suitable for arsenic removal than other commercially available materials, the experiment demonstrated that this combination of characterization, testing and modeling was easier, faster, and less expensive than long-duration pilot testing (Hristovski et al., 2008).

Quantifying adsorption using quilibrium adsorption isotherms. The adsorption capacities of different adsorbent media for a targeted solute can be compared using equilibrium adsorption isotherm equations, which relate the mass of solute adsorbed per unit of adsorbent media to the equilibrium concentration of the solute remaining in the liquid solution (Crittenden et al., 2005). They are created by exposing a known concentration of dissolved solute to different masses of adsorbent media and allowing the system to come to equilibrium. The equilibrium between the adsorbed and dissolved solute phase can be described by Equation 6 (Crittenden et al., 2005).

$$q_e = \frac{V}{m_{Dry}}(C_0 - C_e) \quad (6)$$

Where

q_e = Equilibrium ratio of adsorbed solute: adsorbent, (mg-solute/g-adsorbent)

V = Volume of aqueous-phase added to jar, (L)

m_{Dry} = Mass of dry adsorbent, (g)

C_0 = Initial aqueous-phase concentration of solute, (mg/L)

C_e = Equilibrium aqueous-phase concentration of solute, (mg/L)

There are different versions of the isotherm equation used depending on the particular type of adsorption being described. The Langmuir isotherm model assumes a homogeneous adsorbent surface with all sites having equal adsorption energy for the target adsorbate, and monolayer accumulation of contaminant on the adsorbent surface. However, typically the Freundlich isotherm equation is the one used to describe adsorption onto heterogeneous adsorbents, like those used in this experiment, where the forces governing physical adsorption dominate resulting in multi-layer adsorption on the adsorbent surface (Crittenden et al., 2005).

The Freundlich isotherm model relates the concentration of solute adsorbed onto the surface of an adsorbent to the concentration of the solute remaining in the liquid phase of the solution. Mathematically, it is described by Equation 7 (Crittenden et al., 2005; Zytner, 1991).

$$q_e = K_a C_e^{1/n} \quad (7)$$

Where

q_e = Equilibrium ratio of adsorbed solute: adsorbent, (µg-solute/g-adsorbent)

K_a = Freundlich adsorption capacity parameter, an equilibrium constant indicative of adsorptive capacity, $(\mu g/g)(L/\mu g)^{1/n}$

C_e = Equilibrium concentration of solute A in liquid-phase of solution, (µg/L)

$1/n$ = Freundlich adsorption intensity parameter, (unitless)

The constants K_a and 1/n are determined by linear regression of the log of q_e and C_e. The constant K_a is the intercept and is an indication of the adsorptive capacity of the media in the system, while the constant 1/n indicates adsorption intensity. The adsorptive capacity of the adsorbent for the adsorbate increases with increasing values of K_a and n (Zytner, 1991). Understanding the values of adsorption capacity parameters (like K_a and n) allow the assessment of the relative effectiveness of different adsorbent media for the targeted contaminant.

CHAPTER THREE – METHODOLOGY

This study is comprised of three sections, (1) media synthesis, (2) media characterization, and (3) media evaluation. The methods used in this study are variations of those published in Hristovski et.al. (2009).

Synthesis of Fe-GAC

Table 3 summarizes the two base GACs used as starting materials, both of which are commercially available from NORIT Americas Inc, USA. All GAC was sieved through a 40 mesh screen and the fines were discarded prior to use in the experiment in order to achieve a more representative standard particle size.

Table 3.

Properties of the untreated GAC media

Base Material	*Iodine Number (mg/g)*	*Bed Density (kg/m^3)*	*Source*
Bituminous coal	1020	432.5	(Norit, 2007)
Lignite coal	625	360.4	(Norit, 2007)

Unless otherwise noted, all water used in the experiment was ultrapure water (< 1 µS/cm). Reactant solutions were made immediately prior to use to prevent oxidation.

Synthesis Overview. Three synthesis variations were used on each of the GACs resulting in the synthesis of six Fe-GACs. The HCl/Mn/Fe method followed a three step process consisting of (1) an acid wash followed by, (2)

permanganate pretreatment and finally, (3) iron deposition. The Mn/Fe method omitted the acid wash and only included Steps 2 and 3 (permanganate pretreatment followed by iron deposition). The Fe Only method omitted Steps 1 and 2 and consisted of only the iron deposition step in order to observe the effects of the first two steps on the final iron content of the synthesized media. Treatment conditions are summarized in Table 4 and a schematic of the synthesis process is shown in Figure 2.

Table 4.

Summary of treatment conditions

	Step 1		Step 2		Step 3	
	Acid Wash		$KMnO_4$ Treatment		$FeSO_4$ Oxidation	
Method	[HCl]	Time	[$KMnO_4$]	Time	[$FeSO_4$]	Time
HCl/ Mn/Fe	1 M	1 wk	0.2 N	15 min	1 M	6 hours
Mn/Fe	N/A	N/A	0.2 N	15 min	1 M	6 hours
Fe Only	N/A	N/A	N/A	N/A	1 M	6 hours

Note: N/A indicates that the step is not applicable to the particular method.

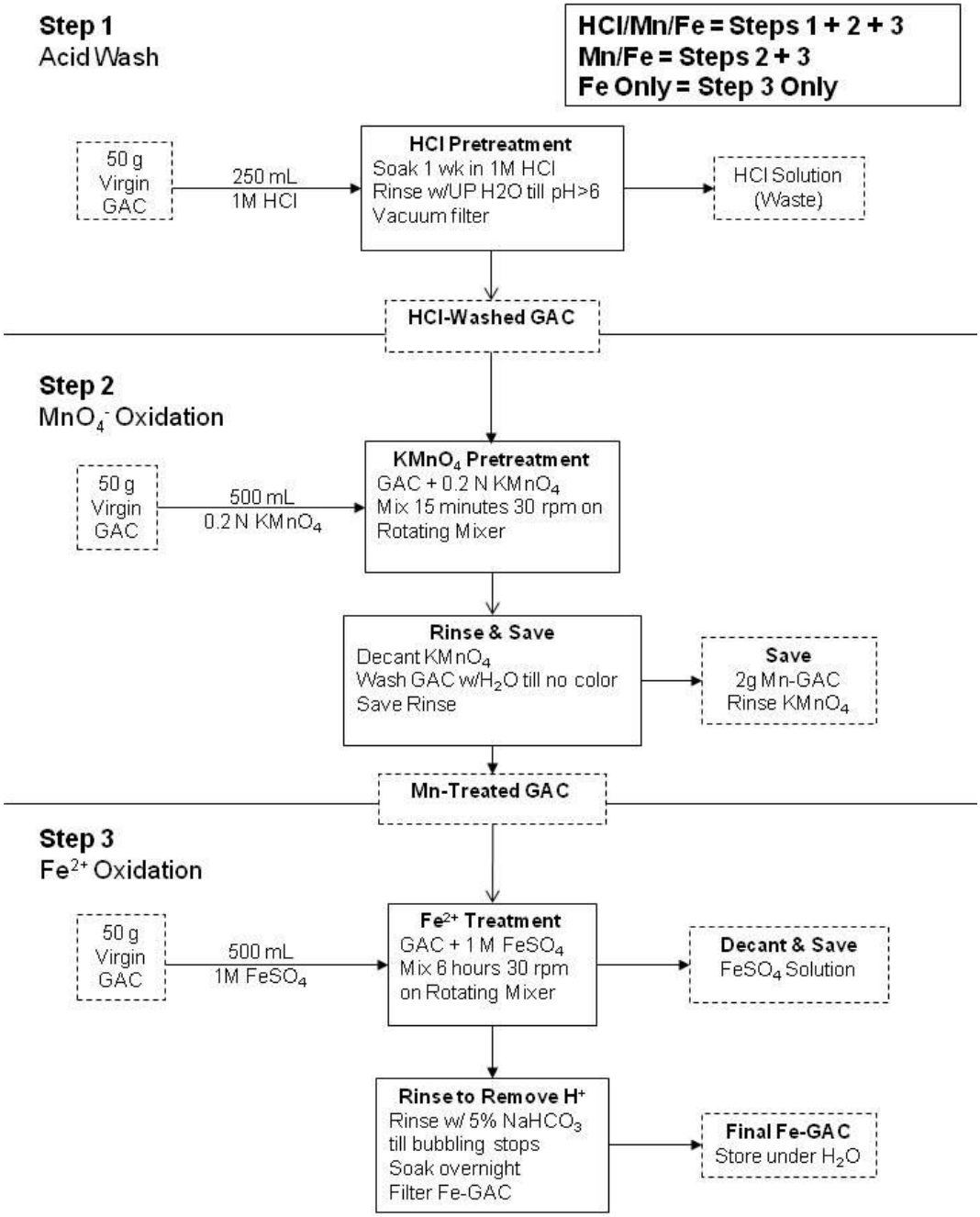

Figure 2 Schematic of synthesis treatment methods

Treatment steps.

Step 1: Acid soak

In this step, 50 g of virgin GAC was soaked in 250 mL of 1M HCl solution for one week in order to remove any surface impurities and acidify the GAC surface. The permanganate ion used in the next step is an anion and any residual positive charge remaining on the GAC surface could minimize potential electrostatic repulsion and facilitate diffusion inside the GAC pores. The acid-soaked GAC was then vacuum filtered and continuously rinsed with water until the rinse water had pH > 6 as measured using Hydrion® pH paper.

Step 2: Permanganate pretreatment

For each GAC-type, a 500 ml 0.2 N $KMnO_4$ solution was prepared by combining 15.8 g $KMnO_4$ (Fluka/Sigma Aldrich, FW = 158.04 g) in a flask with sufficient water to make 500 mL of solution and mixing on a stir plate in a darkened room (to minimize oxidation of the MnO_4^- ion) until dissolved. The solution was added to an amber-glass/Teflon-capped bottle containing 50 g of either the virgin (for the Mn/Fe method) or acid-soaked (for the HCl/Mn/Fe method) GAC and mixed at 30 rpm for 15 minutes on a rotating mixer. The mixing was then stopped and the $KMnO_4$ solution was decanted and saved in a 2 L graduated cylinder. The GAC was continually rinsed with water until there was no observable trace of color from the $KMnO_4$ solution and the rinse added to the cylinder. The reaction vessel and cap were also rinsed and the water added to the cylinder. The volume of the total rinse solution in the cylinder was measured and

saved for analysis and use in the manganese mass balance. A small sample (~1 g) of the rinsed permanganate-treated GAC (Mn-GAC) was also removed for analysis as part of the mass balance.

The concentration and reaction time used in Step 2 were chosen based on prior research performed by Hristovski et al. (2009), in which they determined that a solution concentration between 0.1 N and 0.5 N $KMnO_4$ and reaction time of 15 minutes would be sufficient for permanganate pretreatment of GAC.

Step 3: Iron deposition

For each GAC type, 500 mL of 1 M $FeSO_4$ solution was prepared by combining 139.01 g of $FeSO_4 \bullet 7H_2O$ (Fluka/Sigma Aldrich, FW = 278.02 g) in a flask with sufficient water to make 500 mL solution and mixing on a stir plate until dissolved. The solution was added to an amber-glass/Teflon capped bottle containing either 50 g of virgin (Fe Only method) or Mn-GAC (from HCl/Mn/Fe and Mn/Fe methods) and mixed for 6 hours at 30 rpm on a rotating mixer. After reacting, the $FeSO_4$ solution was decanted and saved for later analysis.

Following iron oxidation, the GAC in the reaction vessel was repeatedly rinsed with 5% $NaHCO_3$ solution until there was no further observable generation of gas bubbles. This step served to neutralize the H^+ released during the Mn^{7+}-reduction/Fe^{2+}-oxidation reaction and to shift the reaction equilibrium in favor of iron (hydr)oxide deposition. The GAC was left to soak overnight in a fresh solution of 5% $NaHCO_3$ and then stirred one final time to release any remaining

CO_2 before it was rinsed with ultrapure water. The resulting Fe-GAC was vacuum filtered and stored wet in a glass Quorpak® jar.

Mass Balance – Mn & Fe Tracking

Sample collection and analysis for mass balance. In order to track Mn and Fe throughout the synthesis process, samples of the initial and final solutions from each reaction step, as well as samples of the virgin GAC, Mn-GAC (from Step 2), and the final Fe-GAC were collected and analyzed for Fe, Mn, and/or MnO_4^-. A schematic of the sample collection and analysis for the mass balance and materials characterization are provided in Figures A1 and A3 of the appendix.

The Fe and Mn content of all samples was measured using acid digestion followed by Flame Atomic Absorption Spectroscopy (FAA, Varian SpectrAA 50B Atomic Absorption Spectrometer). Liquid samples of the initial and final $FeSO_4$ solution, the starting $KMnO_4$ solution and the combined $KMnO_4$ rinse, were digested according to standard methods for examination of water and wastewater (Franson, Eaton, Clescri, & Greenberg, 1995). Solid samples including the untreated GAC, the Mn-GAC and the final Fe-GAC were digested according to US EPA SW846 3050B (United States Environmental Protection Agency [USEPA], 1996). A flowchart of the acid digestion process is included in Figure A2 of the appendix. Settings used for FAA analysis are listed in Tables B1 and B2 of the appendix.

UV/VIS spectrophotometric analysis (Jenway 6405 UV-VIS Spectrophotometer, Barloworld Scientific Ltd., UK) was used to measure the amount of permanganate in solution before and after reacting with the GAC. UV-VIS analysis was performed immediately to prevent reduction of the ion and in accordance with Carus analytic Method 102 (Carus Chemical Company [Carus], 2004). Measurements were taken at 525 nm. The rinse was well homogenized prior to analysis to insure a representative sample.

Mass balance for Mn. The percent of Mn present as unreacted permanganate ion in solution following Step 2 is an indication of the amount of excess Mn used that did not react with the GAC surface and can be described by Equation 8.

$$\%\ Unreacted\ \mathrm{MnO_4^-} = 100\ \times \frac{m(\mathrm{Mn^{7+}})_{Rinse}}{m(\mathrm{Mn^{7+}})_{Start}} \quad (8)$$

Where

$m(\mathrm{Mn^{7+}})_{Start}$ = Initial mass $\mathrm{Mn^{7+}}$ in $\mathrm{KMnO_4}$ solution in Step 2, (mg $\mathrm{Mn^{7+}}$)

$m(\mathrm{Mn^{7+}})_{\boldsymbol{Rinse}}$ = Final mass $\mathrm{Mn^{7+}}$ in $\mathrm{KMnO_4}$ rinse after Step 2, (mg $\mathrm{Mn^{7+}}$)

The mass balance for the percentage of Mn in all oxidation states accounted for after Step 2 can be described by Equation 9.

$$(\mathrm{Mn})_{Start} = m(\mathrm{Mn})_{Rinse2} + m(\mathrm{Mn})_{GAC2} \quad (9)$$

Where

$m(\text{Mn})_{Start}$ = Mass all forms Mn in starting $KMnO_4$ solution Step 2, (mg Mn)

$m(\text{Mn})_{Rinse2}$ = Mass of all forms Mn in $KMnO_4$ rinse after Step 2, (mg Mn)

$m(\text{Mn})_{GAC2}$ = Mass of all forms Mn in treated Mn-GAC after Step2, (mg Mn)

In Step 3, the amount of Mn remaining in the Fe-GAC is equal to the difference between the amount of Mn in the Mn-GAC at the start of the reaction and the amount of Mn found in the $FeSO_4$ rinse after the reaction as described by Equation 10.

$$m(\text{Mn})_{GAC3} = m(\text{Mn})_{GAC2} - m(\text{Mn})_{Rinse3} \quad (10)$$

Where

$m(\text{Mn})_{GAC3}$ = Mass of all forms Mn remaining in Fe-GAC after Step 3, (mg Mn)

$m(\text{Mn})_{GAC2}$ = Mass of all forms Mn in treated Mn-GAC after Step 2, (mg Mn)

$m(\text{Mn})_{Rinse3}$ = Mass of all forms Mn in $FeSO_4$ rinse after Step 3, (mg Mn)

This is important to know as any excess Mn remaining in the final Fe-GAC could serve as a source of contamination to treated water and require removal. The percentage of Mn recovered and accounted for in the mass balance for all steps can be described by Equation 11.

$$\% \text{ Mn Recovered} = 100 \times \frac{m(\text{Mn})_{Rinse2} + m(\text{Mn})_{Rinse3} + m(\text{Mn})_{GAC3}}{m(\text{Mn})_{Start2}} \quad (11)$$

Mass balance for Fe. Iron content of the starting and final $FeSO_4$ solutions, the virgin GAC, and the final Fe-GAC was measured for all samples by the methods described earlier in order to track iron content throughout the synthesis process. The mass balance for iron can be summarized by Equation 12.

$$m(\text{Fe})_{VGAC} + m(\text{Fe})_{Start\ 3} = m(\text{Fe})_{Rinse\ 3} + m(\text{Fe})_{GAC\ 3} \quad (12)$$

Where:

$m(\text{Fe})_{VGAC}$ = Mass of Fe in virgin GAC, (mg Fe)

$m(\text{Fe})_{Start\ 3}$ = Mass of Fe in $FeSO_4$ solution at start of Step 3, (mg Fe)

$m(\text{Fe})_{Rinse\ 3}$ = Mass of Fe in rinse after Step 3, (mg Fe)

$m(\text{Fe})_{GAC\ 3}$ = Mass of Fe in final Fe-GAC after Step 3, (mg Fe)

If the amount of iron in the virgin GAC is negligible and all of the iron comes from the $FeSO_4$ reaction solution, then the $(\text{Fe})_{VGAC}$ term can be eliminated and the percentage of iron recovered and accounted for can be described by Equation 13.

$$\% \, Fe \, Recovered = 100 \times \frac{m(\text{Fe})_{Rinse3} + m(\text{Fe})_{GAC3}}{m(\text{Fe})_{Start3}} \quad (13)$$

Zeta Potential Analysis

Zeta-potential analysis was performed and the isoelectric point (z_{pH}) was estimated on all Fe-GAC and V-GAC samples. Samples were prepared for analysis by grinding a small amount (~0.25 g) of the ground media to a very fine powder and suspending it in 40 mL of 0.01M KNO_3 solution. The suspension was allowed to stand for at least 1 week to insure thorough wetting of the media surfaces. Zeta-potential was measured on the ZetaPALS (Brookhaven Instruments Corporation, Holtsville, NY) using a phase-analysis light-scattering technique.

To perform the analysis, approximately 1 – 2 mL of the GAC-KNO_3 suspension was added to approximately 100 mL of 0.01 M KNO_3 in a 150 mL beaker and stirred on a magnetic stirplate at a speed sufficient to prevent the particles from settling. A calibrated pH meter set to continuously measure pH was placed in the solution and, after it had equilibrated, the initial pH was recorded. A small amount of this solution was used to rinse and then fill a clean, unscratched, polystyrene square cuvette (10 mm square, 4.5 mL). The electrode was placed in the cuvette, checked for bubbles that could cause measurement error, and then placed in the chamber of the analyzer. After the measurements were taken, the cell was removed, shaken slightly to mix, checked for bubbles and then measured again. The pH of the GAC-KNO_3 stirred solution was adjusted by drop wise addition of 1 and 0.1 M acid (HNO_3) or base (KOH), and the zeta-potential was measured at the new pH. A minimum of three runs of six readings

(20 measurements per reading) were taken and averaged at each selected pH interval between the pH of 2 – 11. Average zeta-potential vs. pH was plotted for each point measured and the isoelectric point was estimated as the point at which the graph crossed the x-axis. Two-tailed 95% confidence intervals were calculated and plotted for each average zeta using the method in Equation 14 (Manly, 2001).

$$\alpha_{(2\text{-tailed})} = \frac{t_{95}\sigma}{n^2} \quad (14)$$

Where

$\alpha_{(2-tailed)}$ = the upper and lower confidence interval

t_{95} = Students t for 95% confidence interval

σ = Standard deviation of the mean

n = the number of measurements

Electron Microscopy, Surface Characterization, and Fe and Mn Distribution

Scanning electron microscopy (SEM) equipped with energy dispersive X-ray analysis system (EDX) was used to characterize surface morphology and determine the distribution of iron and manganese on the GAC surface. Samples were prepared by setting the GAC in an epoxy resin then slicing and polishing it to reveal the inner structure of the particle.

Multipoint line-scan EDX microanalysis (SEM/EDX, FEI ESEM XL30, EDAX Inc.) was conducted to investigate the distribution of Mn and Fe

throughout the media particles. Elemental surface mapping of the cross-sectioned particle was also conducted for some samples. A different system (FEI NOVA 200 Nanolab UHR FEG-SEM/FIB) equipped with a backscatter detector and EDX system was used to provide high magnification micrographs of the deposited iron (hydr)oxide nanoparticles within the media pores and mapping of iron throughout the media. This backscatter detector distinguishes heavier elements, like iron, and lighter elements, like carbon, nitrogen, and oxygen, as light areas and dark areas, respectively. High resolution micrographs from this system were used to determine the iron nanoparticles' size and shape.

Pore Size Distribution and Surface Area Analysis

Surface area was measured using the Brunauer Emmett and Teller (BET) model on the Micrometrics Tristar-II 3020 automated gas adsorption analyzer. The BET model calculates the sample surface area from the isotherm data by calculating the monolayer volume of nitrogen gas adsorbed by the sample (Micrometrics Instrument Corporation [MIC], 2008). The same instrument was used to measure the pore size distribution of the media via the method developed by Barrett, Joyner and Halenda (BJH Method) (MIC, 2008).

Prior to the analysis, a small sample (~0.1 to 0.5 g) of the media was added to a pre-weighed, dry, clean, sample tube with stopper. The sample was dried at 300 °C under nitrogen gas for one hour, allowed to cool, and then reweighed. Sample weight was calculated by subtracting the weight of the

stopper and tube from the cooled weight. Surface area analysis was conducted for pore diameter range of 17 to 3000 Å as it was assumed that pores smaller than this would be inaccessible to the iron nanoparticles.

X-ray Diffraction

X-Ray diffraction (XRD) spectra of the untreated and Mn-GAC were used to identify the intermediate manganese species involved in the formation of the iron (hydr)oxide nanoparticles. Spectra were obtained using a high-resolution x-ray diffractometer (PANalytical X'Pert Pro, CuKα source) and then compared with existing library of spectra to identify the intermediate manganese species involved in nanoparticle formation (Laetsch, T., & Downs, R. T., 2006; RRUFF Project, 2006). Samples were dried and then finely powdered and sieved through 200 mesh prior to analysis.

Estimating Equilibrium Adsorption Capacity for Arsenic and TCE

Media were evaluated for arsenate and TCE adsorption capacity via batch equilibrium adsorption testing and isotherm modeling. Arsenate and TCE adsorption were plotted using Equation 7, the Freundlich isotherm model (Crittenden et al., 2005).

Preparation of the test water matrix. Test water containing ~120 µg/L As, ~6 mg/L TCE and buffered with 10 mM $NaHCO_3$ was prepared and mixed in an HDPE-tank immediately prior to use. Sodium arsenate ($Na_2HAsO_4 \bullet 7H_2O$,

MW = 312 g) was used as a source of arsenic for the experiment. Technical grade trichloroethylene from Sigma-Aldrich was used as a source of TCE (MW = 131.39 g/mol). In the first run, the solution pH was measured and adjusted to 7.1 by drop-wise addition of 1M HCl. The pH was confirmed by measuring the remaining test water after the test jars had been filled. In the second run, the pH was not adjusted and the starting pH was approximately 8.2.

Media dosage calculations. Dosages for batch testing were calculated by substituting the Freundlich isotherm equation (Equation 7) for qe in Equation 6 and solving for dry adsorbent mass (m_{Dry}).

$$m_{Dry} = V\frac{(C_0 - C_e)}{K_a C_e^{1/n}} \tag{15}$$

Where

m_{Dry} = Mass of dry adsorbent required to reach equilibrium concentration, (g)

C_0 = Initial concentration of dissolved solute, (µg/L) or (mg/L);

C_e = Equilibrium concentration of dissolved solute, (µg/L) or (mg/L);

V = Solution volume, (L)

K_a = Freundlich adsorption capacity parameter, (µg/g)(L/µg)$^{1/n}$ or (mg/g)(L/mg)$^{1/n}$

$1/n$ = Freundlich intensity parameter, (unitless)

Dosages were estimated by assuming K_a = 250 (µg-As/g-Fe-GAC)(L/µg-As) and *1/n* = 0.45 (based on the findings of Hristovski et.al. (2009), *V* = 0.25 L, and C_0 = 120 µg-As/L. The equilibrium dissolved contaminant concentration C_e was set at 1, 5, 10, 30 and 50 µg-As/L for the purpose of making these calculations.

Percent moisture was accounted for when calculating dosages. Percent moisture was calculated from air-dried samples immediately prior to use. Media was stored in a desiccator between runs to maintain constant moisture level. The actual dried mass was calculated using Equation 16.

$$m_{Dry} = m_{Wet}(1 - \%moisture) \quad (16)$$

Where

m_{Dry} = Net dry mass of adsorbent, (g)

m_{Wet} = Original adsorbent mass, (g)

% moisture = Calculated % moisture for each virgin/Fe-GAC, (%)

Six dosages were calculated for each of the media evaluated. One dosage from each group was run in triplicate in order to observe within group variation. For a between-group difference to be judged significant it must be significantly greater than the observed within-group variation. Dosages used and solution volumes for all test groups are included in Appendix Table E 1 through E 16.

Test procedure. A total of 64 reaction vessels were prepared for each of the two test runs. Reaction vessels were prepared by weighing the calculated adsorbent dose onto the lid of a 250 mL amber-glass/Teflon-capped precleaned I-CHEM 200™ reactor vessel, screwing the reactor vessel onto the cap and then inverting the reactor vessel and tapping on the cap to insure that the measured adsorbent dose was transferred. Reactor vessels were then filled with test water to allow for no head space. The exact volume of test water used for each sample was measured and recorded for accuracy and ranged from 276 – 280 mL. Control samples (blanks) were prepared by filling precleaned 40 mL clear glass/septum-capped I-CHEM™ vials with test water. After filling, reactor vessels were placed in a dark box and agitated on the shaker table on the low setting for 3 days.

After three days, the samples were removed from the shaker and the GAC was allowed to settle with the jars capped. Immediately upon opening, a sample of ~40 mL was decanted into pre-cleaned 40 mL I-CHEM™ clear-glass/septum-capped vials and refrigerated. No head space was allowed to prevent loss of TCE to evaporation. These samples were used for determination of TCE concentration remaining in solution and estimating TCE adsorption capacity. Next, 50 mL from the remaining solution was filtered through a 0.8 µm GN-4 Grid Metricel® membrane syringe filter into an HDPE Nalgene® bottle and refrigerated until analysis. The pH of the solution remaining in the reactor vessel was measured using a pH meter. TCE concentration was analyzed using the solid phase micro extraction (SPME) method on a Varian Saturn 2100 GC/MS/MS and for arsenic

content using a graphite furnace atomic absorption spectrophotometer (GF-AAS) Varian Zeeman Spectra 400. Analysis conditions for arsenic using the GF-AAS are included in Table B 3 of the appendix.

Comparing results with other Fe containing adsorbents. Freundlich adsorption parameters for arsenic adsorption were calculated in terms of mass of iron in the media (K_a^*) as well as mass of dry media (K_a) so that the results can be more easily compared with other iron-containing adsorbents. These values were estimated by dividing K_a by the %Fe content in the media as shown in Equation 17.

$$K_a^* = \frac{K_a}{\%\text{Fe}} \qquad *** \qquad (17)$$

Where

K_a^* = Freundlich adsorption capacity in terms of Fe, (µg-As/g-Fe)(L/µg)$^{1/n}$

K_a = Freundlich adsorption capacity in terms of dry media, (µg-As/g Fe-GAC)(L/µg)$^{1/n}$

%Fe = % Fe in Fe-GAC, (%)

CHAPTER FOUR – RESULTS & DISCUSSION

Media Characterization

Iron content in Fe-GAC. Table 5 summarizes the iron content for the virgin and Fe-GAC fabricated by the different GAC-Synthesis combinations. Both untreated GAC types exhibited similar starting iron concentrations of < 0.2 % iron. However, for all synthesis combinations the lignite based Fe-GAC exhibited higher iron content than did its bituminous-based counterpart. This is significant in that it indicates that base media does play an important role in determining final iron content in the Fe-GAC.

As expected, the media produced using the Fe Only method had the lowest iron concentration, with only a small (1.9 %) difference between the lignite and bituminous Fe-GAC. Using the Mn/Fe method produced media containing approximately twice the amount of iron than did using Fe Only, confirming that permanganate pretreatment is critical to achieving high iron loading. In this case, the lignite GAC resulted in 30% higher iron content than did its bituminous counterpart (Figure 3). Adding the HCl washing step (HCl/Mn/Fe method) resulted in a slight increase in iron content as compared to using Mn/Fe only (0.7% increase for lignite and 1.3% increase for bituminous) and is an indication that acid-washing may not be an efficient way to increase iron loading.

Table 5.

Iron and Mn content in the virgin and Fe-GAC

Method	GAC Type	Weight % Fe	Weight % Mn
Untreated	Bituminous	0.17 %	< 0.05 %
Untreated	Lignite	0.15 %	< 0.05 %
Fe Only	Bituminous	3.6 %	< 0.05 %
Fe Only	Lignite	5.5 %	< 0.05 %
Mn/Fe	Bituminous	8.5 %	0.1 %
Mn/Fe	Lignite	12.1 %	0.7 %
HCl/Mn/Fe	Bituminous	9.2 %	0.2 %
HCl/Mn/Fe	Lignite	13.4 % (± 0.4)	0.7 % (± 0.03)

Notes: Data in parenthesis with ± represent the standard deviation of three independently digested and analyzed samples.

That acid washing did not have a profound effect on iron content could suggest that, for both GAC types, additional iron loading is not possible, perhaps due to blockage of the inner pores by iron (hydr)oxide particles deposited in the larger pores. If this is the case, it could be an indication that iron loading is too high and lower iron content may be needed to avoid pore clogging, which could affect the contaminant adsorption capacity of the media. This is significant because increasing iron loading at the expense of the media's contaminant removal capabilities is undesirable.

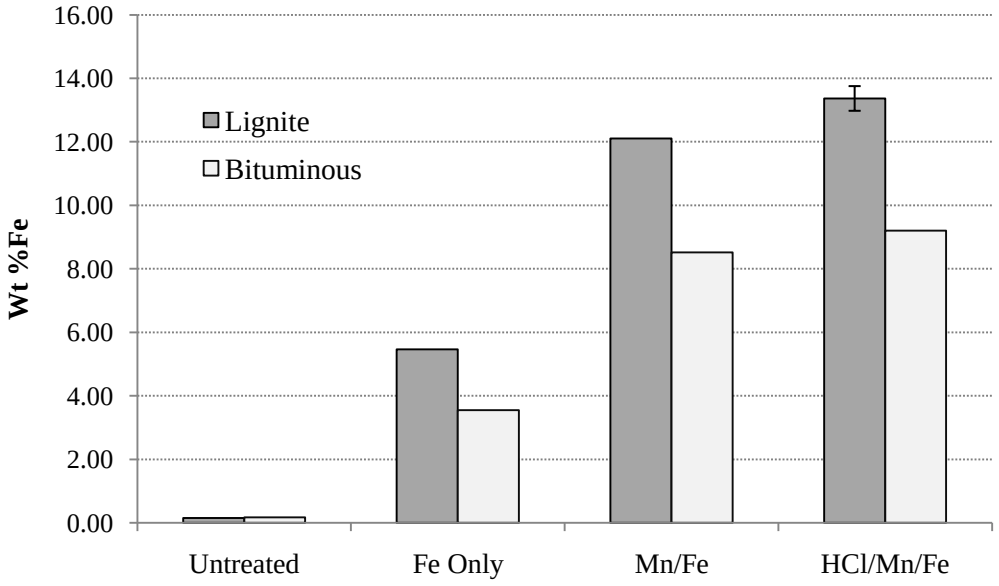

Figure 3. Comparison of Fe content in lignite and bituminous media. Error bars represent the standard deviation of three independently digested and analyzed samples

Iron recovery and mass balance. Iron recovery and a mass balance for iron are summarized in Figure 4. Iron recovery rates were > 80%, with the exception of bituminous Fe-GAC made by the HCl/Mn/Fe method, which had a recovery rate of ~70%. The lower recovery rate is probably a direct result of (1) instrumentation problems which were encountered due to FAA nebulizer interferences and clogging; (2) digestion of non-homogeneous sample; and (3) dilution errors due to high dilution factors. Most of the iron remained in the $FeSO_4$ rinse solution after the six hour period of iron treatment indicating that an

excess of iron is used in this step and further work is needed to determine the optimal quantity of $FeSO_4$ required.

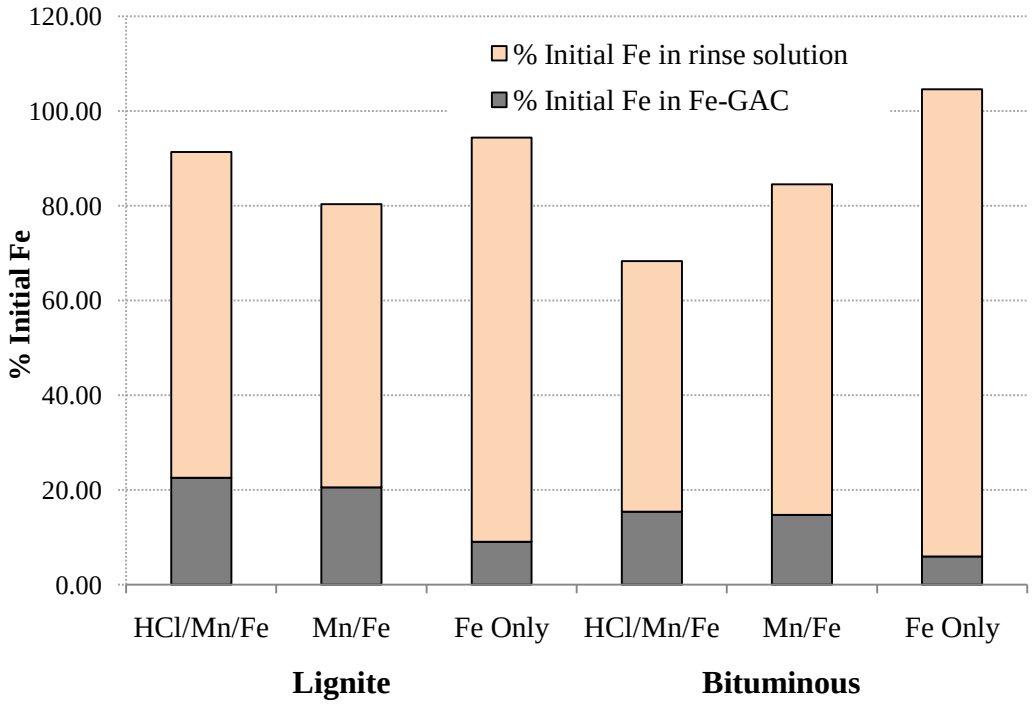

Figure 4. Mass balance for Fe.

Iron distribution in the virgin and Fe-GAC particles. Figure 5 through Figure 12 show SEM micrographs and elemental line scans of cross-sectioned particles of the different media. The path of the line scan is indicated by the red line on the SEM cross-section image. Normalized counts for the elements carbon, oxygen, silicon, manganese and iron at each point on the line are shown on the chart below each image. Images/line scans of the virgin lignite and bituminous media are included for comparison (Figures 5 and 6). Spikes in the iron trace (indicated by the grey trace line in the chart) indicate that some iron is present in

the untreated GAC and appears to be minimal in both media. The lines representing manganese content in the virgin material can be attributed to background noise in the instrument.

For both media types, an increase in iron content over that of the corresponding virgin media is indicated in the SEM/EDX images of Fe-GAC synthesized by the Fe Only method (Figures 7 and 8). However, differences in the pattern of iron distribution can be seen. The presence of iron is concentrated in the outer edges and larger pores of both Fe-GAC types, but appears to have penetrated deeper into the particle for the lignite (Figure 7) than the bituminous media (Figure 8). This corresponds with the results of FAA analysis (Table 5), which indicated higher iron content for the lignite than for the bituminous media. This pattern is representative and similar to the one seen in additional images provided in Appendix C. This could be an indication that the $FeSO_4$ reaction solution in Step 3 was unable to penetrate as far into the smaller micropores of the bituminous GAC, or that the surfaces of the bituminous media were less amenable to iron deposition.

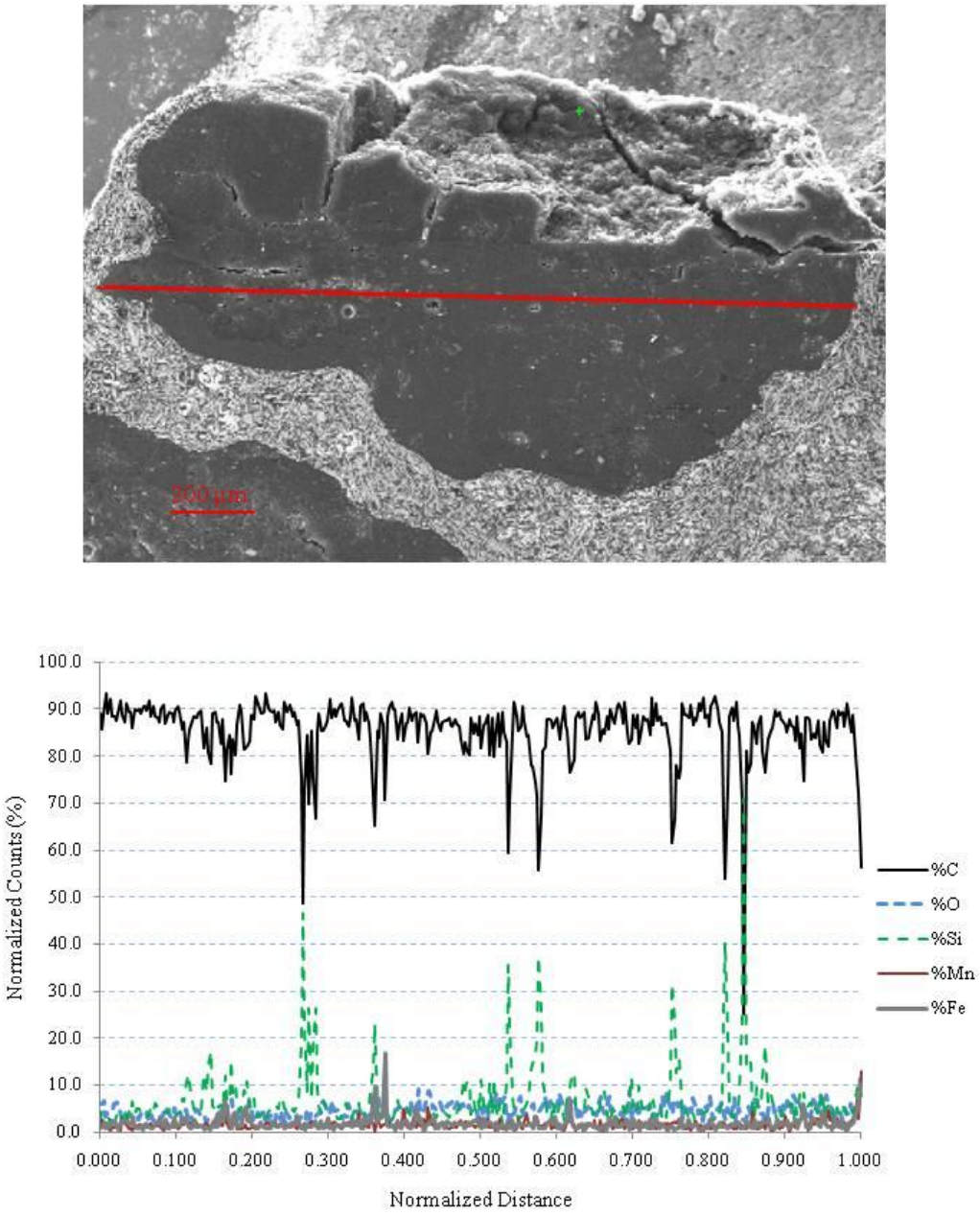

Figure 5. SEM image/EDX line scan of virgin lignite GAC

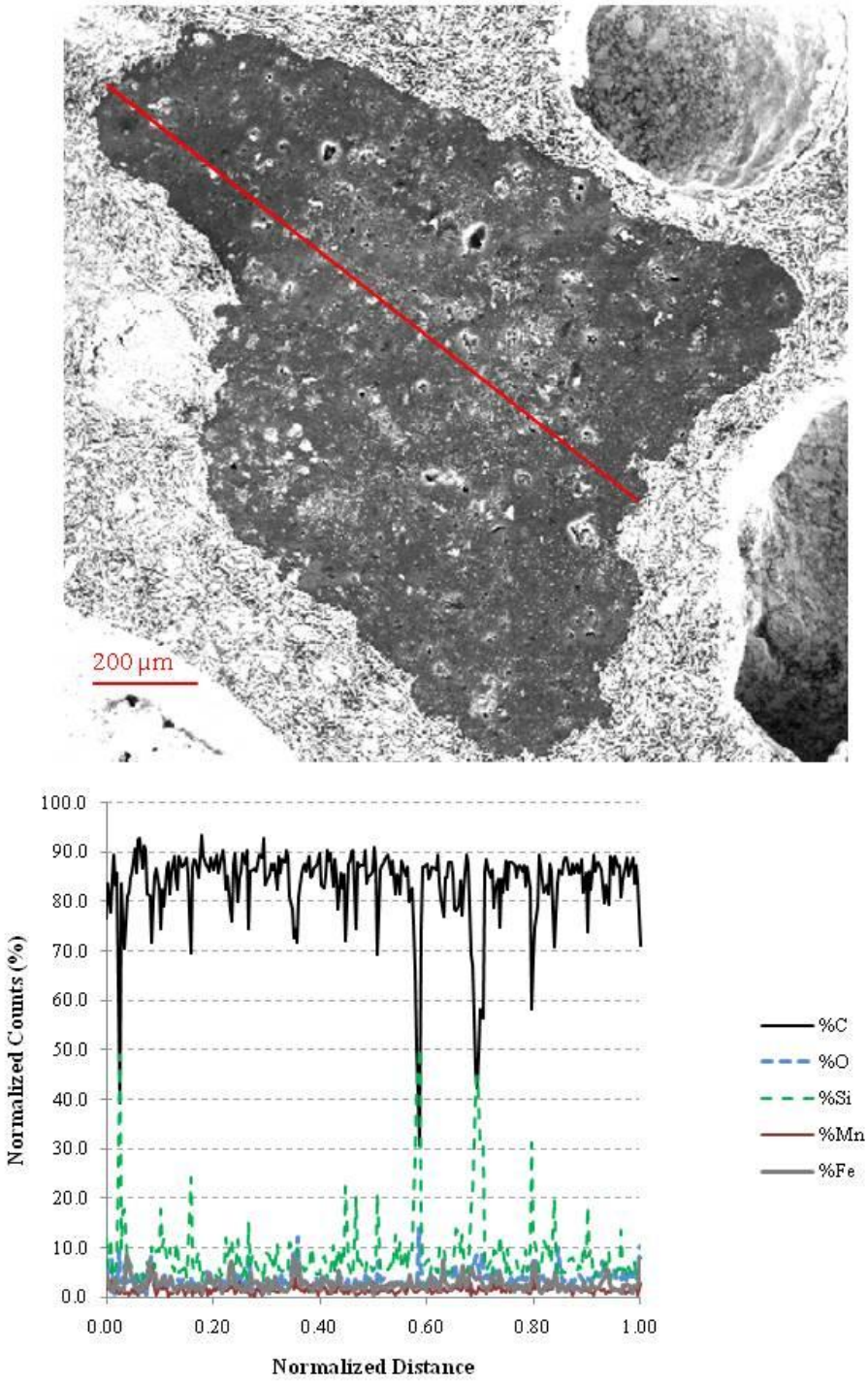

Figure 6. SEM image/EDX line scan of virgin bituminous GAC

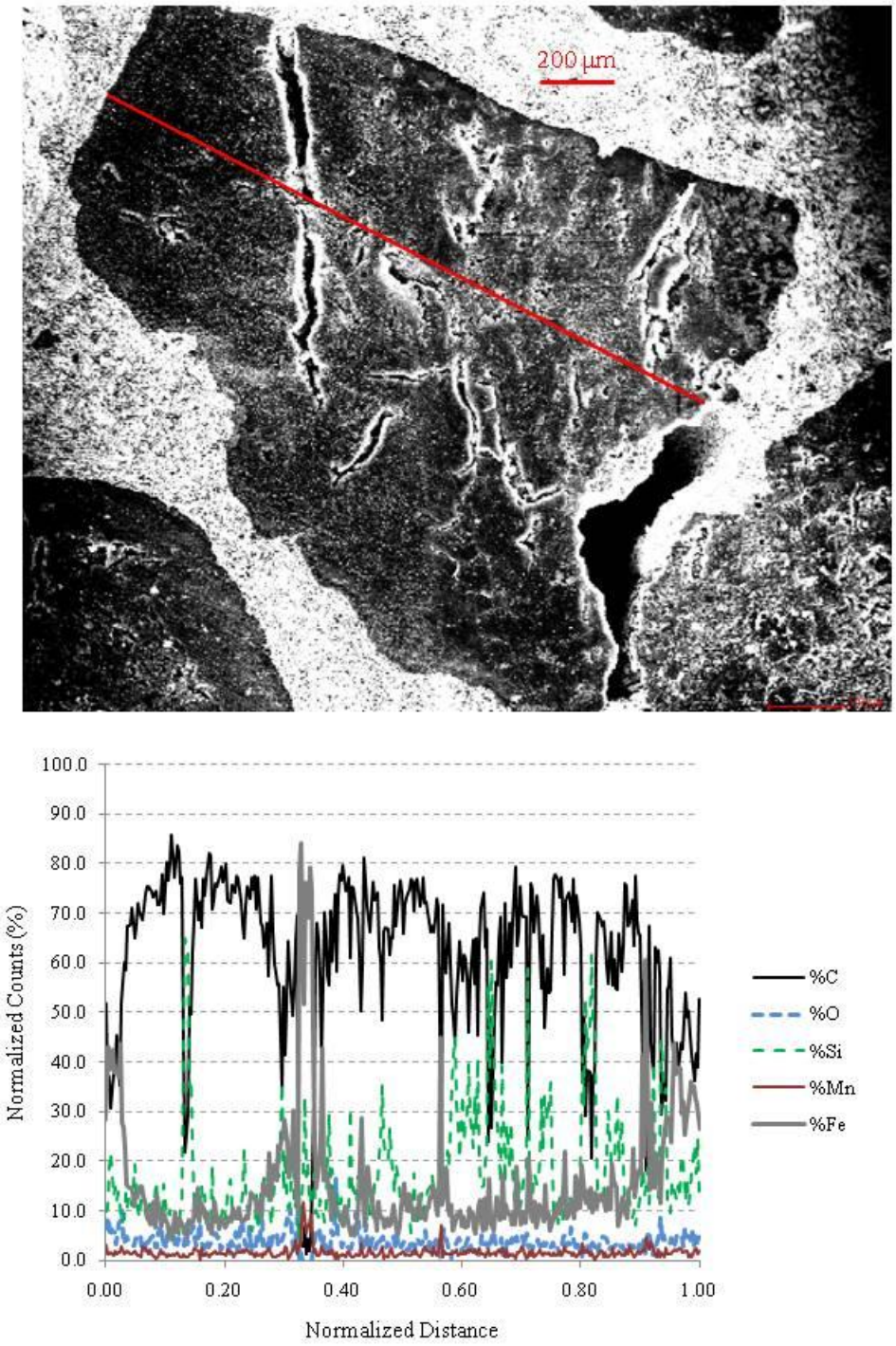

Figure 7. SEM image/EDX line scan of lignite Fe-GAC using Fe Only.

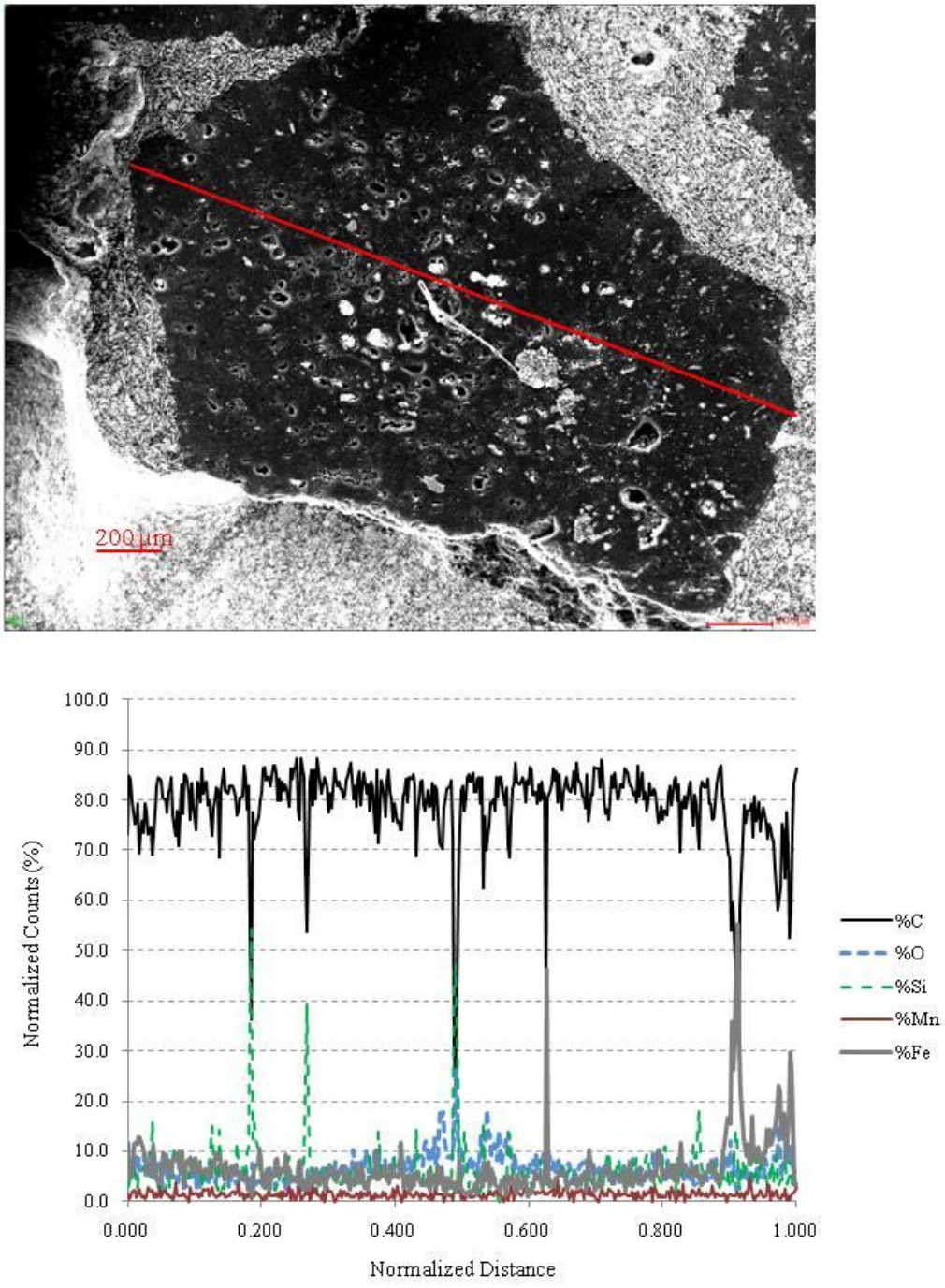

Figure 8. SEM image/EDX line scan of bituminous Fe-GAC by Fe Only.

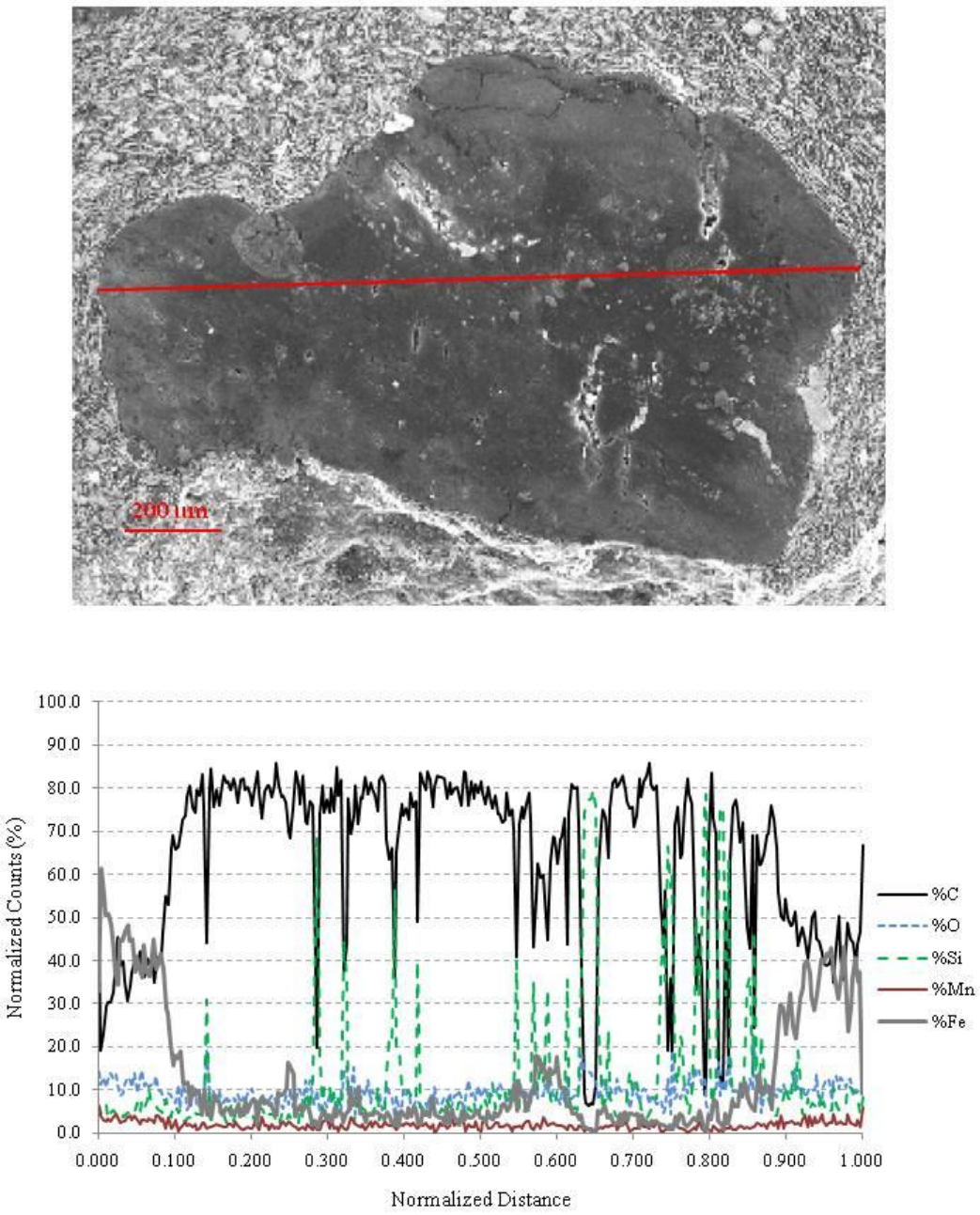

Figure 9. SEM image/EDX line scan of lignite Fe-GAC by Mn/Fe.

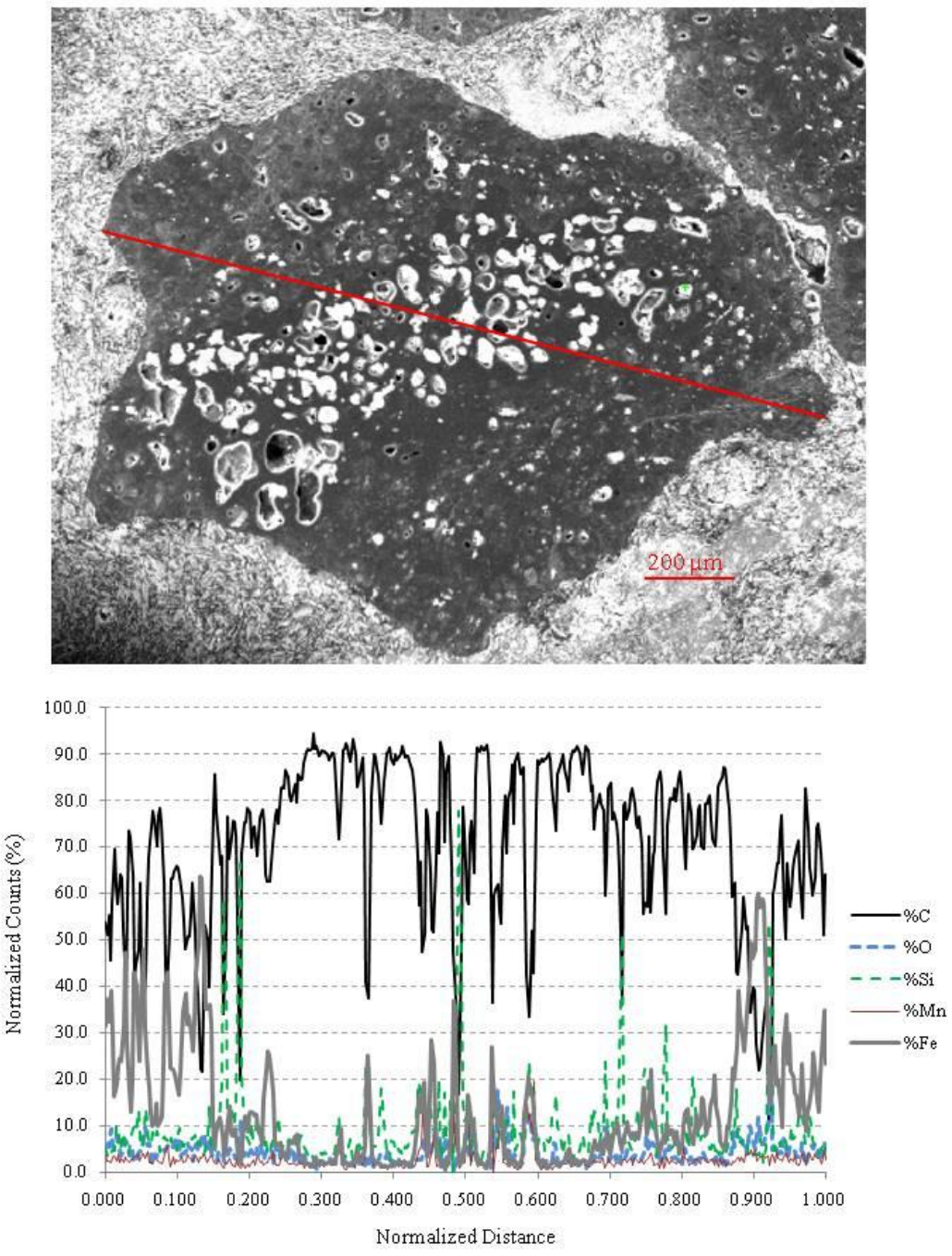

Figure 10. SEM image/EDX line scan of bituminous Fe-GAC by Mn/Fe.

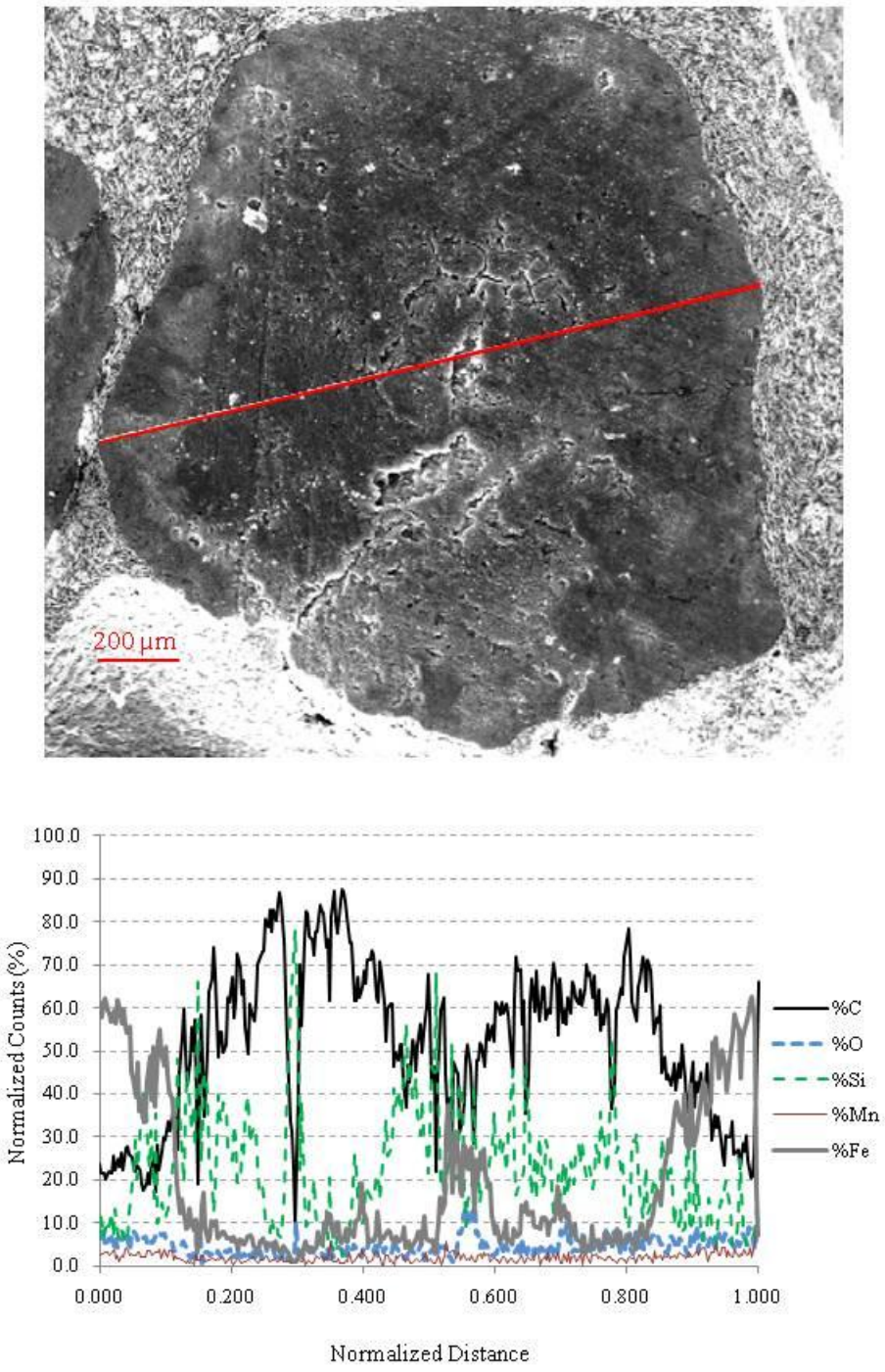

Figure 11. SEM image/EDX line scan of lignite Fe-GAC by HCl/Mn/Fe.

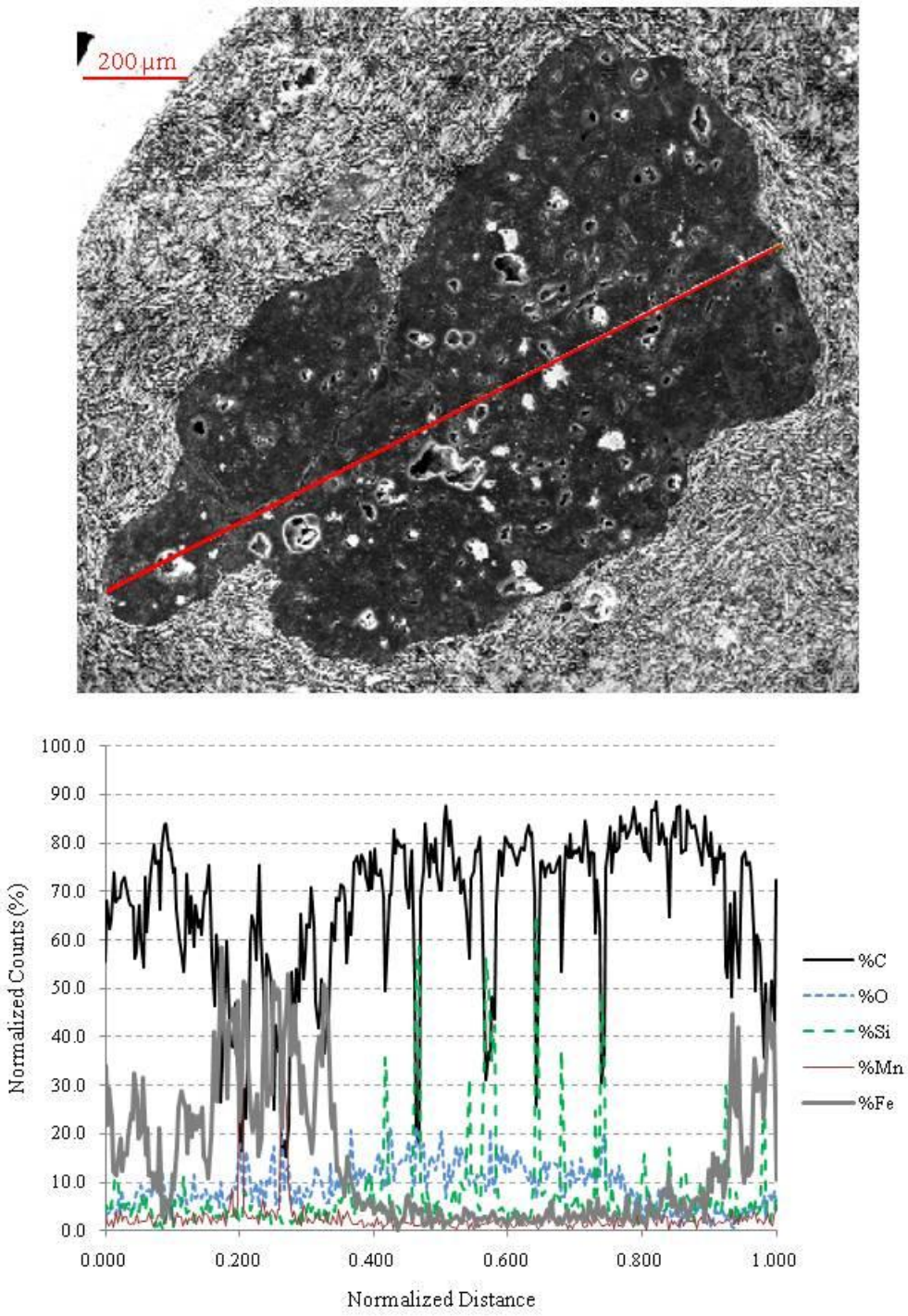

Figure 12. SEM image/EDX line scan of bituminous Fe-GAC by HCl/Mn/Fe.

For Fe-GAC synthesized using the Mn/Fe method (Figures 9 and 10), iron deposition has penetrated even further into the particles of both GAC types than it did using Fe Only (Figures 7 and 8), correlating well with the substantially higher iron content seen in the results of the FAA analysis (Table 5). The presence of iron is indicated in the larger pores of both GAC types, however, once again there appears to be more iron deposited in the lignite than in the bituminous media. This could be further evidence of pore blockage or differences in the surface functional groups present on the different media.

Fe-GAC synthesized using the acid wash step (HCl/Mn/Fe) shows the same pattern as that synthesized without the acid wash (Mn/Fe) (Figures 11 and 12), indicating that acid-washing did not result in a more even distribution of iron throughout the particle. This pattern is representative of the additional images provided in Appendix C.

The location of deposited iron (hydr)oxide in the Fe-GAC was further confirmed by EDAX mapping that was performed on the entire cross-sectioned particle surfaces of Fe-GAC synthesized using the Mn/Fe method. The results of mapping for the elements manganese, iron, carbon, oxygen, and silicon are shown in Figures 13 and 14.

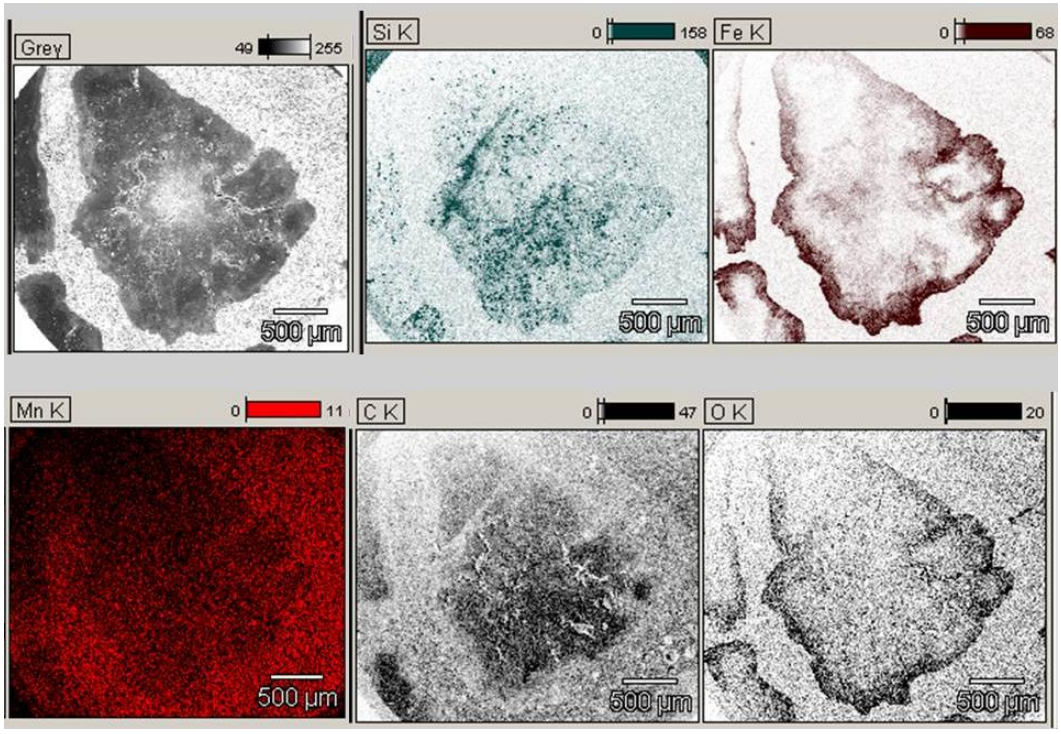

Figure 13. EDAX mapping of lignite Fe-GAC by Mn/Fe method.

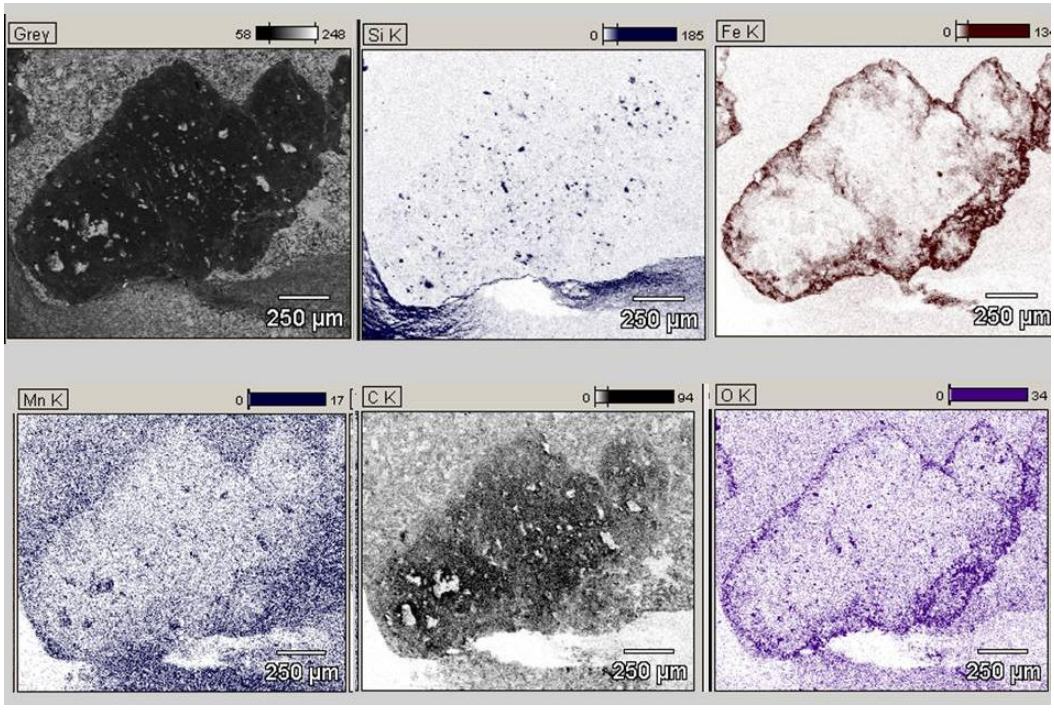

Figure 14. EDAX mapping of bituminous Fe-GAC by Mn/Fe method

In the lignite Fe-GAC, the presence of iron is confirmed to be concentrated in the outer edges and larger pores of the media (Figure 13). In these same regions, carbon content is reduced and oxygen content increased, indicating the presence of iron hydroxides or oxidized carbon groups. This same pattern is seen in the bituminous Fe-GAC (Figure 14). However, in this case, the iron does not appear to have penetrated as deep into the particle.

Iron (hydr)oxide nanoparticles morphology. The type of base GAC did not appear to significantly affect the size or shape of the iron (hydr)oxide nanoparticles in the Fe-GAC. As can be seen from Figures 15 and 16, round sphere-like nanoparticles with diameters between 10 – 50 nm can be seen in both the lignite and bituminous-based Fe-GAC synthesized using the Mn/Fe method. Nanoparticle clusters with diameters of up to 200 – 300 nm were also observed. Further support for these findings are provided by the nanoparticles and clusters shown in the additional images included in Appendix D.

The spherical nature of the particles was somewhat unexpected. In a previous study where Fe-GAC was synthesized in the same way as in the Mn/Fe method, FeOOH nanoparticles were observed with "jagged teeth-like" morphology on the outer surfaces and rounded shapes when deposited on the inner pores" (Hristovski et al., 2009). In that study, it was proposed that the difference in particle structure between the outer and inner surfaces may have been the result of the amount of interaction between the permanganate and the GAC surface. Where there had been greater potential interaction (at the outer

surfaces) deposited particles had a tooth-like structure, whereas they had a rounded shape when deposited on the inner GAC surfaces where there was potentially less MnO_4^-: GAC interaction (Hristovski et al., 2009). Although similar reaction times and conditions were used in the present experiment, the starting GAC was different and it would be interesting to determine whether, the base GAC is responsible for the differences observed in these experiments.

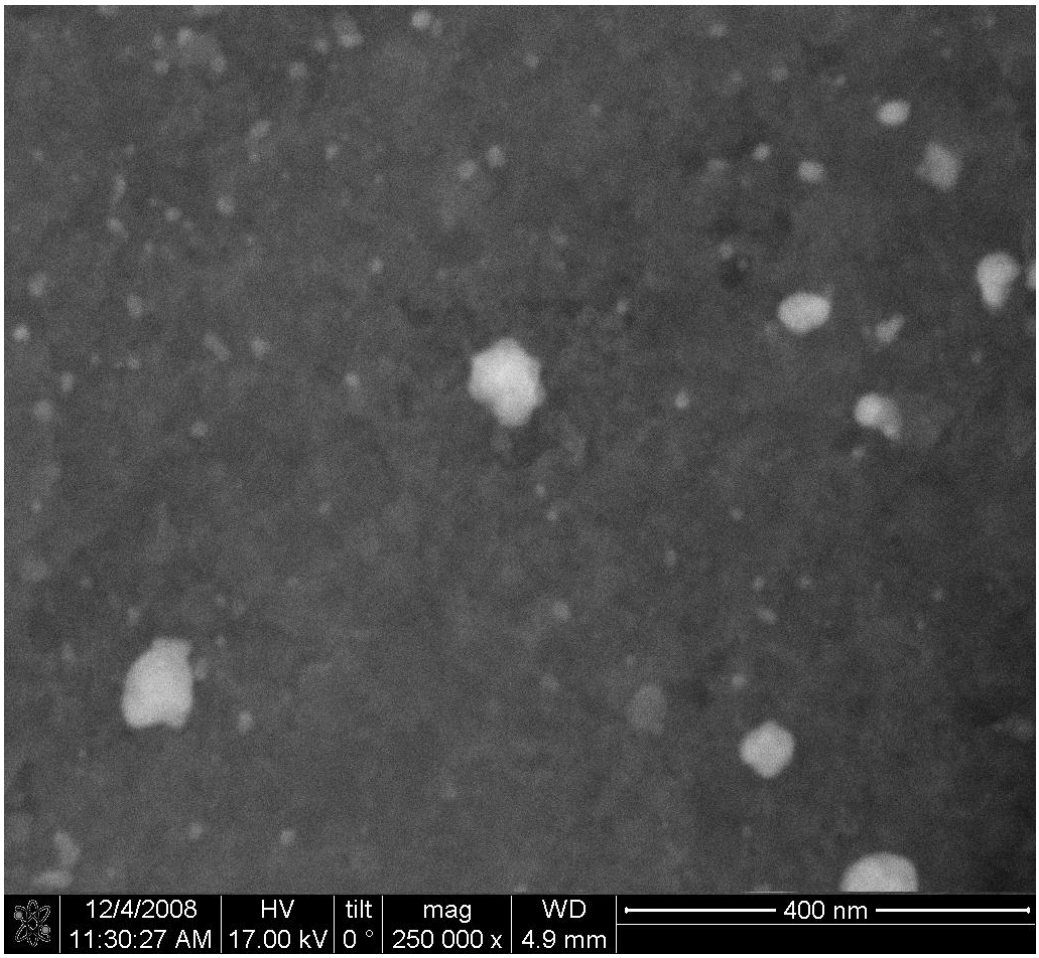

Figure 15. FIB image of FeOOH nanoparticles in lignite Fe-GAC by Mn/Fe method.

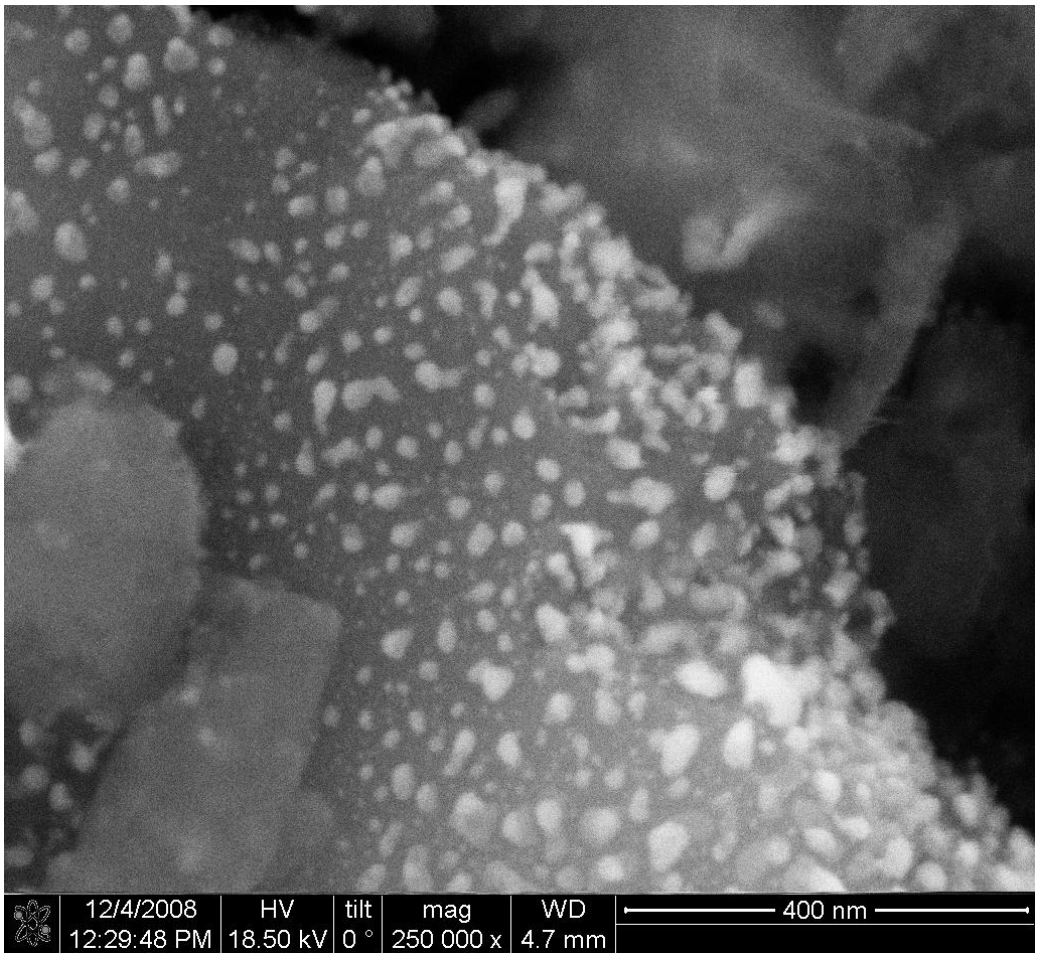

Figure 16. FIB image of FeOOH nanoparticles in bituminous Fe-GAC by Mn/Fe method.

BET surface area and pore size distribution results. The results of BET surface area analysis indicate that, for both GAC types, there is a reduction in available surface area after iron (hydr)oxide impregnation. These results are summarized in Table 6. Iron content in the media (% Fe) is included in the table as a reference for easy comparison.

Table 6.

BET surface area (SA) results for virgin and Fe-GAC

GAC Type	Untreated BET SA (m^2/g)	Fe Only BET SA (m^2/g)	Mn/Fe BET SA (m^2/g)	HCl/Mn/Fe BET SA (m^2/g)
Lignite	696.3 ± 5.4	579.0 ± 4.5	571.5 ± 4.0	524.3 ± 3.6
(% Fe)	(Fe < 0.35 %)	(Fe = 5.5 %)	(Fe = 12.1 %)	(Fe = 13.4 %)
Change in Surface area		-16.8%	-17.9%	-24.7%
Bituminous	847.3 ± 12.2	792.4 ± 11.2	742.0 ± 9.8	729.4 ± 9.9
(% Fe)	(Fe < 0.35 %)	(Fe = 3.6 %)	(Fe = 8.5 %)	(Fe = 9.2%)
Change in Surface area		-6.5%	-12.4%	-13.9%

Surface area reduction was lower for the higher surface area bituminous GAC than for the lignite GAC. In the bituminous media, the reduction ranged from 6.5 – 14% ($\Delta SA \cong 55 – 118\ m^2/g$) after impregnation. In the lignite based media surface area was reduced between 17 – 25% ($\Delta SA \cong 117 – 172\ m^2/g$). When the reduction in surface area was plotted vs. iron content it was evident that the reduction was roughly linear to iron content for both media types (Figure 17).

This correlation was stronger for the bituminous media ($R^2 = 0.99$) than the lignite media ($R^2 = 0.84$), which showed a greater loss in surface area relative to the increase in iron content, particularly for the sample made by the Fe Only method. Excluding this data point gave a correlation factor of $R^2 = 0.96$ for lignite. The reason for this outlier could be the result of the very small amount of media used in the analysis resulting in a non-representative sample.

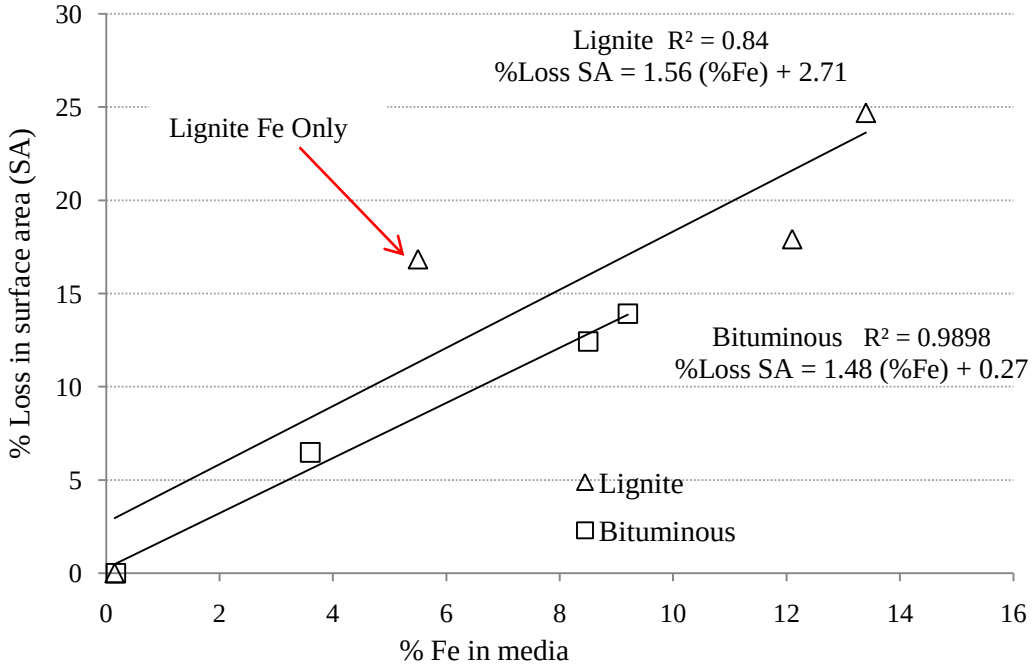

Figure 17. Surface area loss vs. iron content in Fe-GAC

It was expected that impregnation with FeOOH nanoparticles would result in surface area loss as some of the nanoparticles could block narrow pore entrances making their inner surfaces unavailable. Although surface area reduction was greater for the lignite than the bituminous media, pore blockage is

anticipated to be more of a problem for the bituminous media as it contains a greater percentage of micropores.

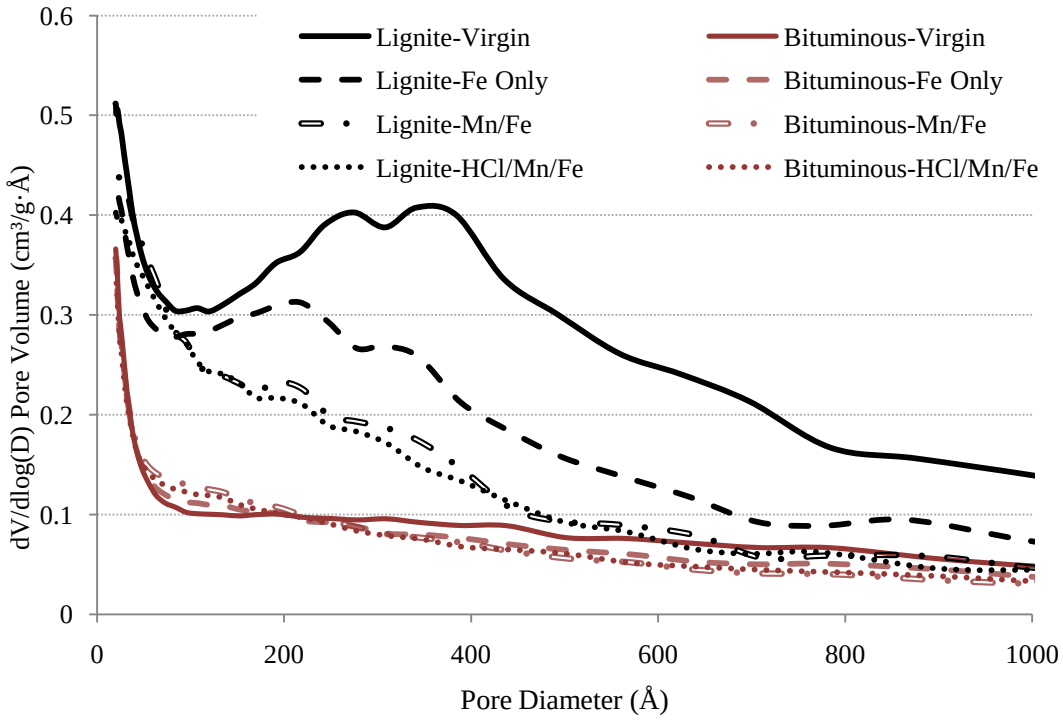

Figure 18. Pore size distribution in media before & after Fe impregnation

The decrease in surface area also correlated well with the decrease in available mesopores and macropores, as illustrated by Figure 18. The results show a greater decrease in available meso and macropores (diameter > 200 Å) for the lignite based media, with the greatest loss in pores of diameter 250 – 400 Å (25 – 40 nm). However for the bituminous Fe-GAC, a slight increase in the differential pore volume in the microporous range following iron impregnation is indicated. The creation of new pores <20 nm (200 Å) could be due to the new surfaces created as a result of iron nanoparticles deposition. The fraction of pores

in this range is significantly greater (2 to 3 times) greater in bituminous than in lignite GAC, which may explain why the increase is more evident for this media type. However, analysis was primarily concentrated on pores in the meso – macro pore range, as this was considered to be the size range most significant for arsenic removal, and so the distribution of pores < 20 Å is not fully characterized, and could be significant for this media type.

The observed change in surface area reinforces the fact that high iron content is not the only factor to consider, especially if it comes at the cost of available adsorption sites, as this could result in reducing the overall adsorption performance of the media. This is especially true for contaminants like TCE, where surface area is linked to adsorptive capacity for the molecule (Karanfil & Dastgheib, 2004). It is important to find the proper level of iron impregnation in the Fe-GAC so that the compromise between surface area reduction and iron content results in the maximum adsorption capacity for the contaminant in question.

If iron deposition has resulted in a decrease in the number of available adsorption sites for TCE, there should be an increase in competition for the remaining sites. This could result in the possible reorganization of the adsorbate on the adsorbent media surfaces leading to less stable thermodynamic states that require higher adsorption energies. The result would be seen as reduced adsorption capacity of the media for the contaminant in question and higher Freundlich adsorption parameters (1/n > 1) (Qin, Gang, Zhang, & Li, 2004).

Zeta potential. With the exception of Fe-GAC synthesized using the acid washing step (HCl/Mn/Fe), the isoelectric points for the final Fe-GAC were increased by 0.8 – 1 pH units over that of the corresponding untreated GAC for both GAC types (Table 7). Isoelectric points for Fe-GAC synthesized by the Mn/Fe method were ~0.3 pH units higher than for Fe-GAC by the Fe Only method. This is not surprising as iron (hydr)oxide and iron oxides have a high isoelectric point ($z_{pH} \approx 8 – 9$) (Tadanier, Schreiber, & Roller, 2005), and therefore an increase in iron content should cause an increase in the isolectric point of the media. This could be favorable for media expected to remove a negatively charged ion, such as arsenate, in the natural pH range of water.

Table 7.

Estimated isoelectric point (z_{pH}) for virgin and Fe-GAC.

GAC Type	Untreated	Fe Only	Mn/Fe	HCl/Mn/Fe
Lignite	2.38	2.95	3.43	1.71
Bituminous	3.17	4.22	4.39	3.39

Results for Fe-GAC synthesized using the HCl/Mn/Fe method were anomalous and showed no change (for bituminous) or a slight decrease (for lignite) in isoelectric point as compared to the corresponding virgin GAC. These results could be due to a greater number of oxidized functional groups remaining on the media surfaces following the acid wash step. Additional measurements were conducted to confirm this trend and eliminate potential error.

The lignite GACs showed lower isoelectric points than their bituminous counterparts before and after impregnation (Table 7). Lower isoelectric points are consistent with more oxidized surfaces and the presence of oxygen containing functional groups, such as hydroxyl, carboxyl and carbonyl groups (Sontheimer et al., 1988). These are more commonly seen in lignite coal (the base material for producing lignite GAC) as it is a geologically younger material and is not exposed to the same reducing conditions and pressures as bituminous coal during the coal aging process (Sontheimer et al., 1988; Buecker, 2006).

Both media exhibited negative surface charge in the natural pH range of water (Figures 19 and 20). However, the surface charge was generally less negative for the Fe-GAC than for the corresponding base media. For both media types, Fe-GAC synthesized using the permanganate pre-treatment step (HCl/Mn/Fe and Mn/Fe) had surface charge in the range of -10 eV to -35 eV in the natural pH range of water (6.5 – 8.5). Surface charge in this pH range was more negative for the (no iron content) virgin and (low iron content) Fe-GACs synthesized without the permanganate pre-treatment (Fe Only). This is also reasonable considering that the higher iron (hydr)oxide content would correspond to an increase in the number of positively charged sites on the GAC surface, which should be greater for media containing higher iron content.

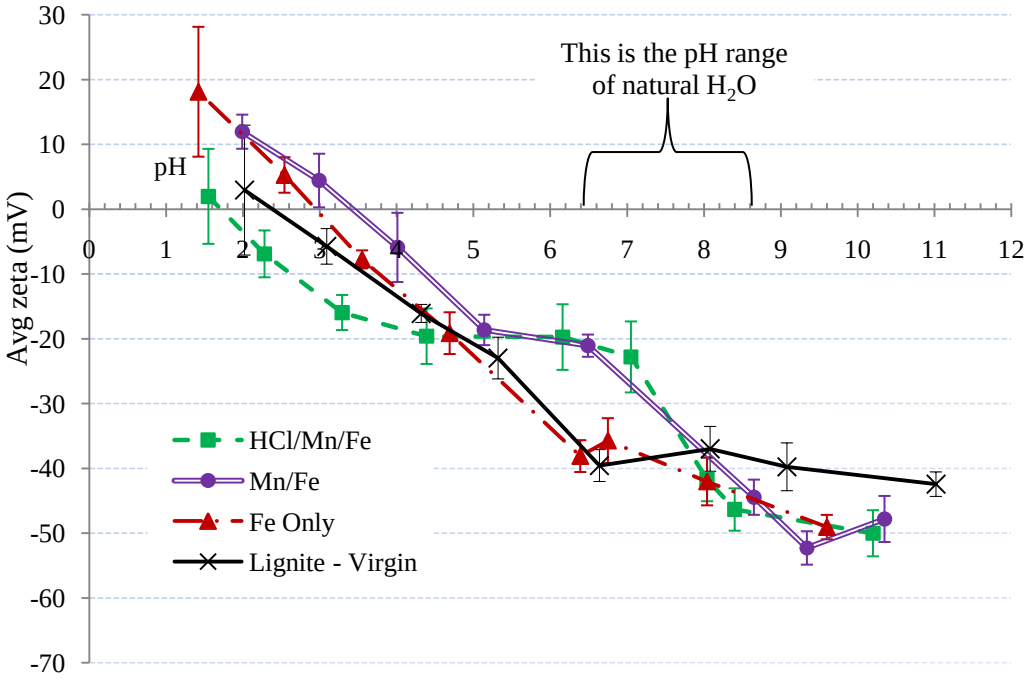

Figure 19. Zeta potential and isoelectric measurements for lignite media. Error bars represent upper and lower 95% confidence intervals.

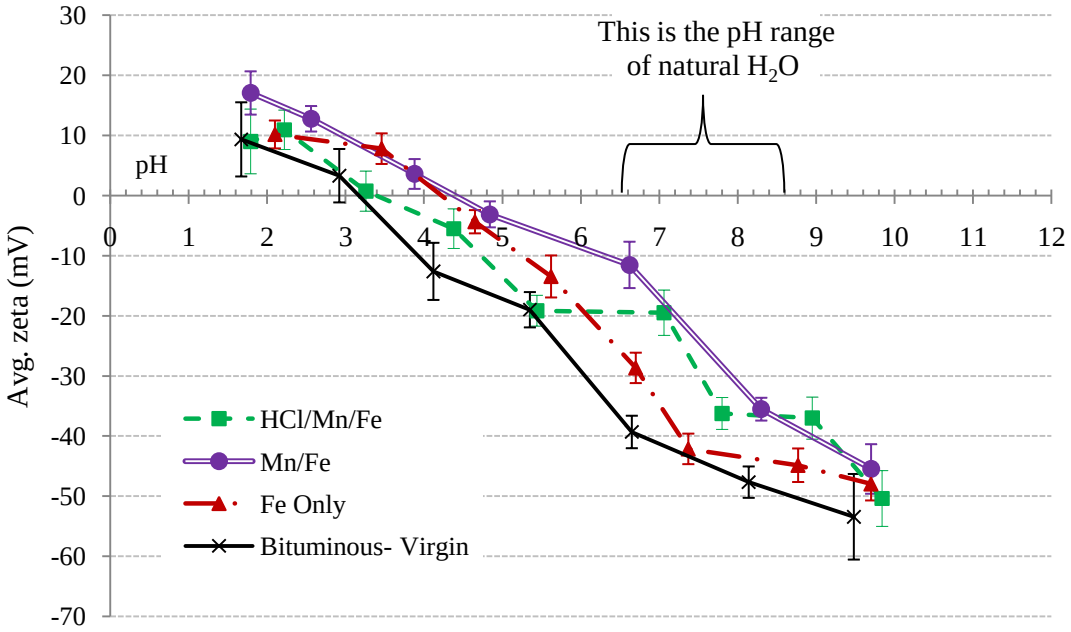

Figure 20. Zeta potential and isoelectric measurements for bituminous media. Error bars represent upper and lower 95% confidence intervals.

The Role of Mn in Nanoparticle Formation

Results of mass balance for Mn. The results of the manganese mass balance and recovery are summarized in Figures 21 – 23. Data used for the Mn mass balance is included in Tables B5 and B6 of the Appendix. Recovery rates for manganese ranged between 88 – 101%. Recovery rates in excess of 100% were the result of experimental error probably due to the degree of dilution required in order to bring the sample into a range suitable for analysis (in some instances > 100X dilution was required).

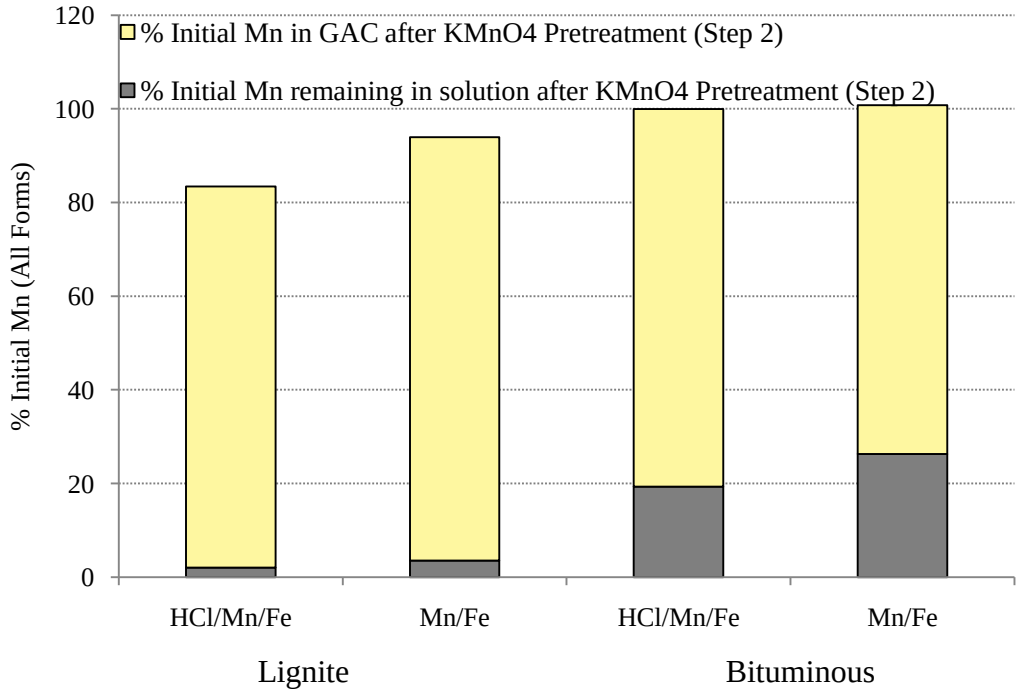

Figure 21. Retention of Mn by the GAC after Step 2 ($KMnO_4$ pretreatment). Results are for Mn in all oxidation states.

Figure 21 illustrates the interaction between the GACs and Mn from the permanganate solution in Step 2 of the synthesis. The lignite GAC retained most of the Mn inside the GAC at the end of Step 2 (> 80% initial Mn retained with and without the HCl pretreatment). The bituminous GAC retained a little bit less for both treatments (between 70 – 80% initial Mn retained). These results indicate that HCl pretreatment had very little effect on the Mn retention by the GAC.

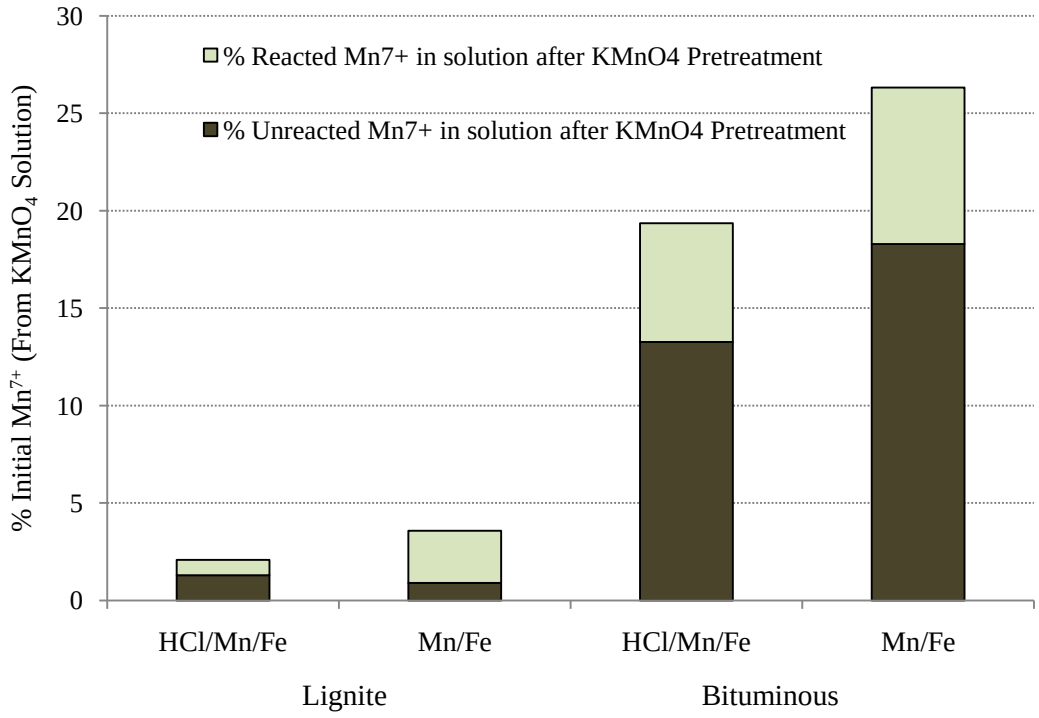

Figure 22. Percent of reacted and unreacted permanganate in solution after Step 2.

A difference in the bituminous and lignite surface reactivity is indicated by the fraction of unreacted permanganate ion remaining in solution following the permanganate pre-treatment in Step 2 of the synthesis (Figure 22). Less than 1.5 % of the initial permanganate remains unreacted (as Mn^{7+}) after contact with the lignite GAC (0.9% and 1.3% with and without the HCl wash step, respectively). Approximately the same amount of reacted permanganate (Mn other than Mn^{7+}) was also in solution. In contrast, the fraction of unreacted permanganate that remained in solution after contact with the bituminous GAC was significantly higher (13.3 and 18.3% for with and without the HCl wash step, respectively). A

greater amount of the reacted permanganate ion was also found in solution (6 – 8%).

These results indicate that the lignite GAC was better able to react with and retain the permanganate than the bituminous GAC and are interesting because they correspond to the final iron content in the Fe-GAC suggesting that Mn loading during the permanganate treatment determines the final iron content in the Fe-GAC.

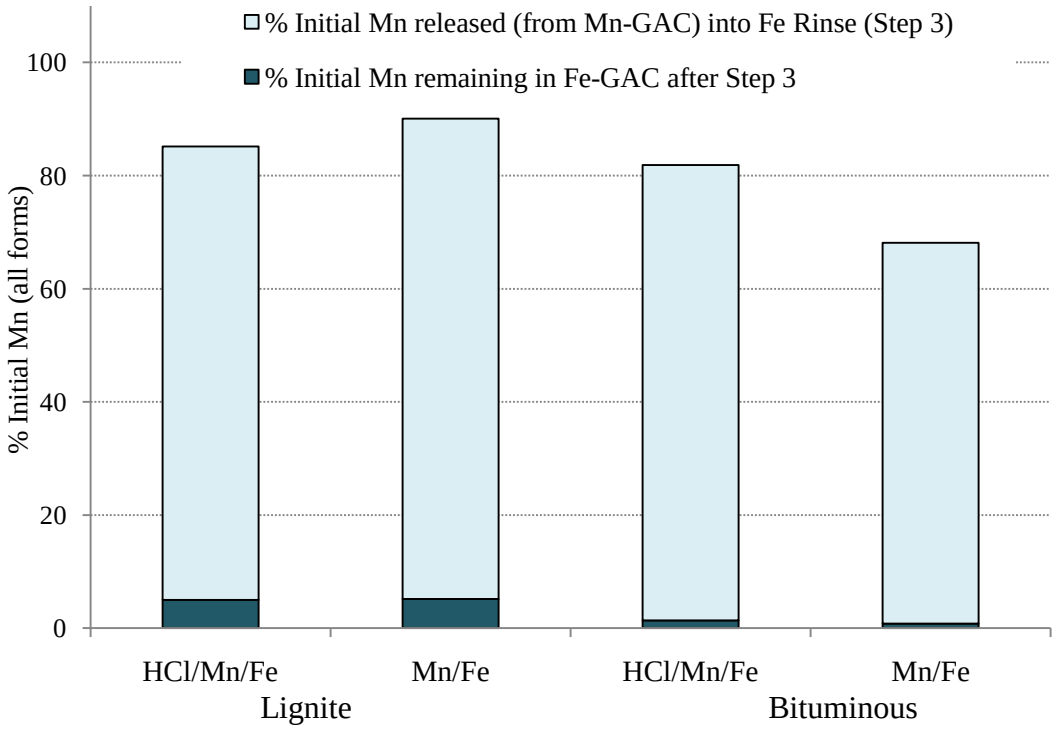

Figure 23. Fraction of initial Mn in solution and GAC following Step 3 ($FeSO_4$ reaction).

Nearly all of the Mn retained by the lignite-based media was released during the $FeSO_4$ reaction in Step 3 (Figure 23). This is important, because

permanganate is a problem contaminant for drinking water. Manganese content in the Fe-GAC synthesized using the permanganate treatment step (HCl/Mn/Fe and Mn/Fe) ranged from 0.1 to 0.7% by weight and was lower for the bituminous-based media (Table 5). This was judged to be acceptable and should not pose a problem for drinking water supplies.

Mn content in Mn-GAC. Further evidence that Mn plays a significant role in preparing the GAC for Fe deposition is provided in the SEM micrographs and elemental line scans of the Mn-GAC samples extracted between Steps 2 and 3 of the synthesis (Figures 24 and 25). Here it can be seen that the location of Mn in the intermediate Mn-GAC coincides with the presence of Fe in the final Fe-GAC. In the lignite Mn-GAC (Figure 24), the presence of Mn is apparent in the outer edges of the particle and in the larger pores and crevices where the permanganate solution could have easily penetrated. This matches the Fe deposition pattern exhibited in Figure 11 for the lignite Fe-GAC synthesized by the same method (HCl/Mn/Fe). However, in the bituminous Mn-GAC shown in Figure 25 (synthesized by the Mn/Fe method), the Mn presence is only seen in the outer edges and does not seem to have penetrated further into the particle. This is the pattern seen in the bituminous Fe-GAC synthesized in the same way (Figure 10). Further evidence of the location of Mn in the Mn-GAC coinciding with the location of Fe in the Fe-GAC can be seen in the additional SEM/EDX images included in Figures C11 through C15 of the appendix.

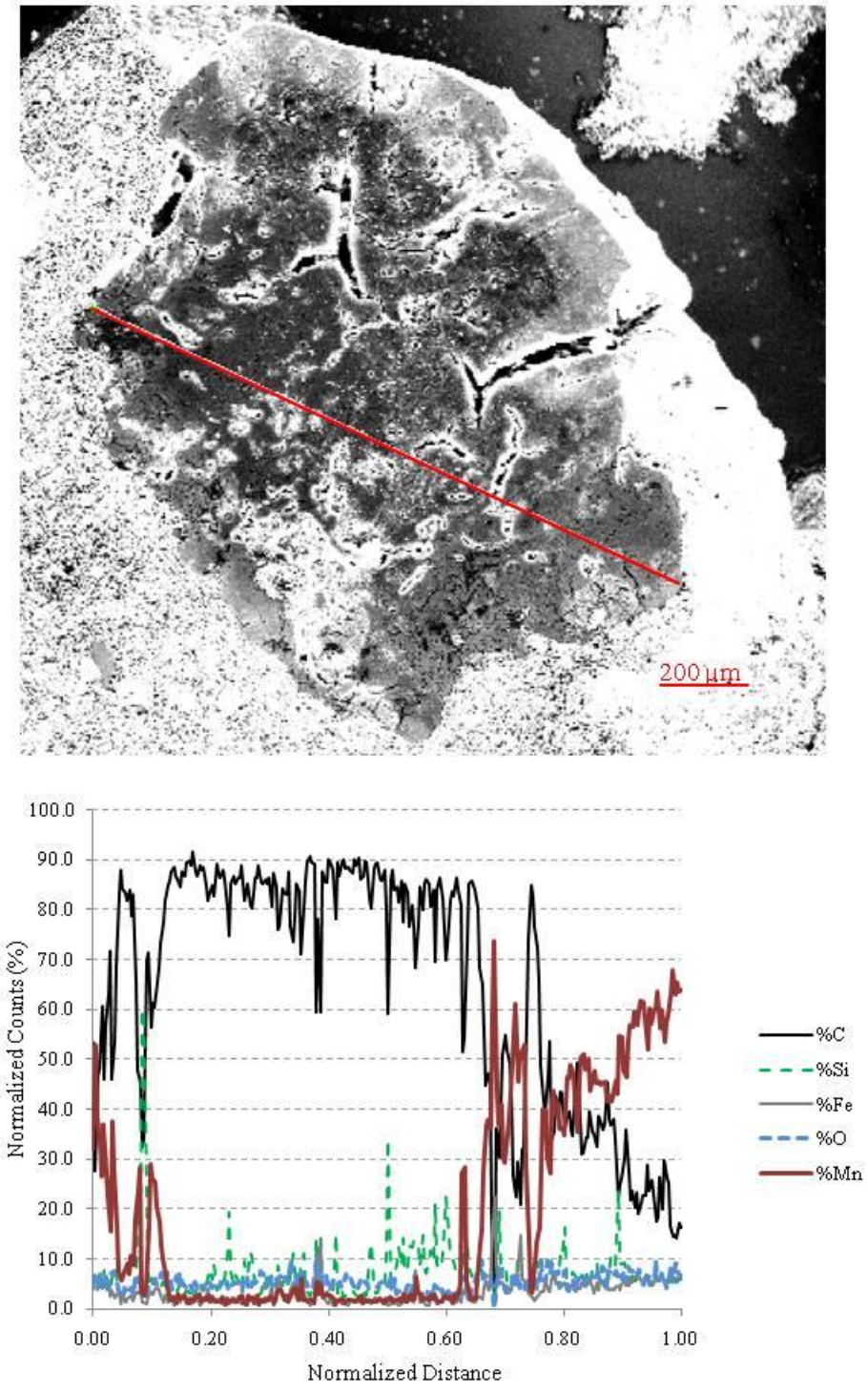

Figure 24. SEM image/EDX line scan of lignite Mn-GAC via HCl/Mn/Fe.

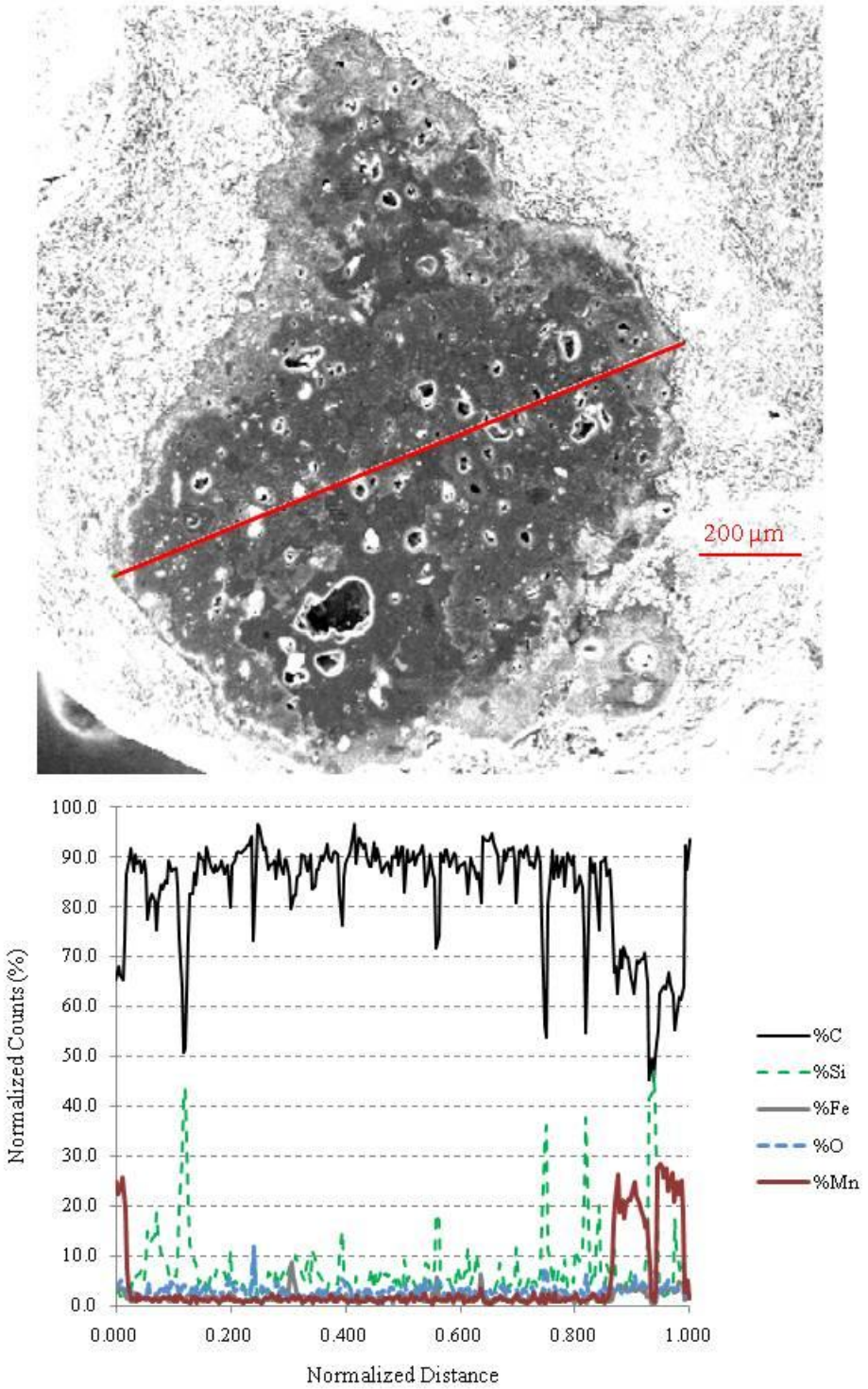

Figure 25. SEM image/EDX line scan of bituminous Mn-GAC from Mn/Fe.

The manganese distribution patterns in the Mn-GAC are interesting because they tend to coincide with the distribution patterns of Fe in the Fe-GAC and imply that iron (hydr)oxide is primarily deposited on surfaces that have interacted with the permanganate solution, another indication that;

1. The permanganate treatment step is critical as it controls the formation and location of iron (hydr)oxide nanoparticles in the Fe-GAC.
2. The ability of the permanganate solution to penetrate the GAC pores and interact with the surface is critical to iron deposition in the Fe-GAC.
3. The permanganate solution is better able to penetrate into the GAC pores and be retained by the lignite than the bituminous media due to differences in the porosity and surface chemistry of the two media.

One explanation for the differences in the ability of the GACs to react with and retain permanganate is that the permanganate solution is more readily able to access and penetrate the inner pores of the lignite media due to its greater fraction of macro and meso pores. Another explanation is that, in the lignite GAC, the permanganate was reduced to a less soluble species, such as Mn^{4+} (e.g. as MnO_2), and so was better retained inside the intermediate Mn-GAC particles. In the bituminous media, the manganese remained as the more soluble Mn^{7+} (as MnO_4^-) which was more easily washed away during the rinse in Step 2.

This latter theory is based on the evidence that, for both methods using a permanganate step, a substantially higher percentage of the initial permanganate solution remained as unreacted MnO_4^- in the rinse from the bituminous, than in

the rinse from the lignite GAC (Figure 22, also Table B6). Between 0.9 and 1.3% of the initial permanganate remained unreacted following interaction with lignite GAC. However, 13 to 18% of the initial permanganate remained in the rinse solution as unreacted permanganate following reaction with the bituminous media.

This suggests that permanganate, a strong oxidizer, is more reactive with the lignite than the bituminous surface. This seems a reasonable explanation as lignite coal is derived from sources closer to the surface and therefore tends to have a more oxidized surface than bituminous which is derived from sources deeper in the earth (Buecker, 2006; Lopez-Ramon, Moreno-Castilla, & Rivera-Utrilla, 1993). It is also reasonable that partially oxidized surfaces, with more oxygen-containing functional groups (like those seen in lignite GAC) can be further oxidized more easily than surfaces that have not been partially oxidized.

Results of XRD analysis – Further evidence of the role of Mn. Further support for the formation of different intermediate manganese species is provided by the XRD data, which is presented in Figure 26. Results are shown for the virgin GAC and for the intermediate Mn-GAC (from the Mn/Fe method only). XRD was not performed on the Mn-GAC from the HCl/Mn/Fe method due to expense and instrument availability. The background has been subtracted and the results plotted using CrystalSleuth software (Laetsch, T., & Downs, R. T., 2006; RRUFF Project, 2006). The spectrum for SiO_2 is included on the bottom for comparison.

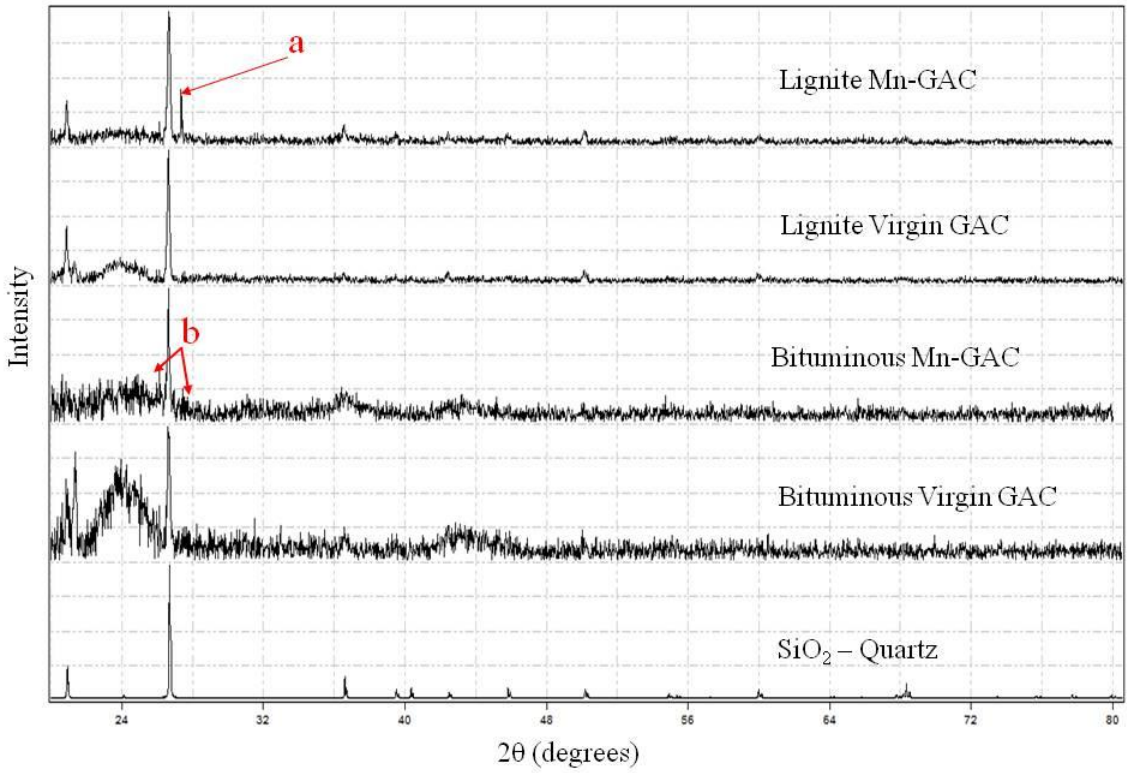

Figure 26. XRD spectra for virgin and Mn-GAC. Peaks a and b suggest the presence of MnO_2 and MnO_4^- respectively.

A very strong peak can be seen at 27.3 two-theta degrees in the lignite Mn-GAC (denoted by red arrow "a") that is not due to the base GAC and is not present in the bituminous Mn-GAC. This strong peak plus the absence of any other strong peaks suggest the presence of MnO_2 species, such as pyrolusite (Kim, Dixon, Chusuei, & Deng, 2002). For the bituminous GAC, two low intensity peaks are suggested at 24.9 and 27.7 two-theta degrees (denoted by red arrows "b"), suggesting the presence of permanganate. However the very low percentage of manganese relative to the amount of silica and carbon in the samples make it

difficult to clearly identify these peaks and these findings require additional support.

The differences in the XRD spectra of the lignite and bituminous Mn-GAC suggest that the formation of the iron (hydr)oxide (as FeOOH) nanoparticles in the two base GAC-types may involve different intermediate steps. Based on the interpretation of the existing XRD spectra, the formation of FeOOH could be described by either Equation 18 or 19, depending on the base media (Lide, 2003; Navrotsky, Mazeina, & Majzlan, 2008; Parc, Nahon, Tardy, & Viellard, 1989; Albert 1969):

$$6H_2O + 5Fe^{2+} + MnO_4^- \rightarrow 5FeOOH\downarrow + 7H^+ + Mn^{2+} \quad \Delta G_0^f = -416.8 \text{ kJ/mol} \quad (18)$$

$$2H_2O + 2Fe^{2+} + MnO_2 \rightarrow 2FeOOH\downarrow + 2H^+ + Mn^{2+} \quad \Delta G_0^f = -112.2 \text{ kJ/mol} \quad (19)$$

It is more likely that, in the bituminous media, FeOOH formation is occurring via the path described in Equation 18, which involves the permanganate ion. However, inside the lignite GAC, FeOOH formation is likely following the path described by Equation 19, which involves MnO_2. The negative Gibbs free energies indicate that both of these mechanisms are thermodynamically favorable under standard conditions. It is likely that other oxidized manganese species in addition to those shown in Equations 18 and 19 are involved to some extent; however, due to their low intensity, the XRD peaks could not provide any additional information.

Isotherm Testing

Arsenic adsorption capacity. The results of batch equilibrium experiments used to evaluate the media's capacity for arsenic removal are summarized in Table 8. As expected, neither of the virgin carbons showed any capacity for arsenic removal, and arsenic adsorption was improved in all of the Fe-GACs over that of the virgin media indicating that arsenic adsorption capability was due to the presence of FeOOH. For this reason, correlation values for the virgin media were low and their isotherms are not included in the charts in the appendix.

In general, the bituminous based Fe-GAC performed better than did the lignite at the lower pH range (pH = 7.2 ± 0.1). Freundlich adsorption capacity parameters (K_a) were higher (indicating greater arsenic adsorption capacity) for the bituminous based Fe-GAC than for the lignite Fe-GAC made by the same method. In this same pH range, Freundlich adsorption intensity parameters were generally favorable ($1/n \leq 1$) for the bituminous media and unfavorable for the lignite Fe-GAC ($1/n \geq 1$). The exception to this was the lignite Fe-GAC synthesized using the HCl/Mn/Fe method which had 1/n = 0.6 indicating favorable adsorption. For both GAC types, Fe-GAC synthesized using the acid wash step performed better than the Fe-GAC synthesized using other methods, perhaps due to functional groups remaining inside the media pores.

With the exception of the bituminous Fe-GAC synthesized using the Fe Only method, Freundlich adsorption capacity was reduced by orders of magnitude at the higher pH range (pH = 8.0 ± 0.1). Results for the bituminous-Fe Only media were anomalous and showed an improvement in performance at the lower pH range. One possible explanation could be that this media showed the lowest loss in surface area and may represent the optimal tradeoff between iron content and surface area reduction.

Table 8.

Estimates of Freundlich adsorption parameters for arsenic

pH = 7.2 ± 0.1	Lignite				Bituminous			
Treatment	K_a	K_a*	1/n	R^2	K_a	K_a*	1/n	R^2
HCl/Mn/Fe	72.6	543	0.6	0.96	31.5	342	0.7	0.92
Mn/Fe	3.7	30.2	1.3	0.96	8.6	101	0.9	0.90
Fe Only	2.0	37.0	1.5	0.93	20.3	572	0.9	0.94
Untreated	0.15	101	1.6	0.01	2.7	1561	0.9	0.00

pH = 8.0 ± 0.1	Lignite				Bituminous			
Treatment	K_a	K_a*	1/n	R^2	K_a	K_a*	1/n	R^2
HCl/Mn/Fe	6×10^{-14}	5×10^{-13}	8.3	0.89	4×10^{-9}	4×10^{-8}	5.4	0.92
Mn/Fe	0.80	6.62	1.5	0.92	6×10^{-6}	7×10^{-5}	3.9	0.94
Fe Only	1×10^{-5}	3×10^{-4}	4.2	0.91	106	2994	0.5	0.94
Untreated	4×10^{-4}	0.27	2.7	0.03	3×10^{-3}	1.51	2.5	0.64

Note: $K_a = (\mu g\text{-As/g-GAC})(L/\mu g\text{-As})^{1/n}$; $K_a^* = (\mu g\text{-As/g-Fe})(L/\mu g\text{-As})^{1/n}$

In general, the Fe-GACs performed better at the lower pH range than at the higher range. For ions like arsenate and arsenite, unfavorable adsorption could be the result of an electrostatic repulsion between the negatively charged $H_2AsO_4^-$ and $HAsO_4^{2-}$ species (pKa = 6.8) and the negatively charged surfaces of the media, which dominate at this pH range for both GAC types. Results from zeta potential measurements indicate that at pH = 7.0, surface charge for the lignite Fe-GACs was approximately -25 eV (Figure 19) and for the bituminous Fe-GACs approximately -15 eV (Figure 20). The surface charge becomes increasingly negative at the higher pH of 8.0 for all Fe-GACs, corresponding to the increasingly unfavorable adsorption capacity at this pH.

Another possibility is that the unfavorable adsorption parameters are due to pore clogging as a result of FeOOH nanoparticle formation, with the problem increasing with higher iron loading. This is supported by a greater decrease in pore availability in the meso and macro pore range of the lignite media (Figure 18) seen in the pore size distribution results. These are the same macropores that would be used to access the smaller micropores in the media, and if they are blocked it is reasonable to expect higher intensity parameters as competition for the remaining available adsorption sites is increased.

Freundlich adsorption parameters were lower than those previously reported for similar media made using the Mn/Fe method. Hristovski et.al. (2009) reported Freundlich adsorption capacity parameters of K_a^* = 2,643 and 294 (µg-As/g-Fe)/(µg-As/L)$^{1/n}$ for pH = 6.4 ± 0.1 and pH = 8.3 ± 0.1, respectively for Fe-

GAC synthesized under similar conditions (0.1 N KMnO4 and 15 minutes reaction time). (Hristovski et al., 2009). Values for 1/n were estimated at 0.41 and 0.62 for the lower and higher pH ranges, both indicating favorable adsorption conditions (Hristovski et al., 2009). This is interesting, as the base media used to synthesize the Fe-GAC was different than the ones used in the present experiment and could be another example of the effect that the base media has on the overall adsorption performance of the synthesized media.

When the Fe-GAC from this experiment was compared with arsenic removal by commercially available GFH, the GFH performed better under similar conditions. Assuming an iron content of 62% for GFH, Badruzzaman et. al. (2004) report $K_a^* = 6{,}365$ (µg-As/g-Fe)(L/µg-As) and 1/n = 0.3 at pH = 7.0 ± 0.02 in a 250 mg/L $NaHCO_3$ solution (3 mM/L). Their value is similar to those reported in similar studies of GFH (for example Driehaus, Srith & Jekel, 1998). Reaction times used in the batch testing of the Badruzzaman study was considerably longer (18 days) than the three days used in the current study and could account for some of the performance difference. However, the advantage of Fe-GAC is its ability to simultaneously remove arsenate and organic contaminants, whereas the commercially available GFH is only able to remove arsenate.

TCE adsorption capacity. The results of batch isotherm testing for TCE adsorption capacity are summarized in Table 9. Data and charts used for these estimates are included in Appendix F. The Freundlich adsorption capacity and

intensity parameters for the untreated lignite and bituminous GACs were very similar, indicating that both had similar TCE adsorption capability before impregnation with FeOOH (Table 9). As was expected, TCE adsorption capacity was reduced in the Fe-GAC when compared to the corresponding virgin media. The exception to this was the bituminous Fe-GAC synthesized using Fe Only, which showed improvement over the untreated bituminous GAC.

Table 9.

Estimates of Freundlich adsorption parameters for TCE

	Lignite			Bituminous		
Method	K_a	1/n	R^2	K_a	1/n	R^2
HCl/Mn/Fe	0.08	4.47	0.52	4.34	1.02	0.92
Mn/ Fe	18.1	0.95	0.90	4.43	1.72	0.95
Fe Only	30.8	1.22	0.95	76.7	0.56	0.66
Untreated	14.5	0.87	0.95	17.0	0.70	0.81

Notes: K_a = (mg-TCE/g-GAC)(L/mg-TCE)$^{1/n}$

With one exception, for the lignite-based media the Freundlich adsorption capacity and intensity parameters (K_a and 1/n, respectively) for TCE were similar before and after iron impregnation suggesting that that the synthesis method did not adversely affect the TCE adsorption capacity of this media (Table 9). The exception to this was the lignite Fe-GAC synthesized by the HCl/Mn/Fe method, which had considerably less favorable Freundlich adsorption and intensity parameters as compared to the virgin GAC.

However, for the bituminous media, Freundlich adsorption capacity parameter was decreased by a factor of four following iron impregnation using the permanganate pretreatment step (HCl/Mn/Fe and Mn/Fe). For these same media, 1/n increased significantly, from the favorable 1/n = 0.7 for the virgin GAC to the increasingly unfavorable 1/n = 1.0 and 1.7 (Mn/Fe and HCl/Mn/Fe respectively). Values of K_a and 1/n for the (low iron content) bituminous Fe-GAC synthesized using Fe Only were similar to those of the virgin media and appear to indicate favorable conditions for TCE adsorption.

In general, TCE adsorption capacity appears to be reduced by increasing iron content in the media. This is not surprising. The deposition of FeOOH nanoparticles onto the GAC surface converts TCE adsorption sites to arsenic adsorption sites, which are no longer available for adsorbing TCE. A reduction in available adsorption sites for TCE increases the competition for the remaining sites, resulting in higher adsorption intensity parameters and a reduction in TCE adsorption capacity. This is observed in the higher Freundlich intensity parameters for the Fe-GAC.

The availability of TCE adsorption sites is further reduced as the smaller micropores in the media are rendered inaccessible due to pore clogging by the formation and deposition of iron (hydr)oxide nanoparticles, leading to an increase in competition and higher adsorption energies. In spite of the reduction in TCE adsorption sites, it appears that, due to their high surface areas, both the lignite and bituminous Fe-GAC should retain TCE adsorption capacity after iron

(hydr)oxide impregnation and that this media would remain effective in its capacity to remove organic contaminants.

Detailed TCE isotherm data is included in Appendix F. Solvent loss through evaporation was the greatest source of experimental error in evaluating TCE adsorption capacity as the volatile nature of TCE made working with this contaminant problematic. This resulted in lower than expected correlation ($R^2 <$ 0.90) for some of the isotherms.

CHAPTER FIVE – CONCLUSIONS & RECOMMENDATIONS

While hybrid adsorbent media may offer a viable solution to the problem of simultaneously removing multiple contaminants with different chemistries from water; an increase in the media's removal capacity for one contaminant may come at the expense of a reduction in the removal capacity for another. In this study, the synthesis of iron (hydr)oxide nanoparticles may have resulted in a hybrid Fe-GAC media with improved arsenic removal capabilities while seriously reducing the organic co-contaminant removal capacity of the underlying GAC. This tradeoff may be controlled by several factors; however the type and properties of the virgin GAC, which are directly related to the properties and variability of the coal used as a raw material in its manufacture, appear to play the most important role in the overall contaminant removal capability of the resulting hybrid Fe-GAC media. Even though new pores and adsorption sites are created in the Fe-GAC as a result of iron (hydr)oxide nanoparticle impregnation, they may have different chemistries as a result of the use of strong oxidizers or different reaction mechanisms used during the FeOOH deposition process. As a result of these different chemistries, the pores and surface sites may have reduced ability to adsorb organic co-contaminants. Additionally, iron (hydr)oxide nanoparticles could block the existing micropores and limit access to the remaining surface adsorption sites capable of adsorbing organics. These adsorption-restricting processes may be more prevalent in microporous GAC media. In the specific example of this study, the more microporous bituminous GAC resulted in Fe-

GAC with poor TCE removal capability as compared to the ability of the more macroporous lignite-based media. Additionally, the arsenic removal ability of the lignite-based Fe-GAC was better than that of the bituminous-based Fe-GAC, implying that, when synthesizing Fe-GAC using the methods employed in this study (i.e. permanganate/$FeSO_4$), a more macroporous GAC may make a better base media and minimize the effects of this tradeoff.

The results of this study clearly show that synthesizing a hybrid media by impregnating a GAC with metal (hydr)oxide has much greater implications for the media's overall contaminant removal capability than merely improving its arsenic removal capacity. As seen in this study, the nanoparticle impregnation can result in changes in the media's properties, which could consequently reduce its ability to remove other non-competing contaminants. Therefore, when engineering nanoparticle-containing hybrid media for removal of arsenic and co-contaminants, it is important to examine how each step of the "hybridization" process, and the properties of the underlying base media, affects the overall performance of the new hybrid media.

Recommendations for future research

This study specifically focused on the effect that differences in the properties of lignite and bituminous carbon had on the synthesized Fe-GAC and its ability to simultaneously remove arsenic and the organic co-contaminant TCE. However while carrying out this research, new questions were raised. Future

research needs to be conducted to answer these questions and better understand how the conclusions of this research apply to the broader field of the development of nanomaterials for contaminant removal. The following are some of my recommendations for future research:

- Re-examine the Fe-GAC synthesized in this experiment using a less volatile model organic co-contaminant. Solvent loss through evaporation of the TCE, was problematic and made it difficult to definitively determine how severely the organic co-contaminant removal capacity of the media was diminished in the Fe-GAC. A less volatile model organic co-contaminant would allow a more accurate quantitative assessment..
- Re-examine the Fe-GAC used in this study with a water model containing different types of background contaminant ions to examine how base media affects competitive adsorption in the Fe-GAC.
- Investigate how MnO_2 influences nanoparticles precipitation by synthesizing Fe-GAC (via Mn/Fe and Fe Only methods) in an oxygen free environment. Does iron (hydr)oxide precipitation occur in the absence of oxygen?
- Synthesize Fe-GAC from other base carbon materials, for example from anthracite or coconut shells, to determine how their properties (surface chemistry, pore size distribution) affect the Fe-GAC and its contaminant removal capacity. Examining a broader range of carbons with different

chemistries and porosities will provide a better understanding how these differences affect the synthesized media.

- Determine whether the results of this study are true for iron (hydr)oxide impregnated media synthesized from lignite and bituminous carbons in other forms, for example activated carbon fibers or powdered activated carbon.
- Use a higher strength acid solution to wash the GAC prior to permanganate treatment. In this study, soaking the GAC in HCl did not substantially increase iron content in the Fe-GAC, however this could be due to the low concentration used.
- Study the differences in Mn species retained in the Mn-GAC to confirm the reaction mechanisms proposed by this research. Extended X-ray fine structure spectroscopy (EXAFS) or EDAX mapping of the entire cross-sectioned Mn-GAC particle can be used to examine the location and ratio of Mn and O across the particle to better understand the reaction mechanisms involved.
- Explore the effects of base carbon on Fe-GAC synthesized by other methods to gain a broader understanding of the interactions of base carbon properties and synthesis method on the Fe-GAC.
- Impregnate lignite and bituminous GAC with other nanomaterials, for example zirconium, to determine how the GAC properties affect other types of hybrid media.

REFERENCES

Agency for Toxic Substances and Disease Registry. (2001, January). *Case studies in environmental medicine: Trichloroethylene (TCE) toxicity* (Case Study Monograph ATSDR-HE-CS-2002-0004). Retrieved from ATSDR Website: www.atsdr.cdc.gov/HEC/CSEM/

Agency for Toxic Substances and Disease Registry. (2005). *ToxFAQs for trichloroethylene* [Fact sheet]. Retrieved from http://www.atsdr.cdc.gov/tfacts19.html

Albers, P., Deller, K., Despeyroux, B. M., Prescher, G., Schafer, A., & Seibold, K. (1994). SIMS/XPS investigations on activated carbon catalyst supports. *Journal of Catalysis, 150,* 368-375.

Albert, R. A. (1969, June 25). Standard Gibbs free energy, enthalpy, and entropy changes as a function of pH and pMg for several reactions involving adenosine phosphates. *Journal of Biological Chemistry, 244*(12), 3290-3302. Retrieved from www.jbc.org

Altundogan, H. S., Altundogan, S., Tuemen, F., & Bildik, M. (2000). Arsenic removal from aqueous solutions by adsorption on red mud. *Waste Management,* 20, 761-767.

Amirtharajah, A., & O'Melia, C. R. (1999). *Water quality and treatment* (5th ed.). Denver, CO: American Water Works Association.

Arizona Department of Environmental Quality (2004, April). *Site registry report (final) - Water Quality Assurance Revolving Fund site, 56th Street and Earl Drive, Phoenix, Maricopa county, Arizona*. Retrieved from ADEQ Superfund/WQARF Registry website: http://www.azdeq.gov/environ/waste/sps/phxsites.html

Arizona Department of Environmental Quality. (n.d.). *Site registry report for the West Central Phoenix East Grand Avenue site* (West Central Phoenix Water Quality Assurance Fund). Phoenix, AZ: Arizona Department of Environmental Quality.

Axe, L., & Trivedi, P. (2002). Intraparticle surface diffusion of metal contaminants and their attenuation in microporous amorphous Al, Fe, and Mn oxides. *Journal of Colloid and Interface Science, 247,* 259-265. doi: 10.1006/jcis.2001.8125

Badruzzaman, M., & Westerhoff, P. K. (2004). Intraparticle diffusion and adsorption of arsenate onto granular ferric hydroxide (GFH). *Water Research*, *38*(18), 4002-4012.

Bayer, P., & Finkel, M. (2005). Modeling of sequential groundwater treatment with zero valent iron and granular activated carbon. *Journal of Contaminant Hydrology, 78*, 129-146.

Bedient, P. B., Rifai, H. S., & Newell, C. J. (1999). *Groundwater Contamination: Transport and Remediation* (2nd ed.). New Jersey: Prentice Hall.

Brunauer, S., Emmett, P. H., & Teller, E. (1938, February). Adsorption of gases in multimolecular layers. *Journal of the American Chemical Society*, *60*(2), 309-313. doi: 10.1021/ja01269a023

Buecker, B. (2006, November). Coal: What your parents never taught you. *Power Engineering*, 104-114.

Carlson, L., Bigham, J. M., Schwertmann, U., Kyek, A., & Wagner, F. (2002). Scavenging arsenic from acid mine drainage by schwertnite and ferrihydrite: A comparison with synthetic analogues. *Environmental Science and Technology, 36*, 1712-1719.

Carter, M. C., & Weber, W. J., Jr. (1994). Modeling adsorption of TCE by activated carbon preloaded by background organic matter. *Environmental Science and Technology, 28*, 614 - 623.

Carus Chemical Company (2004, January). *Analytic method 102: Determination of Cairox potassium permanganate residual for drinking water treatment*. Retrieved from Carus Chemical Corporate Website: www.caruschem.com

Chakravarty, S., Dureja, V., Bhattacharyya, G., Maity, S., & Bhattacharjee, S. (2002). Removal of arsenic from groundwater using low cost ferruginous manganese ore. *Water Research, 36*, 625-632.

Chen, J. P., & Lin, M. (2001). Equilibrium and kinetics of metal ion adsorption onto a commercial H-type granular activated carbon: Experimental and modeling studies. *Water Research*, *35*(10), 2385-2394.

Chen, J. P., & Wang, L. (2004). Characterization of metal adsorption kinetic properties in batch and fixed-bed reactors. *Chemosphere, 54*, 397-404.

Chen, W., Parette, R., & Cannon, F. S. (2008). Arsenic adsorption via iron-preloaded activated carbon and zero-valent iron. *Journal of the American Water Works Association*, *100*(8), 96 - 105.

Christophi, C.A.; & Axe, L. (2000). Competition of Cd, Cu, and Pb adsorption on goethite. *Journal of Environmental Engineering, 121*(1), 66-74.

Chuang, C. L., Fan, M., Xu, M., Brown, R. C., Sung, S., & Saha, B. (2005,). Adsorption of arsenic(V) by activated carbon prepared from oat hulls. *Chemosphere*, *61*, 478-483.

Crittenden, J. C., Trussell, R. R., Hand, D. W., Howe, K. J., & Tchobanoglous, G. (2005). *Water treatment: Principles and practice* (2nd ed.). Hoboken, NJ: John Wiley and Sons.

Coughlin, B., & Stone, A. T. (1995). Nonreversible adsorption ofdivalent metal ions [Mn(II), Co(II), Ni(II), Cu(II), and Pb(II)] onto goethite: Effects of acidification, Fell addition, and picolinic acid additions. *Environmental Science and Technology, 29*, 2445-2455.

Dastgheib, S. A., Karanfil, T., & Cheng, W. (2004). Tailoring activated carbons for enhanced removal of natural organic matter from natural waters. *Carbon*, *42*, 547-557. doi: 10.1016/j.carbon.2003.12.062

Daus, B., Wennrich, R., & Weiss, H. (2004). Sorption materials for arsenic removal from water: A comparative study. *Water Research*, *38*, 2948-2954.

De Laeter, J. R., Bohlke, J. K., De Bievre, P., Hidaka, H., Pieser, H. S., Rosman, K. J., & Taylor, P. D. (2003). Atomic weights of the elements. Review 2000 . *Pure and Applied Chemistry*, *75*(6), 683-800. doi: 10.1351/pac200375060683

Deliyanni, E. A., Bakoyannakis, D. N., Zouboulis, A. I., & Matis, K. A. (2003). Sorption of As(V) ions by akaganeite-type nanocrystals. *Chemosphere, 50*, 155-163.

Dong, L., Zini, P. V., Cowen, J. P., & Ming, L. C. (2009). Iron coated pottery granules for arsenic removal from water. *Journal of Hazardous Materials*, *168*, 626-632.

Driehaus, W., Jekel, M., Hildebrandt, U. (1998). Granular ferric hydroxide – A new adsorbent for the removal of arsenic from natural water. *Journal of Water Supply: Research and Technology*, *47*(1), 30 – 35.

Driehaus, W., Srith, R., & Jekel, M. (1994). Oxidation of arsenate(III) with manganese oxides in water treatment. *Water Research, 29*(1), 279-305.

Dubinin, M. M. (1989). Fundamentals of the theory of adsorption in micropores of carbon adsorbents: Characteristics of their adsorption properties and micro porous structures. *Pure & Applied Chemistry, 61*(11), 1841-1843.

Edwards, M. A. (1994, September). Chemistry of arsenic removal during coagulation and Fe-Mn oxidation. *Journal of the American Water Works Association*, 64-77.

Farrell, J. (2002, May/June). Assessing arsenic removal technologies. *Southwest Hydrology*, 20-22.

Fitts, C. R. (2002). *Groundwater Science*. San Diego, CA: Academic Press.

Florea, A., Yamaha, E. N., & Dopp, E. (2005). Intracellular calcium disturbances induced by arsenic and its methylated derivatives in relation to genomic damage and apoptosis induction. *Environmental Health Perspectives, 113*(6), 659-664.

Franson, M. A., Eaton, A. D., Clescri, L. S., & Greenberg, A. E. (Eds.). (1995). *Standard methods for the examination of water and wastewater* (19th ed.). Washington, DC: American Public Health Association.

Frazer, L. (2005, June). Metal attraction: An ironclad solution to arsenic contamination. *Environmental Health Perspectives, 113*(6), 398-401.

Gu, Z., Fang, J., & Deng, B. (2005). Preparation and evaluation of GAC-based iron-containing adsorbents for arsenic removal. *Environmental Science and Technology, 39*, 3833-3843.

Hayes, K. F., Papelis, C., & Leckie, J. O. (1988). Modeling ionic strength effects on anion adsorption at hydrous oxide/solution interfaces. *Environmental Engineering and Science, 125*(2), 717-726.

Hingston, F. J., Atkinson, R. J., Posner, A. M., & Quirk, J. P. (1967). Specific adsorption of anions. *Nature, (215)*, 1459-1461.

Hristovski, K. D., Baumgardner, A., & Westerhoff, P. K. (2007). Selecting metal oxide nanomaterials for arsenic removal in fixed-bed columns: From nanopowders to aggregated nanoparticle media. *Journal of Hazardous Materials, 147*, 265-274. doi: 10.1016/j.hazmat.2007.01.017

Hristovski, K. D., Ngyuen, H. P., & Westerhoff, P. K. (2009). Removal of arsenate and 17 a-ethinyl estradiol (EE2) by iron (hydr)oxide modified activated carbon fibers. *Journal of Environmental Science and Health Part A, 44*, 354-361. doi: 10.1080/10934520802659695

Hristovski, K. D., Westerhoff, P. K., Crittenden, J., & Olson, L. (2008). Arsenate removal by iron (hydr)oxide modified granulated activated carbon: Modeling arsenate breakthrough with the pore surface diffusion model. *Separation Science and Technology, 43,* 3154-3167.

Hristovski, K. D., Westerhoff, P. K., Moller, T., & Sylvester, P. (2009). Effect of synthesis conditions on nano-iron (hydr)oxide impregnated granular activated carbon. *Chemical Engineering Journal*, *146,* 237-243. doi: 10.1016/j.cej.2008

Hristovski, K., Westerhoff, P., & Crittenden, J. (2008). An approach for evaluating nanomaterials for use as packed bed adsorber media: A case study of arsenate removal by titanate nanofibers. *Journal of Hazardous Materials*, *156*, 604 - 611.

Hristovski, K., Westerhoff, P., Moller, T., Sylvester, P., Condit, W., & Mash, H. (2008). Simultaneous removal of perchlorate and arsenate by ion-exchange media modified with nanostructured iron (hydr)oxide. *Journal of Hazardous Materials*, *152*, 397 - 406.

International Agency for Research On Cancer. (2008). *IARC Monographs on the evaluation of carcinogenic risks to humans: Group 1 carcinogenic to humans* [Fact sheet]. Retrieved from http://monographs.iarc.fr/ENG/Classification/crthgr01.php

Ishikazi, C., & Marty, I. (1981). Surface oxide structures on a commercial activated carbon. *Carbon*, 19(6), 410-412.

Jain, A., Raven, K. P., & Loeppert, R. H. (1999). Arsenate and arsenite adsorption ferrihydrite: Surface charge reduction and net OH- release stoichiometry. *Environmental Science and Technology*, *33,* 1179-1184.

Johnson, D. L. (1972, November 3). Bacterial reduction of arsenate in seawater. *Nature*, *240*, 44-45.

Kabata-Pendias, A., & Pendias, H. (2001). *Trace elements in soils and plants* (3rd ed.). [Google Books]. doi: ISBN-0-84931

Karanfil, T., & Dastgheib, S. A. (2004). Trichloroethylene adsorption by fibrous and granular activated carbons: Aqueous phase, gas phase, and water vapor adsorption studies. *Environmental Science and Technology*, *38*, 5834-5841.

Karanfil, T., & Kilduff, J. A. (1999). Role of granular activated carbon surface chemistry on the adsorption of organic compounds. 1. Priority pollutants. *Environmental Science and Technology*, *33*(18), 3217-3224.

Karanfil, T., Kitis, M., Kilduff, J. E., & Wigton, A. (1999). Role of granular activated carbon surface chemistry on adsorption of organic contaminants: 2. Natural organic matter. *Environmental Science and Technology*, *33*, 3225-3233. doi: 10.1021/es9810179

Kartinen, E. O., & Martin, C. J. (1995). An overview of arsenic removal processes. *Desalination*, *103*, 79-88.

Katsoyiannis, I. A., & Zouboulis, A. I. (2002). Removal of arsenic from contaminated water sources by sorption onto iron-oxide-coated polymeric materials. *Water Research*, *36*, 5141-5155.

Kim, J. G., Dixon, J. B., Chusuei, C. C., & Deng, Y. (2002). Oxidation of chromium(III) to (VI) by manganese oxides. *Soli Science of America Journal*, *66*, 306-315.

Klecka, G. M., McDaniel, E. G., Wilson, P. S., Carpenter, C. L., Clark, J. E., Thomas, A., & Spain, J. C. (1996, Summer). Field Evaluation of a granular activated carbon fluidized-bed bioreactor for treatment of chlorobenzene in groundwater. *Environmental Progress*, *15*(2), 93-107.

Korngold, E., Belayev, N., & Aronov, L. (2001). Removal of arsenic from drinking water by anion exchangers. *Desalination*, *141*, 81-84.

Laetsch, T., & Downs, R. T. (2006). CrystalSleuth [Computer software]. http://www.geo.arizona.edu/xtal/group/software.htm

Langer, V., Novakowski, K., & Woodbury, A. (1999). Sorption of trichloroethylene onto stylolites. *Journal of Contaminant Hydrology*, *40*, 1-23.

Larsen, E. H., & Hansen, S. H. (1992), Separation of arsenic species by ion-pair and ion-exchange high performance liquid chromatography. *Mikrochimica Acta*, *109*, 47-51.

LeVan, D. M., Carta, G., & Yon, C. M. (1997). Chapter 16: Adsorption and ion exchange. In R. D. Perry & D. W. Green (Eds.), *Perry's Chemical Engineers' Handboook* (pp. -). New York: McGraw-Hill.

Lee, M. C., Snoeyink, V. L., & Crittenden, J. C. (1981,). Activated carbon adsorption of humic substances. *American Water Works Association*, 81, 440-446.

Lide, D. R. (2003). *CRC Handbook of Chemistry and Physics* (84th ed.). Boca Raton, FL: CRC Press.

Liu, G. J., Zhang, X. R., McWilliams, L., Talley, J. W., & Neal, C. R. (2008). Influence of ionic strength, electrolyte type. and NOM on As(V) adsorption onto TiO_2. *Journal of Environmental Science and Health Part A, 43*, 430-436. doi: 10.1080/10934520701795749.

Liu, Y., Majetich, S. A., Tilton, R. D., Scholl, D. S., & Lowry, G. V. (2005,). TCE dechlorination rates, pathways and efficiency of nanoscale iron particles with different properties. *Environmental Science and Technology*, *39*, 1338 - 1345.

Livesey, N. T., & Huang, P. M. (1981, February). Adsorption of arsenate by soils and its relation to selected chemical properties and anions. *Soil Science, 131*(2), 88-94.

Lopez-Ramon, M. V., Moreno-Castilla, N. C., & Rivera-Utrilla, J. (1993). Activated carbons from a subbituminous coal: Pore texture and electrokinetic properties. *Carbon, 31*(5), 815-819.

Lopez-Ramon, M. V., Stoeckli, F., Moreno-Castilla, C., & Carrasco-Marin, F. (1999). On the characterization of acidic and basic surface sites on carbons by various techniques. *Carbon, 37*, 1215-1221.

Lorenzen, L., Van Deventer, J. S., & Landi, W. M. (1995). Factors affecting the mechanism of the adsorption of arsenic species on activated carbon. *Mineral Engineering, 8*(4/5), 557-569.

Lu, Q., & Sorial, G. A. (2004). The role of adsorbent pore size distribution in multicomponent adsorption on activated carbon. *Carbon, 42*, 3133-3142. doi: 10.1016/jcarbon.2004.07.025

Mandal, B. K., & Suzuki, K. T. (2002). Arsenic round the world: A review. *Talanta, 58*, 201-235.

Manly, B. F. (2001). *Statistics for environmental science and management*. Boca Raton, FL: CRC Press.

Mattigod, S. V., Frampton, J. A., & Lim, C. H. (1985). Effect of ion-pair formation on boron adsorption by kaolinite. *Clays and Clay Minerals, 33*(5), 433-437.

Matis, K. A., Zouboulis, A. I., Zamboulis, D., & Valtadorou, A. V. (1999). Sorption of As(V) by goethite particles and study of their flocculation. *Water, Air, and Soil Pollution, 111*, 297-316.

McNab Jr., W. W., Ruiz, R., & Reinhard, M. (2000). In-situ destruction of chlorinated hydrocarbons in groundwater using catalytic reductive dehalogenation in a reactive well: Testing and operational experiences. *Environmental Science and Technology, 34*, 149-153. doi: 10.1021/es9903936

Mehran, M., Olsen, R. L., & Rector, B. M. (1987, May-June). Distribution coefficient of trichloroethylene in soil-water systems. *Ground Water, 25*(3), 275-282.

Meng, X., Bang, S. B., & Korfiatis, G. P. (2000). Effect of silicate, sulphate and carbonate on arsenic removal by ferric chloride. *Water Research, 34*(4), 1255-1261.

Meng, X., Korfiatis, P. G., Christodoulatos, C., & Bang, S. (2001). Treatment of arsenic in Bangladesh well water using a household co-precipitation and filtration system. *Water Research, 35*(12), 2805-2810.

Micrometrics Instrument Corporation. (2008). *Tristar II 3020: Operator's manual* (V1.02 ed.). Norcross, GA: Author. Retrieved from www.micrometrics.com

Mohan, D., & Pittman, C. U., Jr. (2007). Arsenic removal from water/wastewater using adsorbents - A critical review. *Journal of Hazardous Materials, 142*(1-2), 1-53.

Mondal, P., Balomajumder, C., & Mohanty, B. (2007). A laboratory study for the treatment of arsenic, iron, and manganese bearing ground water using Fe3+ impregnated activated carbon: Effects of shaking time, pH, and temperature. *Journal of Hazardous Materials, 144*, 420-426.

Mondal, P., Majumder, C. B., & Mohanty, B. (2006). Laboratory based approaches for arsenic remediation from contaminated water: Recent developments. *Journal of Hazardous Materials*, *B137*, 464-479.

Navrotsky, A., Mazeina, L., & Majzlan, J. (2008). Size driven structure and thermodynamic complexity in iron oxides. *Science*, *319*, 1635-1638.

Ng, K. S., Ujang, Z., & Le-Clech, P. (2004). Arsenic removal technologies for drinking water treatment. *Reviews in Environmental Science and Biotechnology*, *3*, 43-53.

Norit Americas Inc. (2007). *Norit GAC 1240 datasheet* [Fact sheet]. Retrieved from www.norit-americas.com

Norit Americas Inc. (2007, October). *Understanding activated carbons* (White Paper 00-010-TP). Marshall, TX: Norit Americas .

Norit Americas, Inc. (2007). *Datasheet Darco 12X40 GAC* [Fact sheet]. Retrieved from www.norit-americas.com

Nriagu, J. O., & Azcue, J. M. (1990). Part I: Cycling and characterization. In J. O. Nriagu (Ed.), *Arsenic in the environment* (pp. 1-15). New York: John Wiley and Sons.

Ona-Nguema, G., Morin, G., Juillot, F., Calas, G., & Brown, G. E. (2005). EXAFS analysis of arsenite adsorption onto two-line ferrihydrite, hematite, goethite, and lepridocrocite. *Environmental Science and Technology*, *39*(23), 9147-9155.

Parc, S., Nahon, D., Tardy, Y., & Viellard, P. (1989). Estimated solubility products and fields of stability for cryptomelane, insutite, birnessite, and lithiophorite based on natural lateritic weathering sequences. *American Mineralogist*, *74*, 466-475.

Pattanayak, J., Mondal, K., Matthew, S., & Lalvani, S. B. (2000,). A parametric evaluation of the removal of As(V) and As(III) by carbon-based adsorbents. *Carbon*, *38*, 589-596.

Payne, K. B., & Abdel-Fattah, T. M. (2005). Adsorption of arsenate and arsenite by iron-treated activated carbon and zeolites: Effects of pH, temperature, and ionic strength. *Journal of Environmental Science and Health*, *40*, 723-749. doi: 10.1081/ESE-200048254.

Petrusevski, B., Sharma, S., Van der Meer, W. G., Kruis, F., Khan, M., Barua, M., & Schippers, J. C. (2008). Four years of development and field testing of IHE arsenic removal family filter in rural Bangladesh. *Water Science & Technology*, *58.1*. doi: 10.2166/wst.2008.335

Pokonova, Y. V. (1997,). Carbon adsorbents for the sorption of arsenic. Carbon, *36*, 457-459.

Pollard, S. J., Fowler, G. D., Sollars, C. J., & Perry, R. (1992). Low-cost adsorbents for waste and wastewater treatment: A review. *The Science of the Total Environment*, *116*, 31-52.

Qin, Y. W., Gang, P., Zhang, M. M., & Li, X. L. (2004). Adsorption of zinc on manganite (MnOOH): Particle concentration effect and adsorption reversibility. *Journal of Environmental Sciences*, *16*(4), 627-630.

Quinlivan, P. A., Li, L., & Knappe, D. R. (2005). Effects of activated carbon characteristics on the simultaneous adsorption of aqueous organic micropollutants and natural organic matter. *Water Research*, *39*, 1663-1673. doi: 10.1016/jwatres.2005.01.029

RRUFF Project. (2006). RRUFF Project integrated database of Raman spectra, x-ray diffraction and chemistry data for minerals [Database and software]. Retrieved from http://rruff.info/

Raven, K. P., Jain, A., & Loeppert, R. H. (1998). Arsenite and arsenate adsorption on ferrihydrite: Kinetics, equilibrium and adsorption envelopes. *Environmental Science Technology*, *32*, 344-349.

Reed, B. E., & Arunachalam, S. (1994). Use of GAC columns for Pb removal. *Journal of Environmental Engineering*, *120*(2), 416-436.

Reed, B. E., & Nonavinakere, S. K. (1992,). Metal removal by activated carbon: Effects of complexing ligands, competing adsorbates, ionic strength, and background electrolyte. *Separation Science and Technology*, *27*(14), 1985-2000.

Reed, B. E., Vaughan, R., & Jiang, L. (2000). As(III), As(V), Hg and Pb removal by Fe-oxide impregnated activated carbon. *Journal of Environmental Engineering*, *126*(9), 869-873.

Reitner, L., Falk, H., Groat, C., & Coussens, C. M. (2004). *From Source Water to Drinking Water: A Workshop Summary*. Retrieved from http://books.nap.edu/openbook.php?record_id=11142&page=47

Russell, H. H., Matthews, J. E., & Sewell, G. W. (1992, January). *TCE removal from contaminated soil and groundwater* (Issue Brief USEPA EPA/540/S-92/002). Ada, OK: Agency Superfund Technology Support Center for Ground Water.

Sadiq, M. (1997). Arsenic chemistry in soils: An overview of thermodynamic predictions and field observations. *Water, Air and Soil Pollution, 93*, 117-136.

Sato, Y., Kang, M., Kamei, T., & Magara, Y. (2002). Performance of nanofiltration for arsenic removal. *Water Research, 36*, 3371-3377.

Schwertman, U., & Taylor, R. M. (1989). Iron oxides. *Minerals in Soil Environments,* 2nd Ed., SSSA Book Series No. 1, Soil Science of America, Madison, WI, 379-427.

Sengupta, A. K., & Cumbal, L. H. (2005). *U.S. Patent No. 20,050,156,136*. Washington, DC: U.S. Patent and Trademark Office.

Sherman, D. M., & Randall, S. R. (2003). Surface complexation of arsenic(V) to iron(III) (hydr)oxides Structural mechanism from ab initio molecular geometries and EXAFS. *Geochim Cosmochim Acta, 67*(22), 4223-4230.

Snoeyink, V. L., Weber, W. J. Jr., & Mark, H. B. (1969). Sorption of phenol and nitrophenol by active carbon. *Environmental Science and Technology, 3*(10), 918-926.

Sontheimer, H., Crittenden, J., & Summers, S. (1988). *Activated carbon for water treatment* (2nd ed.). Karlsruhe, Germany: DVGW-Forschungsstelle, Engler-Bunte Institut.

Stumm, W., & Morgan, J. (1981). *Aquatic Chemistry.* John Wiley & Sons, NY, NY.

Subcommittee on Arsenic in Drinking Water, National Research Council. (1999). *Arsenic in drinking water* Washington, D.C.: National Academies Press. Retrieved from http://books.nap.edu/catalog.php?record_id=6444

Subramanian, K. S., Viraraghavan, T., Phommavong, T., & Tanjore, S. (1997). Manganese greensand for removal of arsenic in drinking water. *Water Quality Research Journal of Canada, 32*(3), 551-561.

Summers, R. S., & Roberts, P. V. (1988). Activated carbon adsorption of humic substances II: Size exclusion and electrostatic interactions. *Journal of Colloid and Interface Science, 122*(2), 382-397.

Suzuki, M. (1994). Activated carbon fiber: Fundamentals and applications. *Carbon*, *32*(4), 577-586.

Suzuki, T. M., Bomani, J. O., Matsunaga, H., & Yokoyama, T. (2000). Preparation of porous resin with crystalline hydrous zirconium oxide and its application to the removal of arsenic. *Reactive and Functional Polymers*, *43*, 165-172.

Szecsody, J. E., Fruchter, J. S., Williams, M. D., Vermeul, V. R., & Sklarew, D. (2004). In situ chemical reduction of aquifer sediments: Enhancement of reactive iron phases and TCE dechlorination. *Environmental Science and Technology*, *38*, 4656 - 4663.

Tadanier, C., Schreiber, M., & Roller, J. (2005). Arsenic mobilization through microbially mediated deflocculation of ferrihydrite. *Environmental Science and Technology, 39*, 3061-3068.

Thirunavukkarasu, O. S., Viraraghavan, T., Subramanian, K. S., & Tanjore, S. (2002). Organic arsenic removal from drinking water. *Urban Water, 4*, 415-421.

United States Army Corp of Engineers. (2001). *Adsorption design guide* (DG 1110-1-2). Washington, DC: U.S. Government Printing Office.

United States Department of Health & Human Services, Agency for Toxic Substances & Disease Registry. (1997, September). *Toxicological profile for trichloroethylene* (Toxicological Profile). Retrieved from Agency for Toxic Substances and Disease Registry website: http://www.atsdr.cdc.gov/toxprofiles/tp.asp?id=173&tid=30

United States Department of Health and Human Services (Ed). (2007). *Toxicological profile for arsenic* (White Paper). Washington, DC: US Department of Health and Human Services.

United States Environmental Protection Agency Website. (2009). http//www.epa.gov/safewater/contaminants/basicinformation/trichloroethylene.html

United States Environmental Protection Agency. (1987). *Safe Drinking Water Act Amendment*. Retrieved December 26, 2008, from http//www.epa.gov

United States Environmental Protection Agency. (1996). *Test methods for evaluating solid waste* (Physical/chemical Methods SW-846). Washington, DC: US EPA.

United States Environmental Protection Agency. (2000). *Arsenic in drinking water rule: Economic assessment* (EPA 815-R-00-026). Washington, DC: U.S. Government Printing Office.

United States Environmental Protection Agency. (2000). *Technologies and costs for removal of arsenic from drinking water* (EPA 815-R-00-028). Washington, DC: U.S. Government Printing Office.

United States Environmental Protection Agency. (2003). *Water treatment technology feasibility support document for chemical contaminants: In support of EPA six-year review of national primary drinking water regulations* (EPA 815-R-03-004). Washington, DC: U.S. Government Printing Office.

United States Environmental Protection Agency. (2006). *EPA National primary drinking water standards* [Fact sheet]. Retrieved from http://www.epa.gov/safewater/contaminants/index.html#1

United States Environmental Protection Agency. (2006). *Technical factsheet on: Trichloroethylene* [Fact sheet]. Retrieved from http://www.epa.gov/OGWDW/dwh/t-voc/trichlor.html

United States Environmental Protection Agency. (2009). *Basic information about trichloroethylene in drinking water* (Fact Sheet). Retrieved from USEPA Website: http://www.epa.gov/safewater/contaminants/basicinformation/trichloroethylene.html

United States Environmental Protection Agency. (2009). *Six year review 2: Health effects assessment survey report* (EPA-R-09-006). Washington, DC: U.S. Government Printing Office.

United States Environmental Protection Agency. (2009). *Water treatment technology feasibility support document for chemical contaminants for the second six year review of national primary drinking water regulations.* (EPA 815-B-09-007). Washington, DC: U.S. Government Printing Office.

Vaishya, R. C., & Gupta, S. K. (2003,). Arsenic removal from groundwater by iron impregnated sand. *Journal of Environmental Engineering*, *129*(1), 89-92.

Vaughan, R. L., Jr., & Reed, B. E. (2005,). Modeling As(V) removal by a iron oxide impregnated activated carbon using the surface complexation approach. *Water Research*, *39*, 1005-1014.

Vaughan, R. L., Jr., Reed, B. E., Viadero, R. C., Jr., Jamil, M., & Berg, M. (1999,). Simultaneous removal of organic and heavy metal contaminants by granular activated carbon (GAC) columns. *Advances in Environmental Research; an international journal of research in environmental science, engineering and technology*, *3*(3), 229-242.

Wang, L. K., Hung, Y. -T., & Shammas, N. (Eds.). (2004). *Handbook of environmental engineering* (Vols.3-3). doi: ISBN:9781592598205

Wilkie, J. A., & Hering, J. G. (1996). Adsorption of arsenic onto hydrous ferric oxide: Effects of adsorbate/adsorbent ratios and co-occurring solutes. *Colloids and Surfaces A: Physiochemical and Engineering Aspects*, *107*, 97-110.

Woolson, E. A. (1975). Arsenical pesticides. In *Bioaccumulation of arsenicals* (pp. 97-107). Beltsville, MD: American Chemical Society.

Yang, J. –K., Lee, S. –M., & Davis, A. P. (2006). Effect of background electrolytes and pH on the adsorption of Cu(II)/EDTA onto TiO_2. *Journal of Colloid and Interface Science*, *295*, 14-20. doi: 10.1016/j.jcis.2005.08.019.

Yang, R. T. (2003). *Adsorbents: Fundamentals and applications*. Hoboken, NJ: John Wiley & Sons.

Zhang, Y., Yang, M., & Huang, X. (2003). Arsenic(V) removal with a Ce(IV)-doped iron oxide adsorbent. *Chemosphere*, *51*, 945-952.

Zytner, R. G. (1991). Adsorption-desorption of trichloroethylene in granular media. *Water, Air and Soil Pollution*, *65*, 245-255.

APPENDIX A

ADDITIONAL FLOWCHARTS & SCHEMATICS

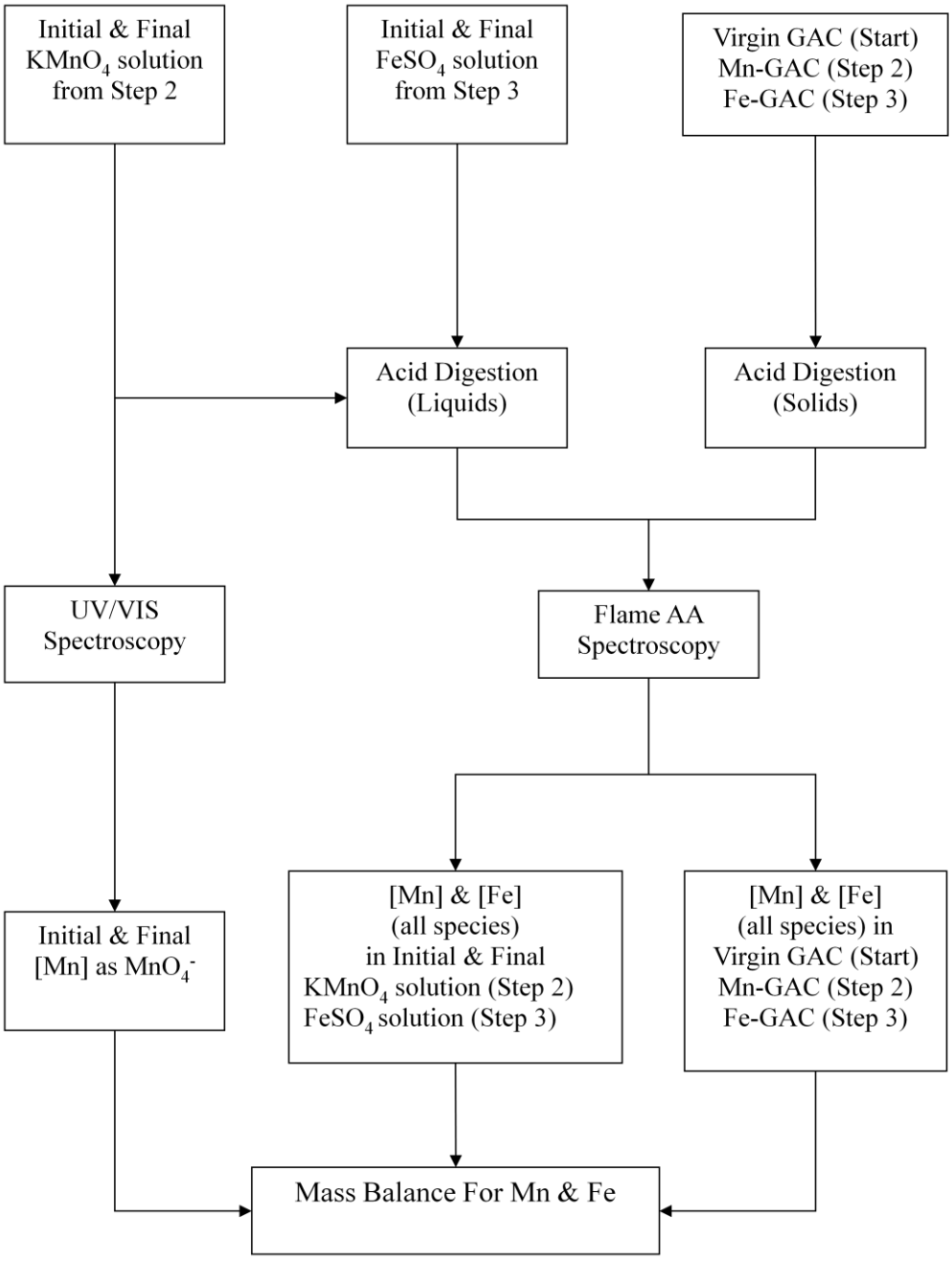

Figure A 1. Schematic of sample collection for mass balance.

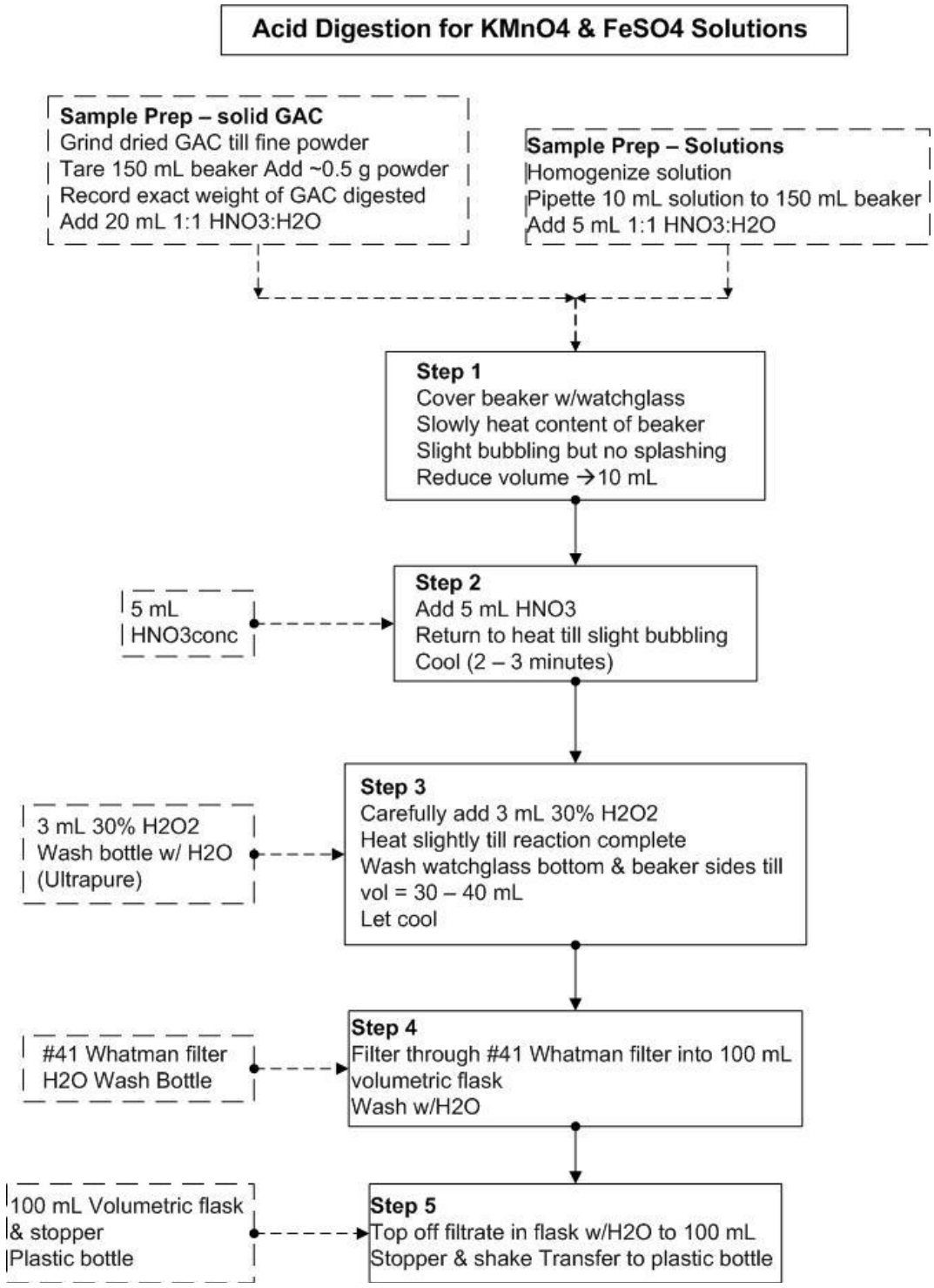

Figure A 2. Flowchart for acid digestion process

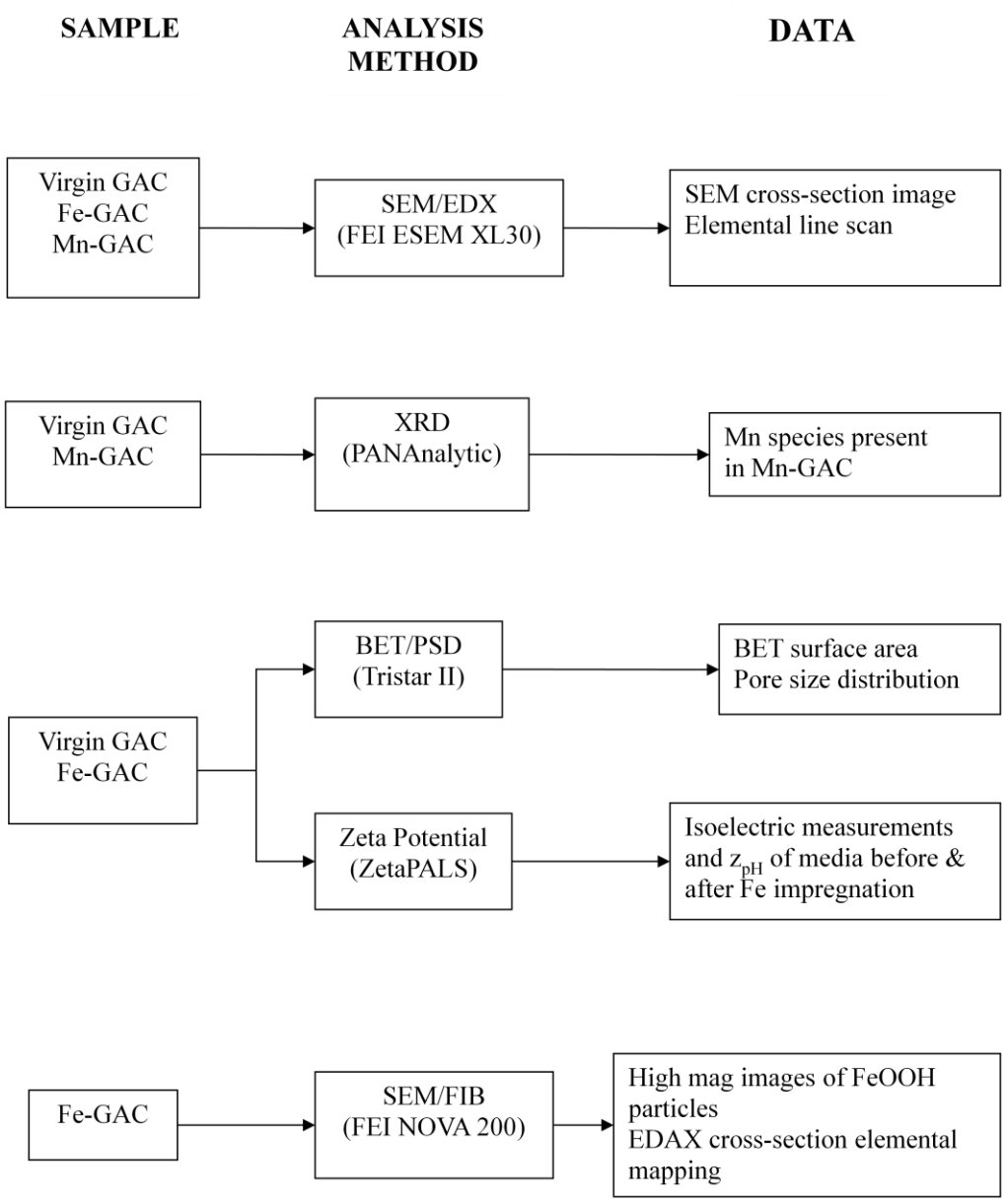

Figure A 3. Materials characterization and analysis flowchart

APPENDIX B

ADDITIONAL TABLES & FIGURES

Table B 1.

Instrument settings for FAA analysis of Mn.

Working Conditions (Fixed)	
Lamp Current	5 mA
Fuel	acetylene
Support	air
Flame Stoichiometry	oxidizing
Bulb	Mn

Working Conditions (Variable)		
Wavelength (nm)	Slit Width (nm)	Optimum Working Range (µg/mL)
403.1	0.2	0.5 – 60
321.7	0.2	100 – 14000

Table B 2.

Instrument settings for FAA analysis of Fe.

Working Conditions (Fixed)	
Lamp Current	5 mA
Fuel	acetylene
Support	air
Flame Stoichiometry	oxidizing
Bulb	Fe

Working Conditions (Variable)		
Wavelength (nm)	Slit Width (nm)	Optimum Working Range (μg/mL)
386.0	0.2	1.5 – 200

Table B 3.

Instrument settings for GF-AAS analysis

Category	Setting
Solution Matrix:	0.1 % HNO3
Atomizer:	Pyrolytic coated partitioned graphite tube
Temperature Range:	85 – 2600 °C
Lamp Current:	10 mA
Spectral Band Width:	0.2 nm
d2:	0.5 nm
Wavelength (λ):	193.7 nm
Max Absorbance:	0.95
MSR:	86%

Table B 4.

Iron recovery and mass balance

	Total Mass of Fe (mg)				Fraction of Initial Fe (%)		
	A	B	C	B+C=D	E	F	G
Treatment Base GAC	Initial (mg)	Rinse (mg)	Media (mg)	Total Fe (mg)	In Rinse (%Initial)	In GAC (%Initial)	Recovery (%Initial)
Method = Fe Only							
Lignite	30082	25666	2729	28395	85.3	9.1	94.4
Bituminous	30082	29673	1785	31458	98.6	5.9	104.6
Method = Mn/Fe							
Lignite	29498	17648	6054	23701	59.8	20.5	80.4
Bituminous	29796	20798	4386	25184	69.8	14.7	84.5
Method = HCl/Mn/Fe							
Lignite	29641	20387	6683	27070	68.8	22.6	91.3
Bituminous	29796	15760	4603	20363	52.9	15.5	68.3

Table B 5.

Manganese mass balance (mg Mn)

	In $KMnO_4$	Mn recovered AFTER KMnO4 step				Mn Recovered after Fe Step	
	Initial Mn	In solution	In solution	In Mn-GAC	Total	In $FeSO_4$	In final
	(Prereaction)	(as MnO_4^-)	(All forms)	(All forms)	Recovered	Rinse	Fe-GAC
Method	(mg Mn)	(mg Mn)	(mg Mn)	(mg Mn)	(mg Mn)	(mg Mn)	(mg Mn)
GAC Type	A	B	C	D = F + G	E = C + D	F	G
Mn/Fe							
Lignite	6118	55	218	5529	5747	5194	335
Bituminous	5906	1080	1554	4397	5951	3977	62
HCl/Mn/Fe							
Lignite	6297	81	131	5124	5255	5048	332
Bituminous	5749	762	1113	4631	5744	4627	93

Table B 6.

Manganese recovery rate (% Mn)

	AFTER Mn Pretreatment step				AFTER FeSO4 treatment step		
	% Initial Mn in SOLUTION as			% in SOLID	% Initial Mn in		
	All Mn (% Initial) A	Unreacted (% Initial) B	Reacted (% Initial) C = A + B	In Mn-GAC (% Initial) D	Fe Rinse (% Initial) E	Fe-GAC (% Initial) F	Total (% Initial) A + E + F
Mn/Fe							
Lignite	3.56	0.90	2.66	90.4	84.9	5.48	94.0
Bituminous	26.3	18.3	8.03	74.5	67.3	1.04	94.7
HCl/Mn/Fe							
Lignite	2.07	1.29	0.78	81.4	80.2	5.27	87.5
Bituminous	19.4	13.3	6.10	80.6	80.5	1.63	101

APPENDIX C

ADDITIONAL SEM IMAGES & EDX LINE SCANS

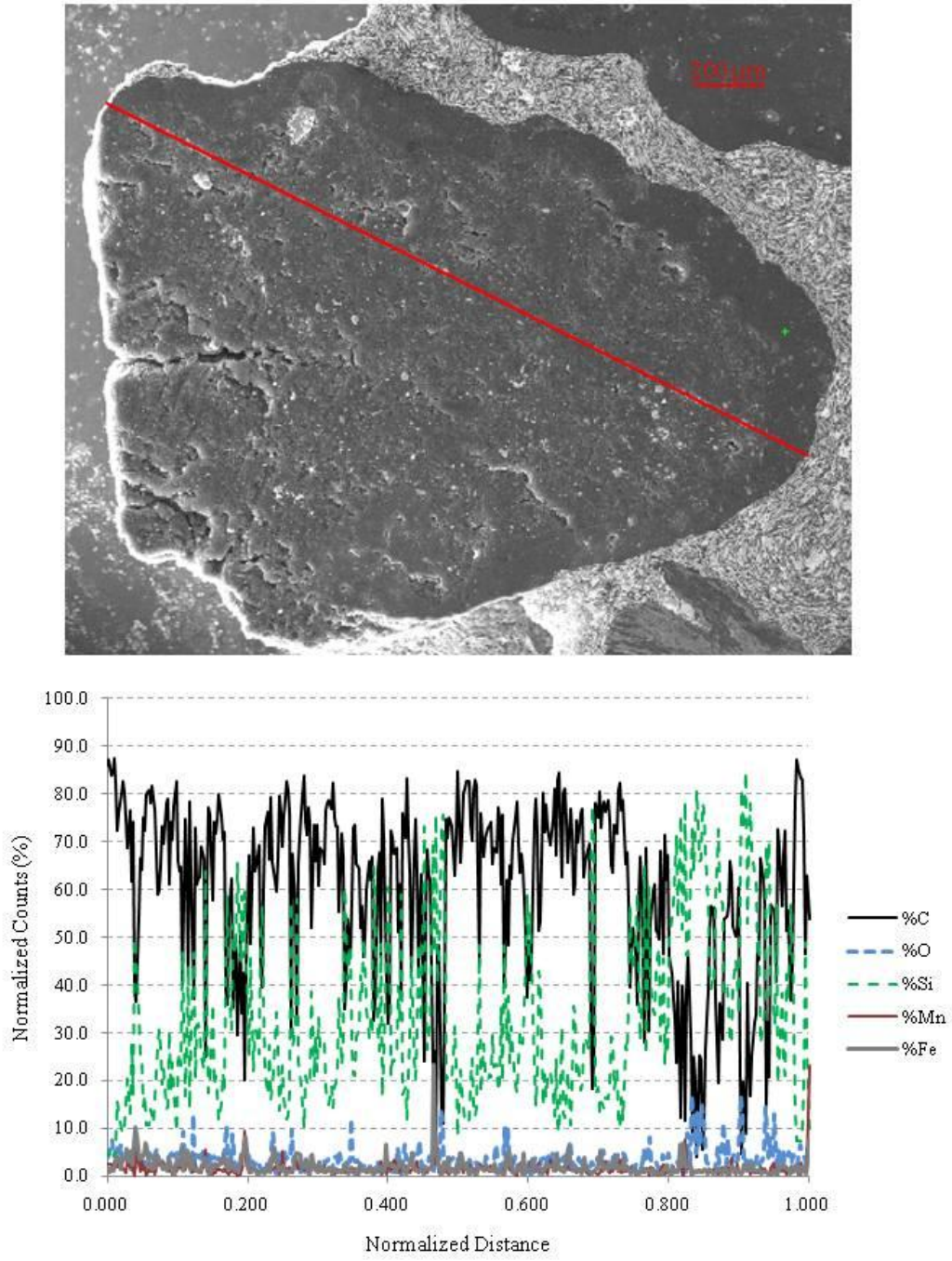

Figure C 1. SEM image and EDX line scan of virgin lignite GAC

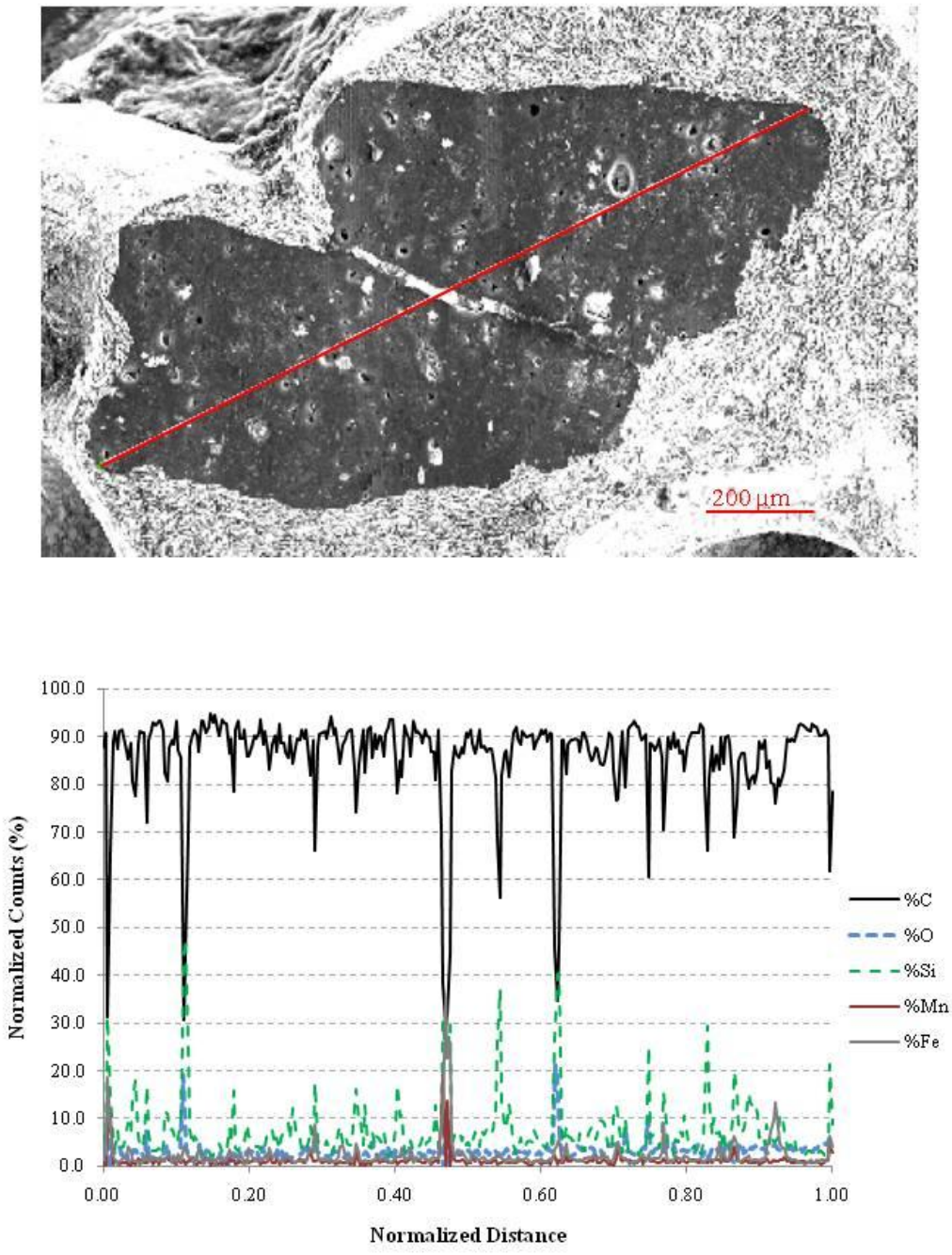

Figure C 2. SEM image and EDX line scan of virgin bituminous GAC

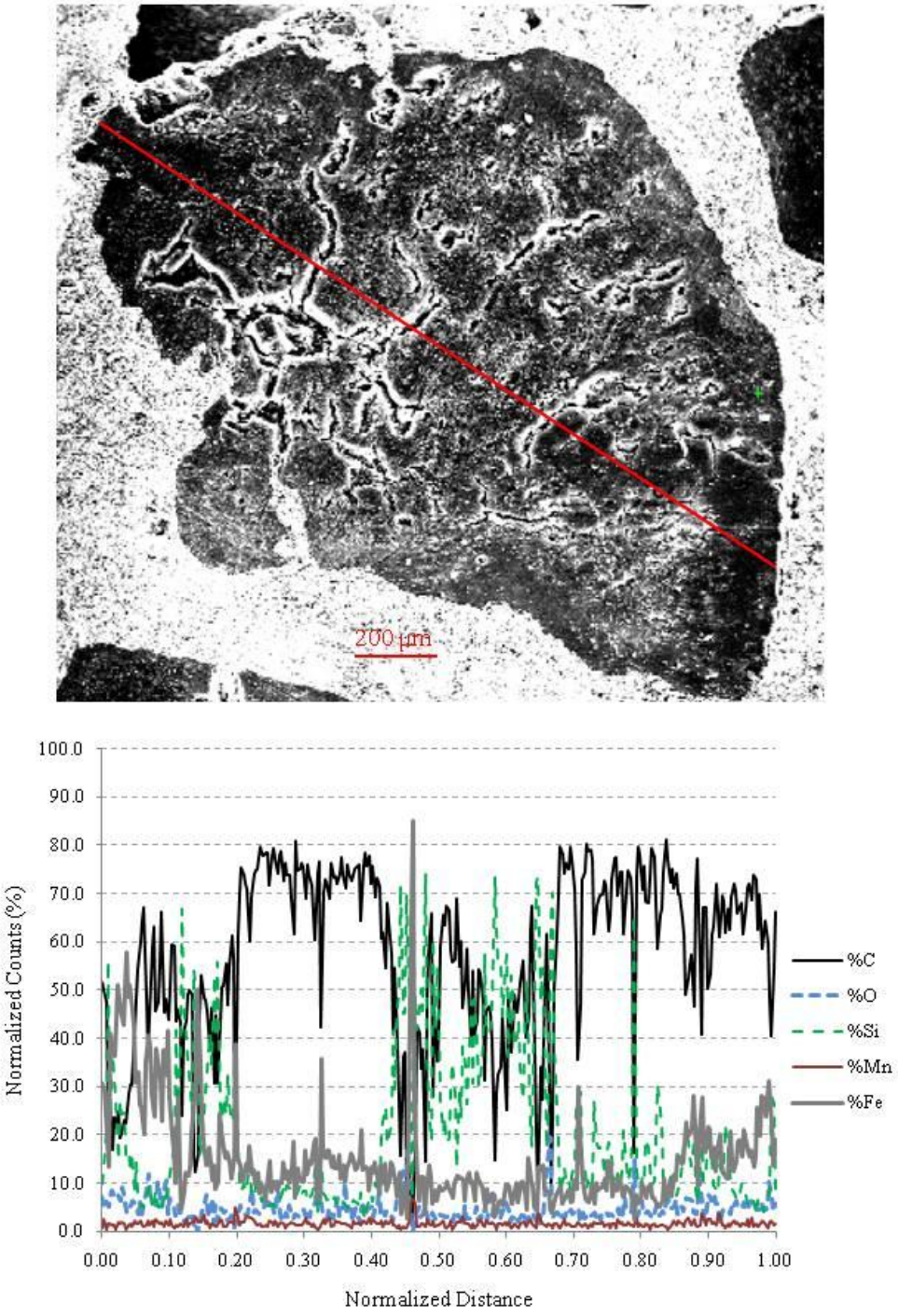

Figure C 3. SEM image and EDX line scan of lignite Fe-GAC by Fe Only method.

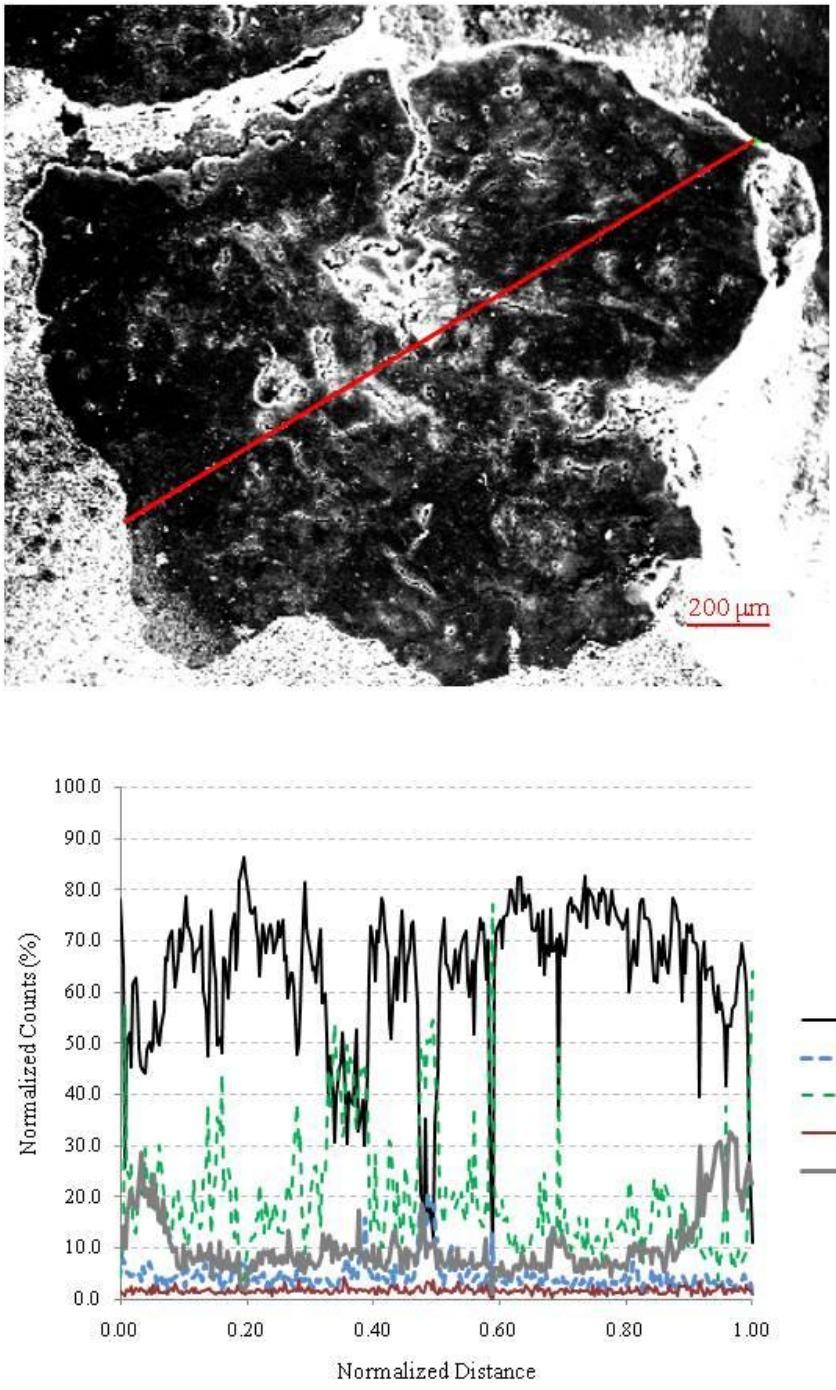

Figure C 4. SEM image and EDX line scan of lignite Fe-GAC by Fe Only.

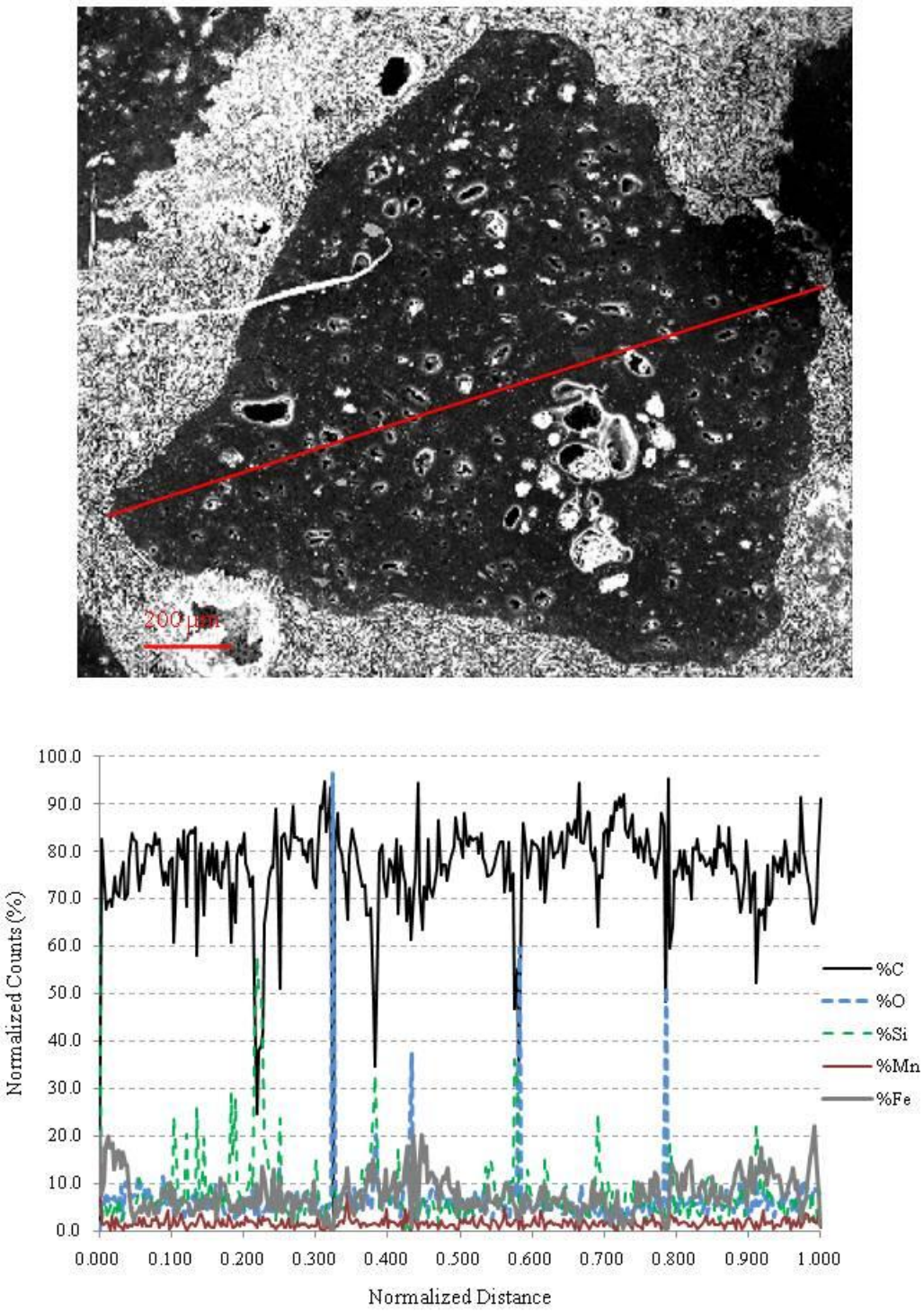

Figure C 5. SEM image and EDX line scan of bituminous Fe-GAC by Fe Only.

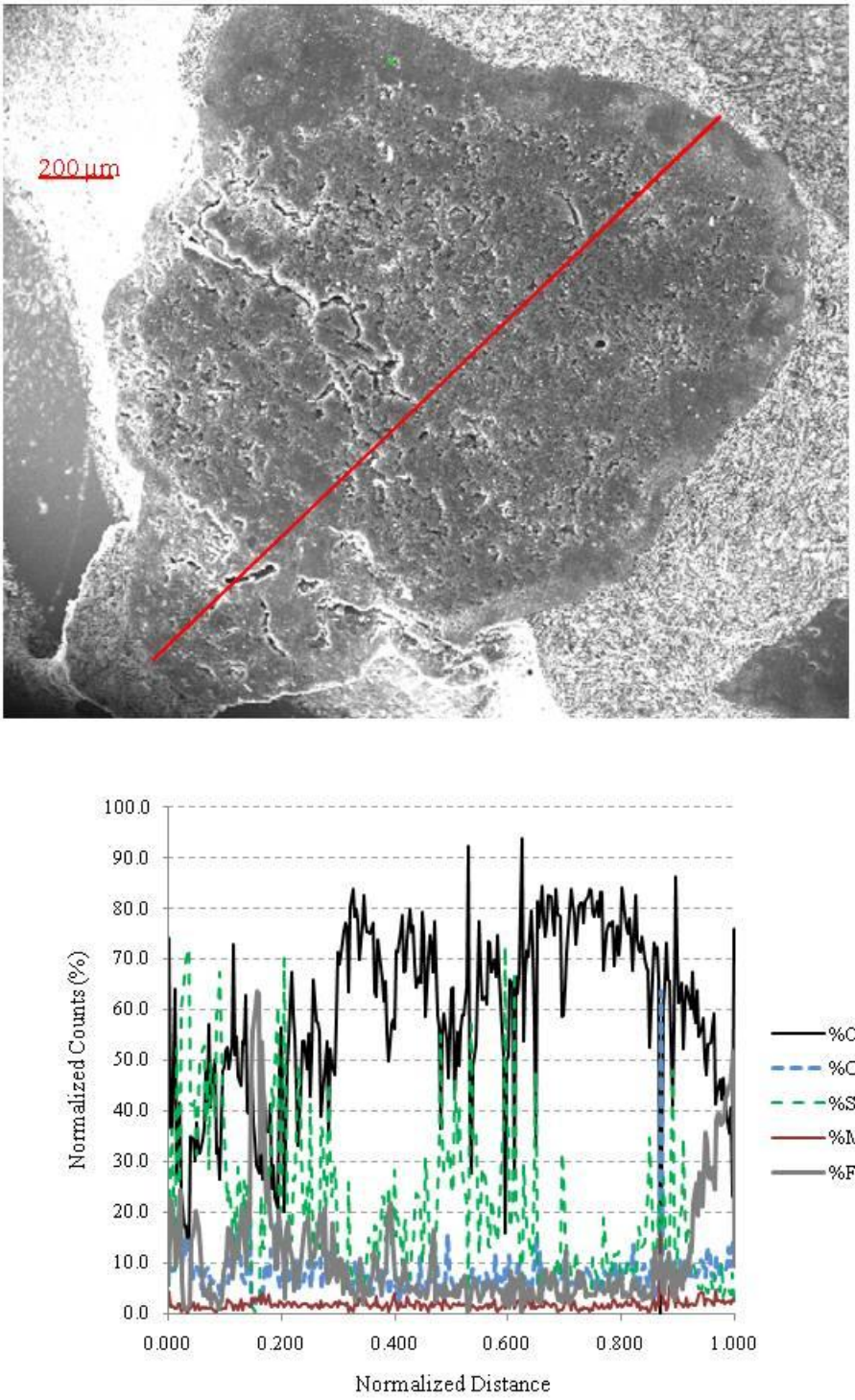

Figure C 6. SEM image and EDX line scan of lignite Fe-GAC by Mn/Fe.

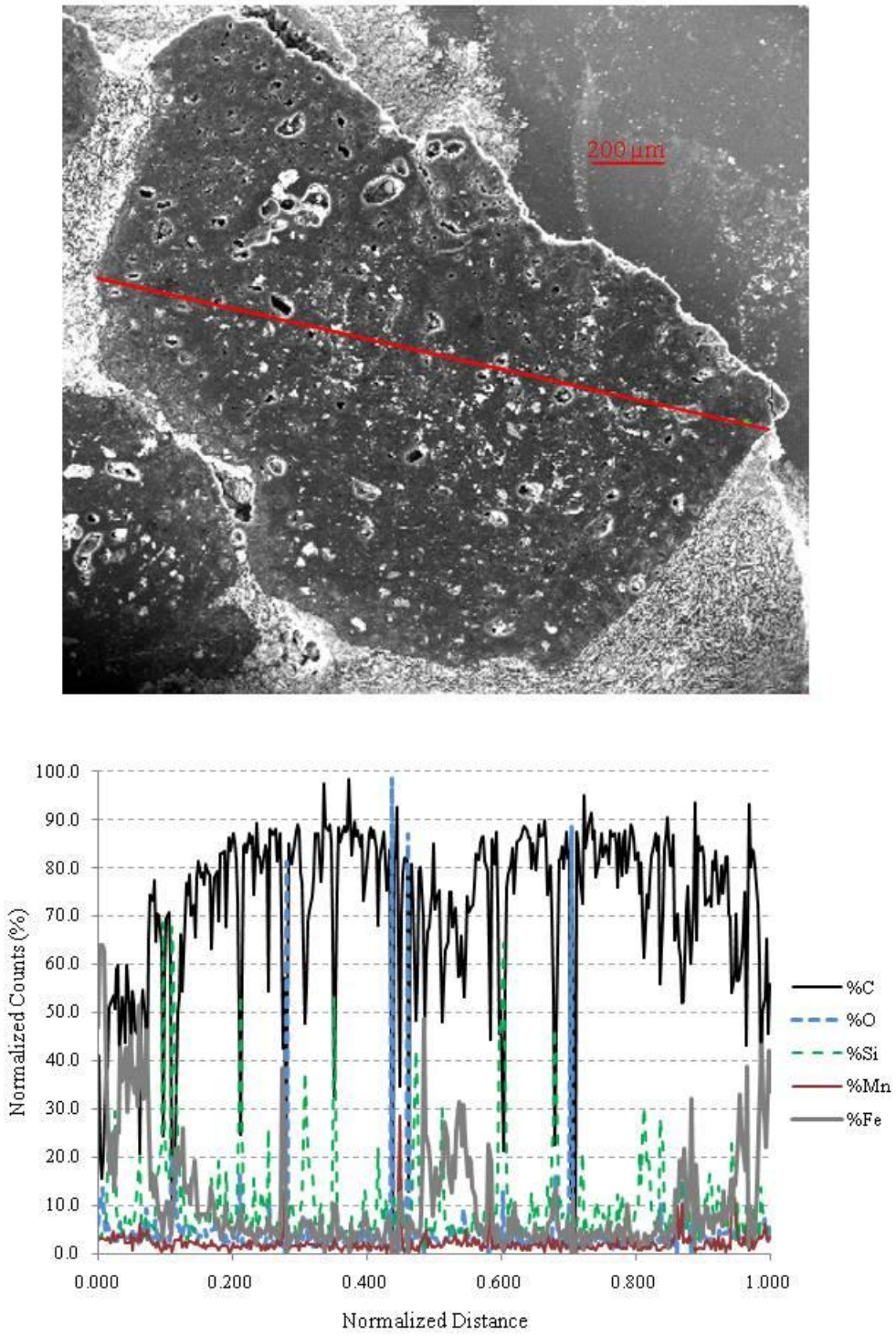

Figure C 7. SEM image and EDX line scan of bituminous Fe-GAC by Mn/Fe.

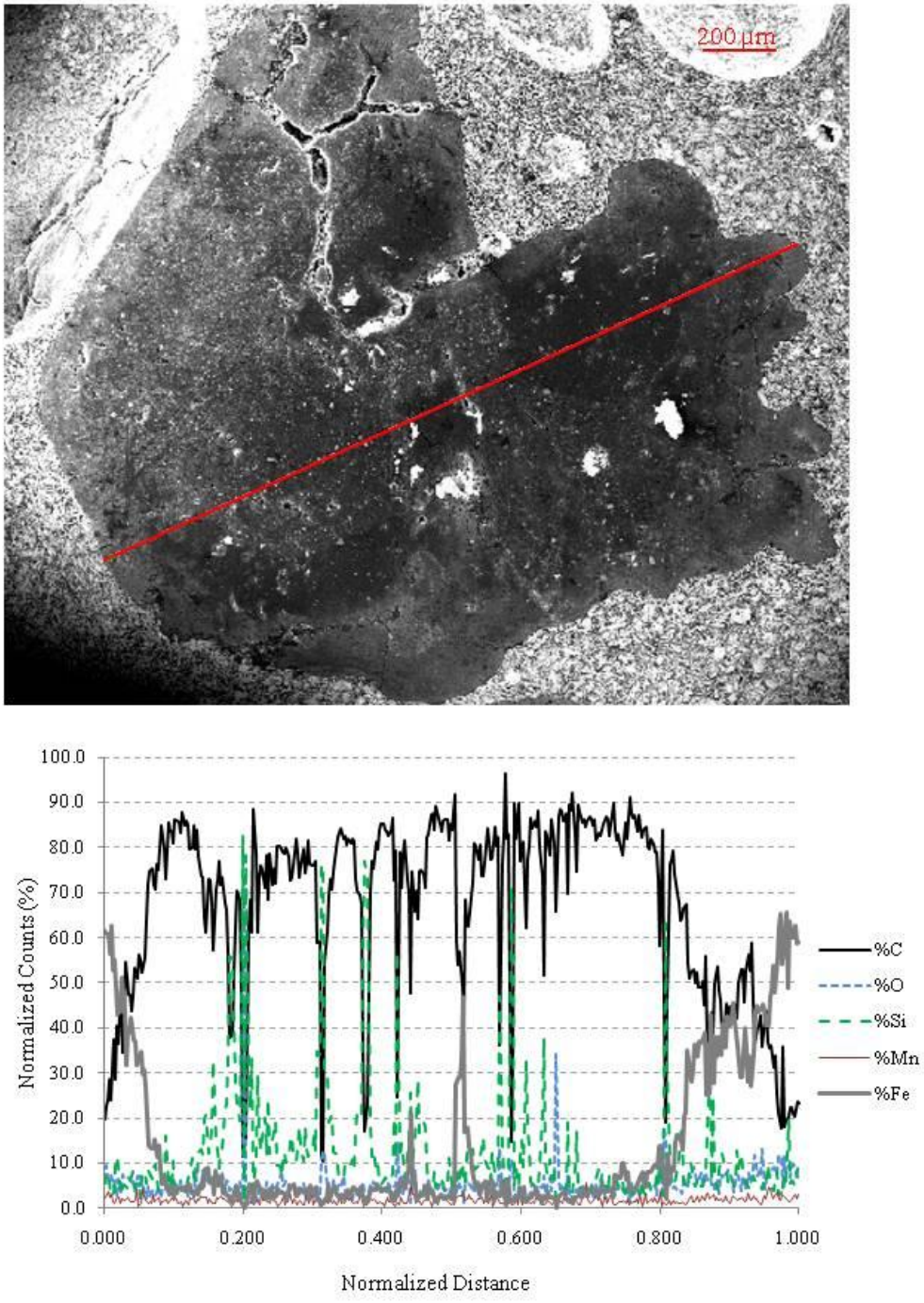

Figure C 8. SEM image and EDX line scan of lignite Fe-GAC by HCl/Mn/Fe.

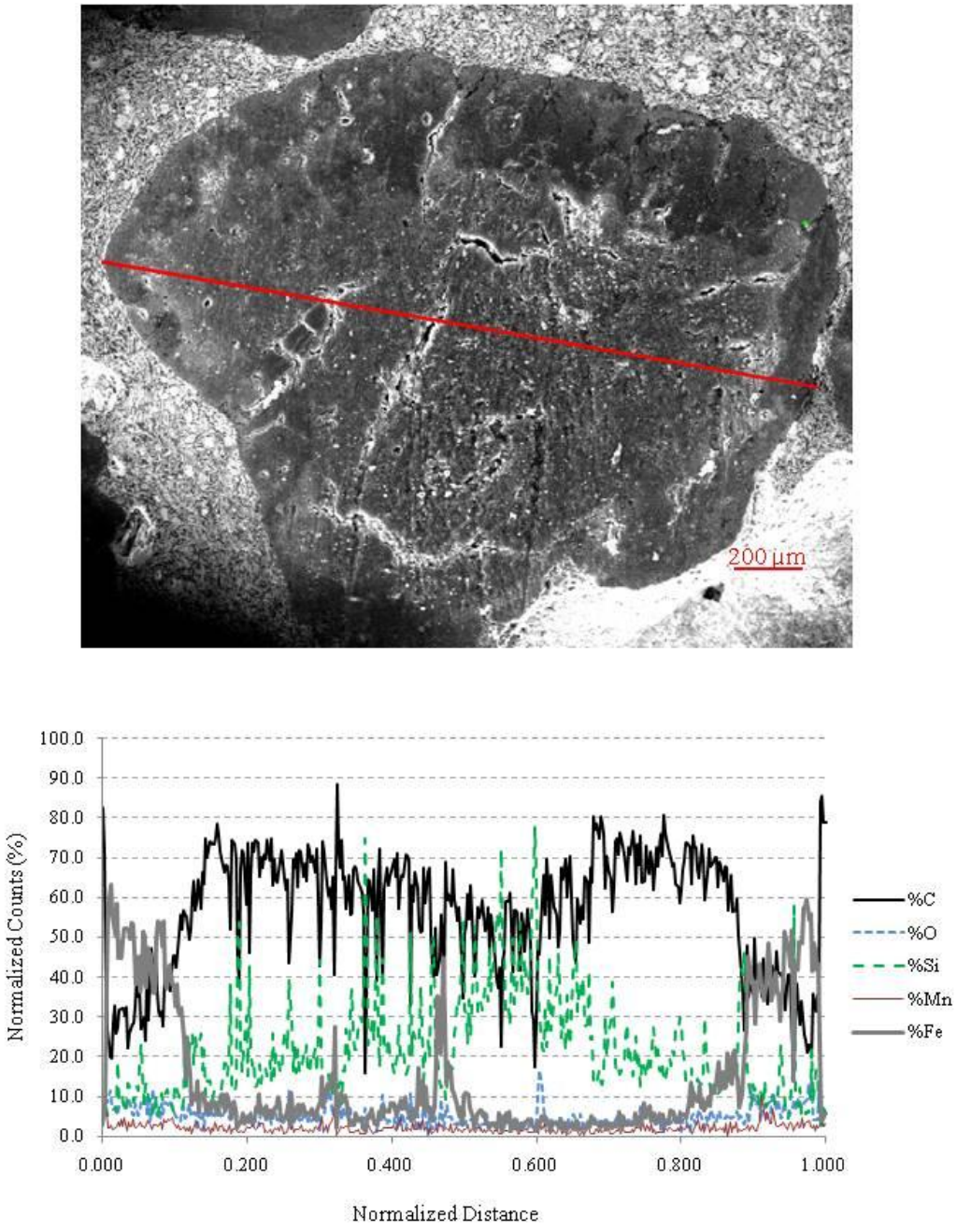

Figure C 9. SEM image and EDX line scan of lignite Fe-GAC by HCl/Mn/Fe.

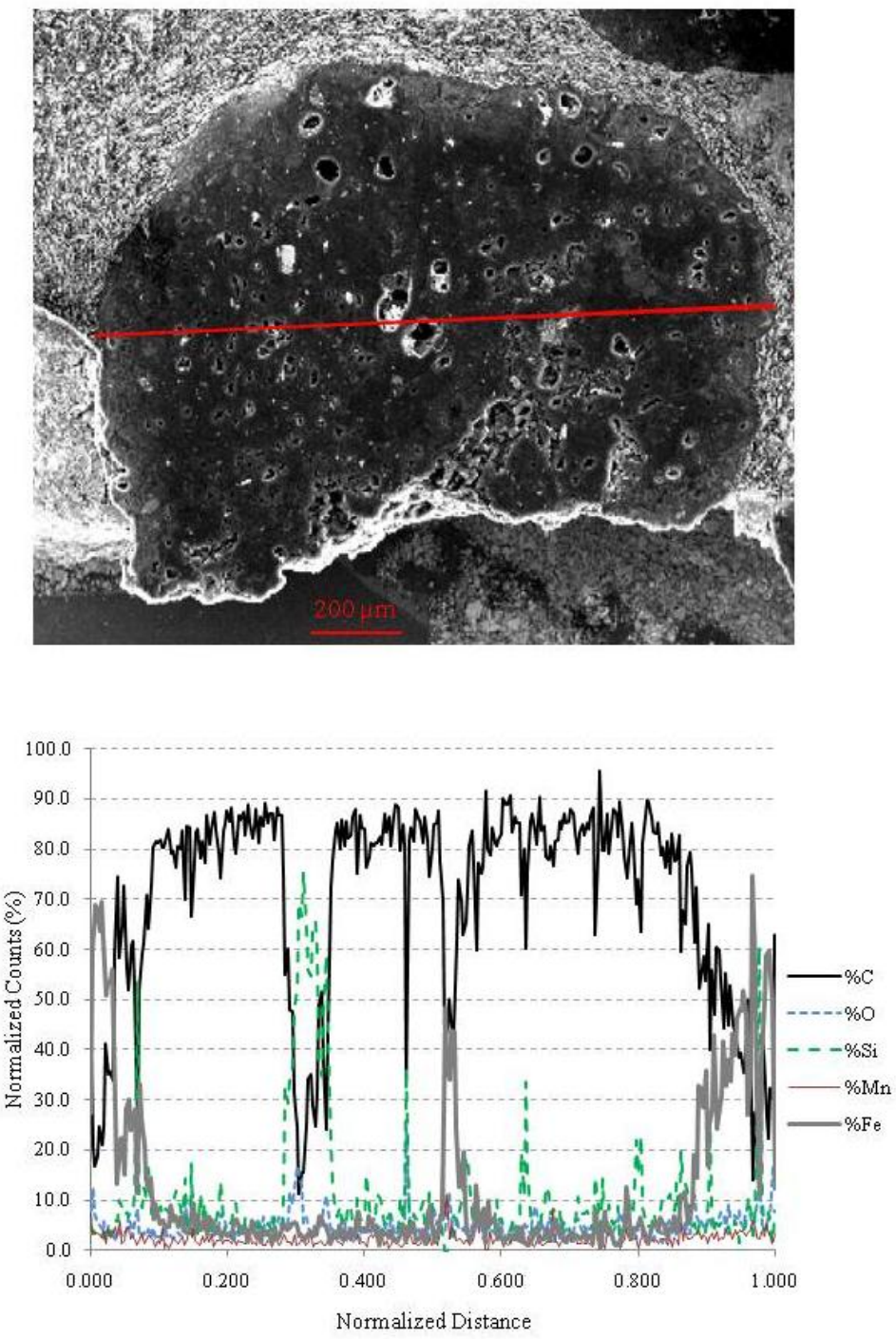

Figure C 10. SEM image and EDX line scan of bituminous Fe-GAC by HCl/Mn/Fe.

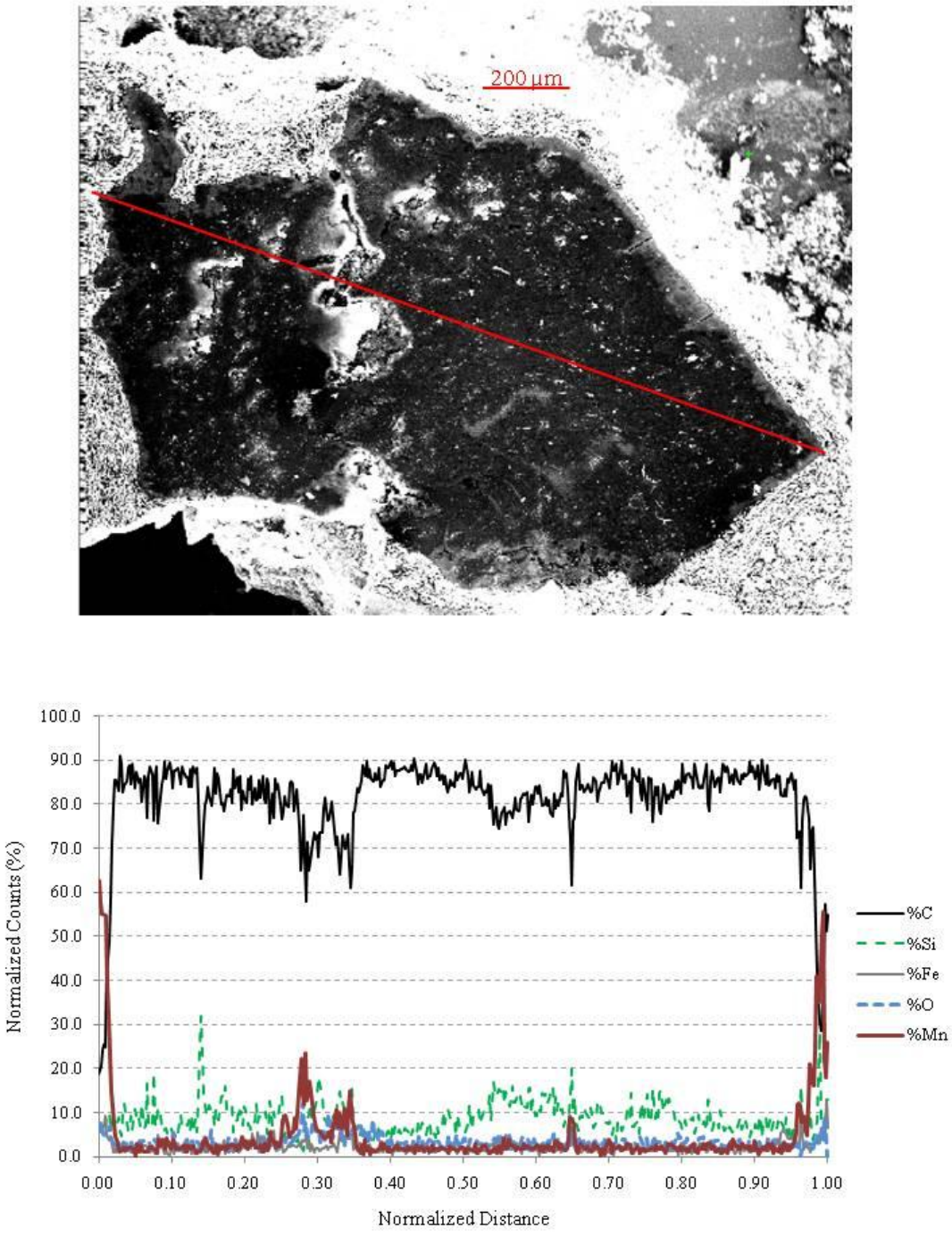

Figure C 11. SEM image and EDX line scan of lignite Mn-GAC by HCl/Mn.

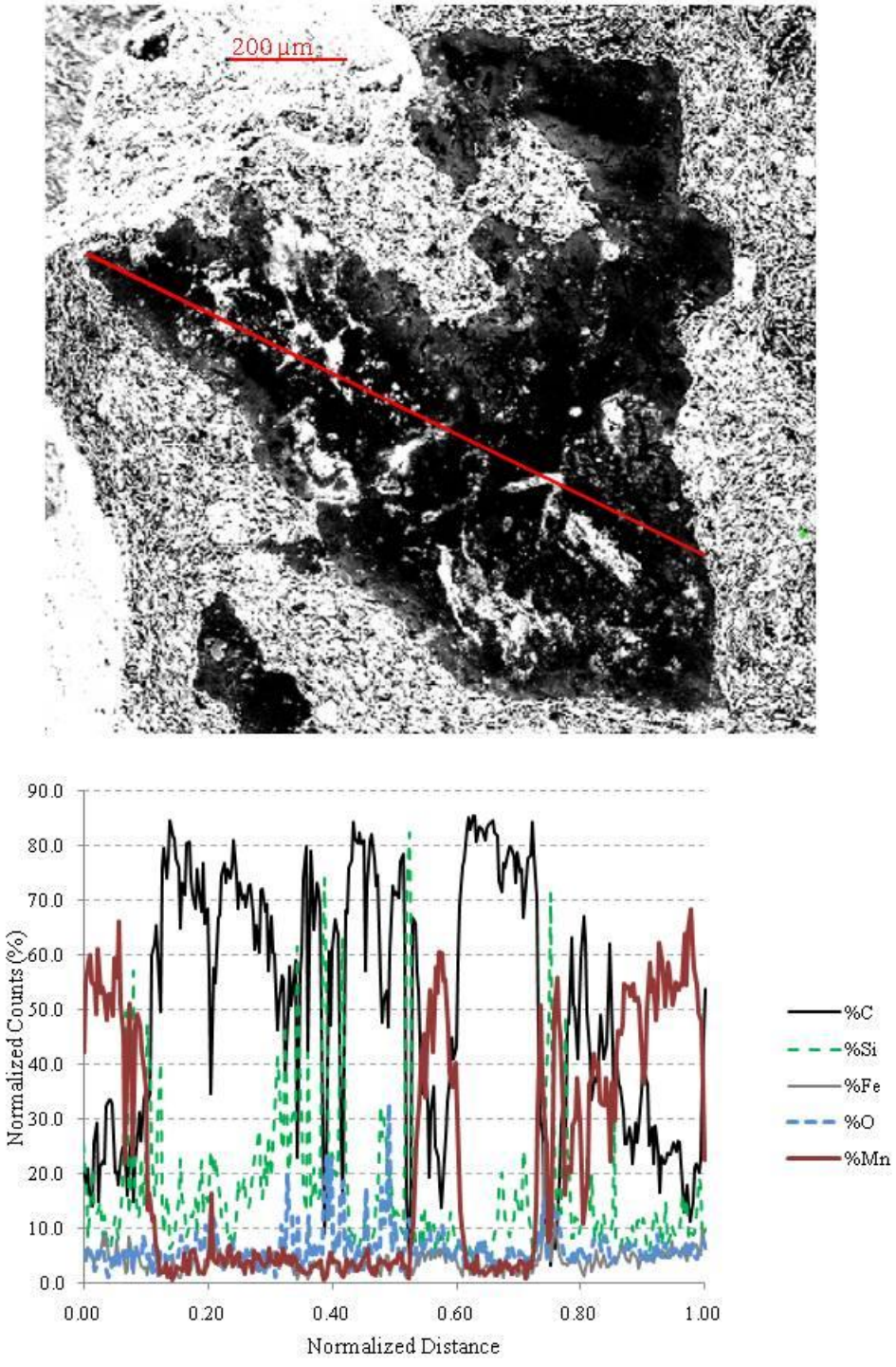

Figure C 12. SEM image and EDX line scan of lignite Mn-GAC by HCl/Mn.

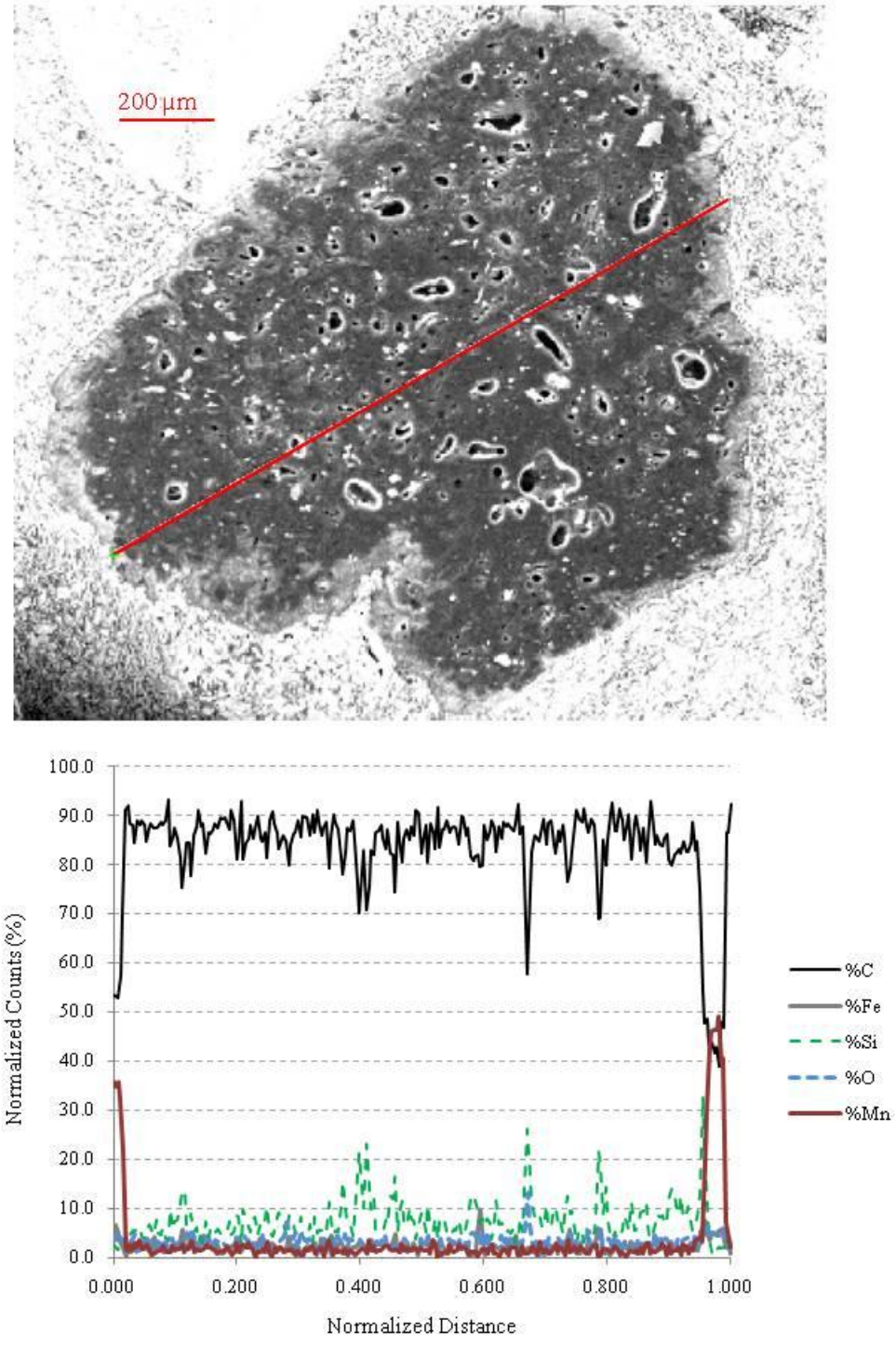

Figure C 13. SEM image and EDX line scan of bituminous Mn-GAC by Mn only.

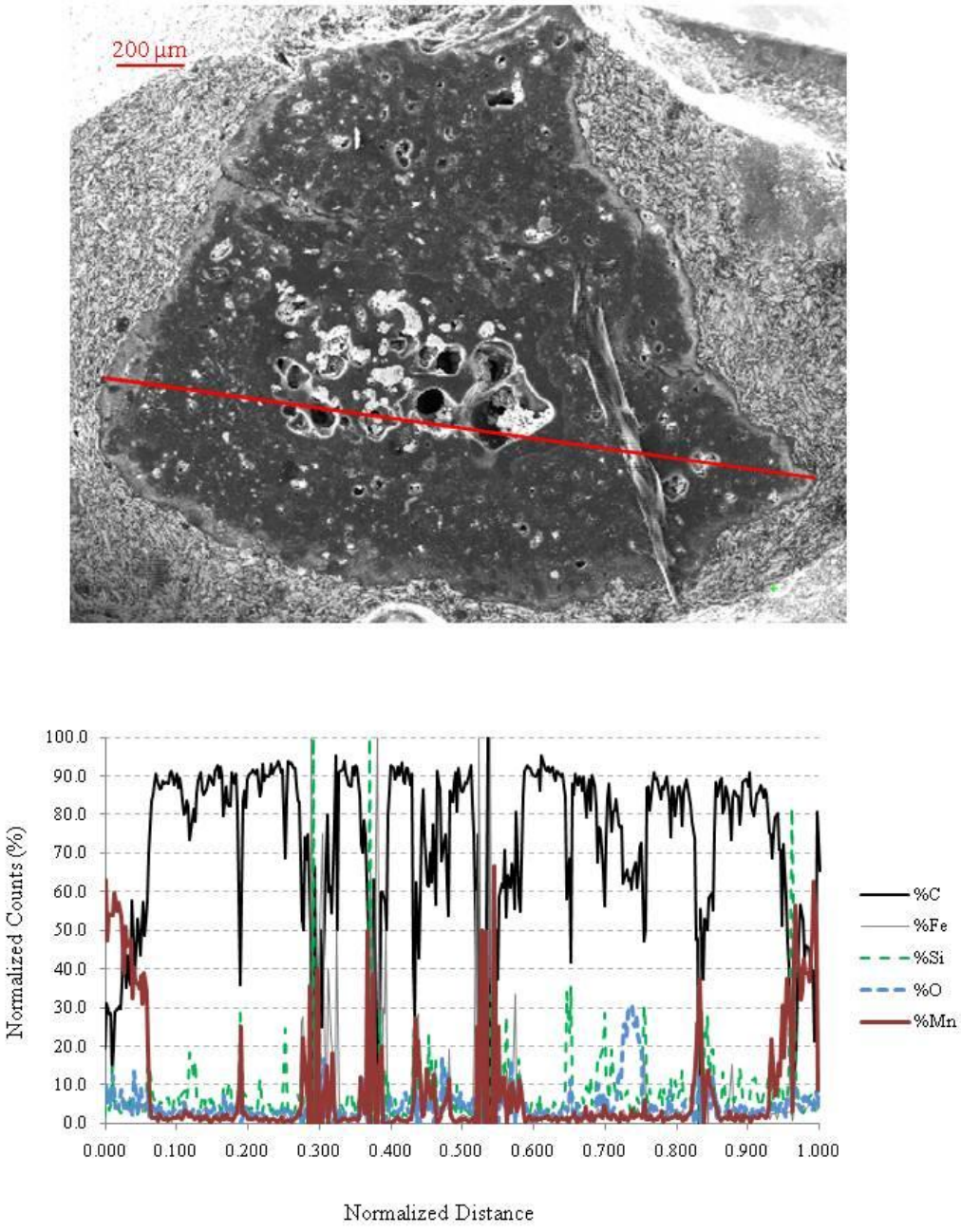

Figure C 14. SEM image and EDX line scan of bituminous Mn-GAC by Mn Only

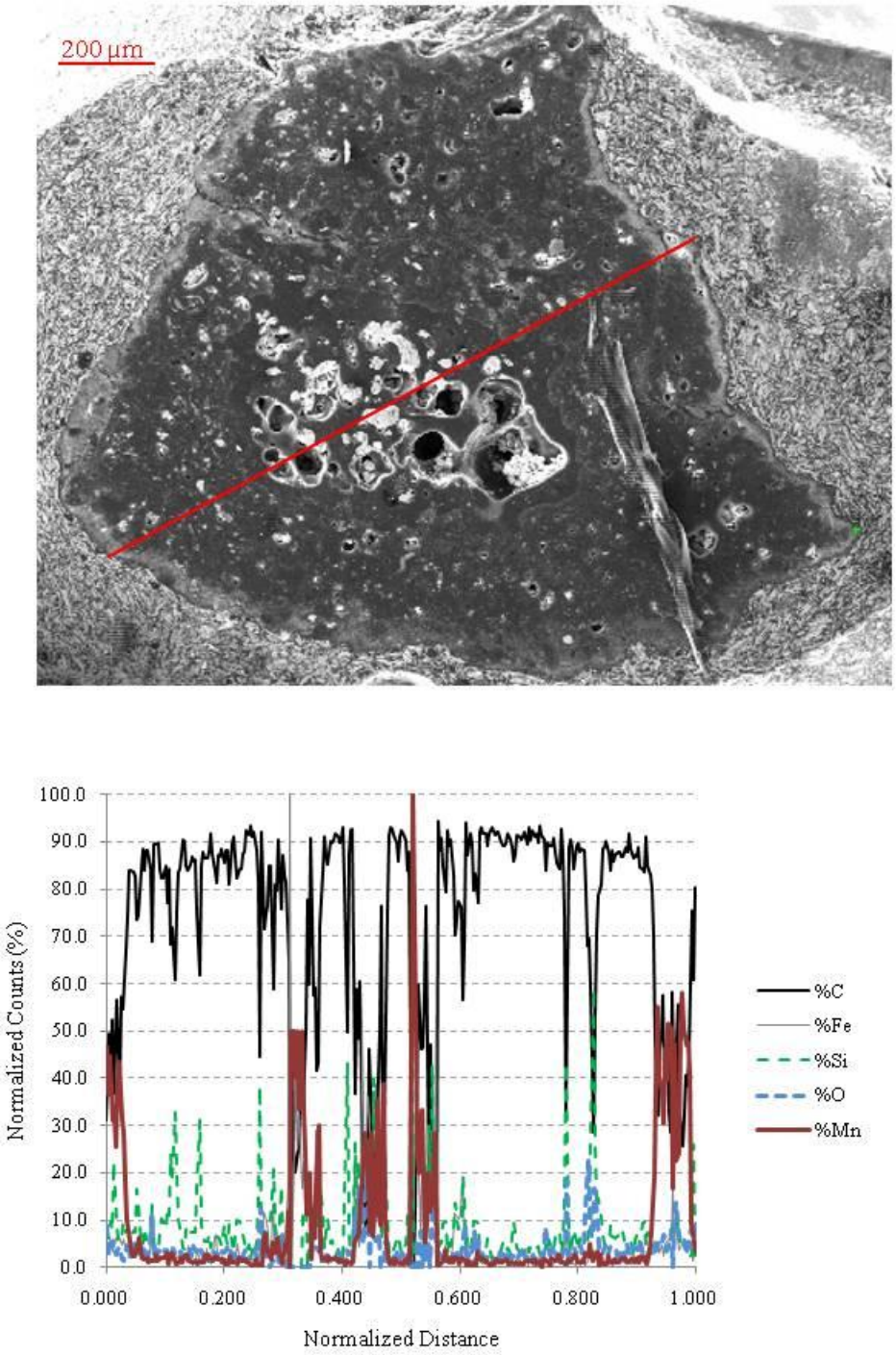

Figure C 15. SEM image and EDX line scan of bituminous Mn-GAC Mn only.

APPENDIX D

ADDITIONAL FIB IMAGES

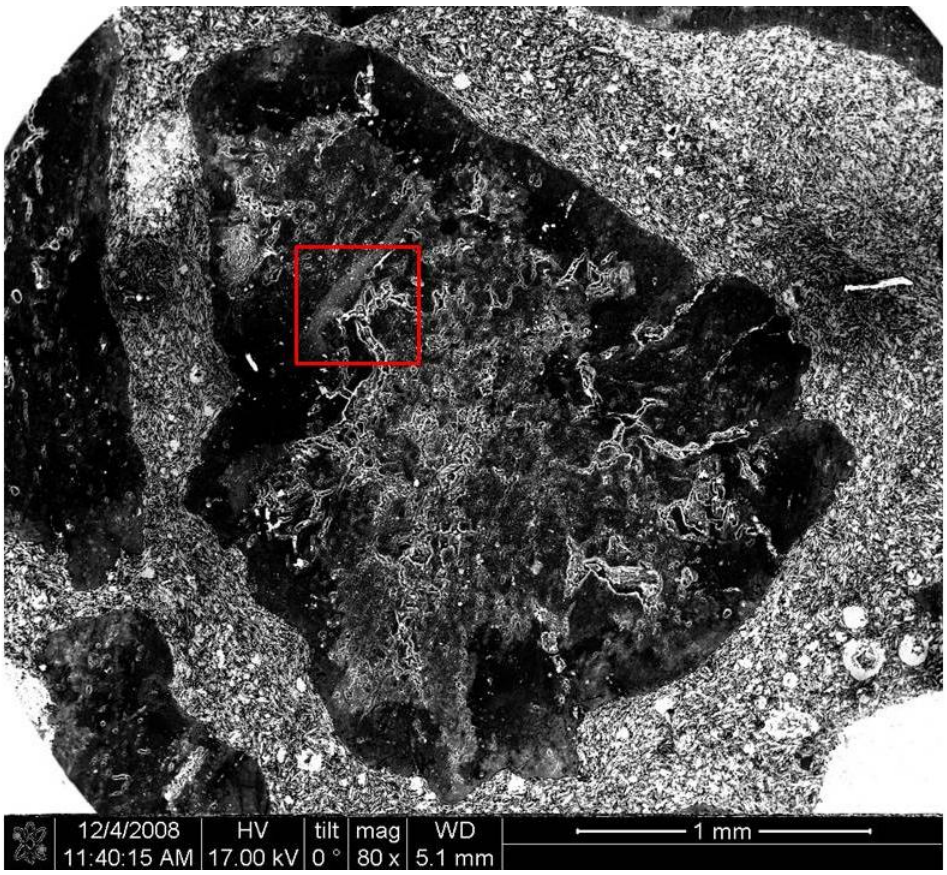

Figure D 1. FIB image of particle of lignite Fe-GAC by Mn/Fe. Red square corresponds to approximate location of next image.

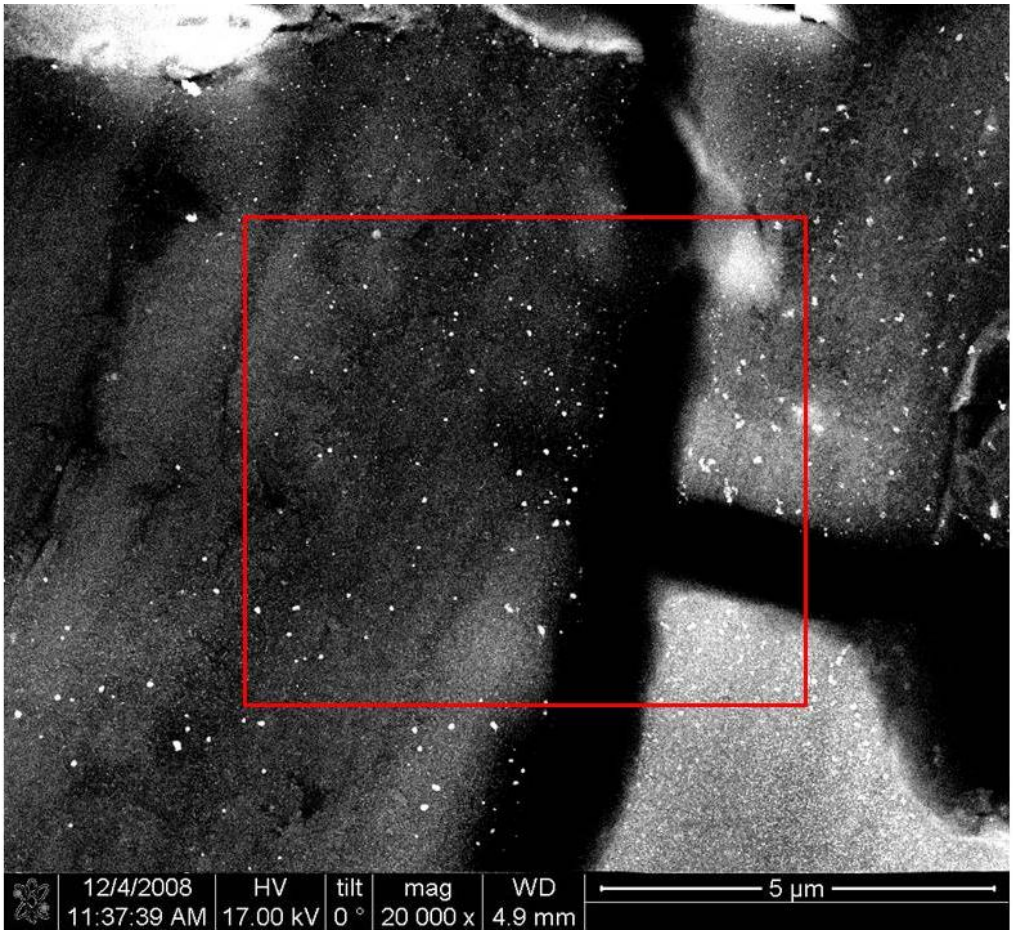

Figure D 2. FIB image of particle of lignite Fe-GAC by Mn/Fe.

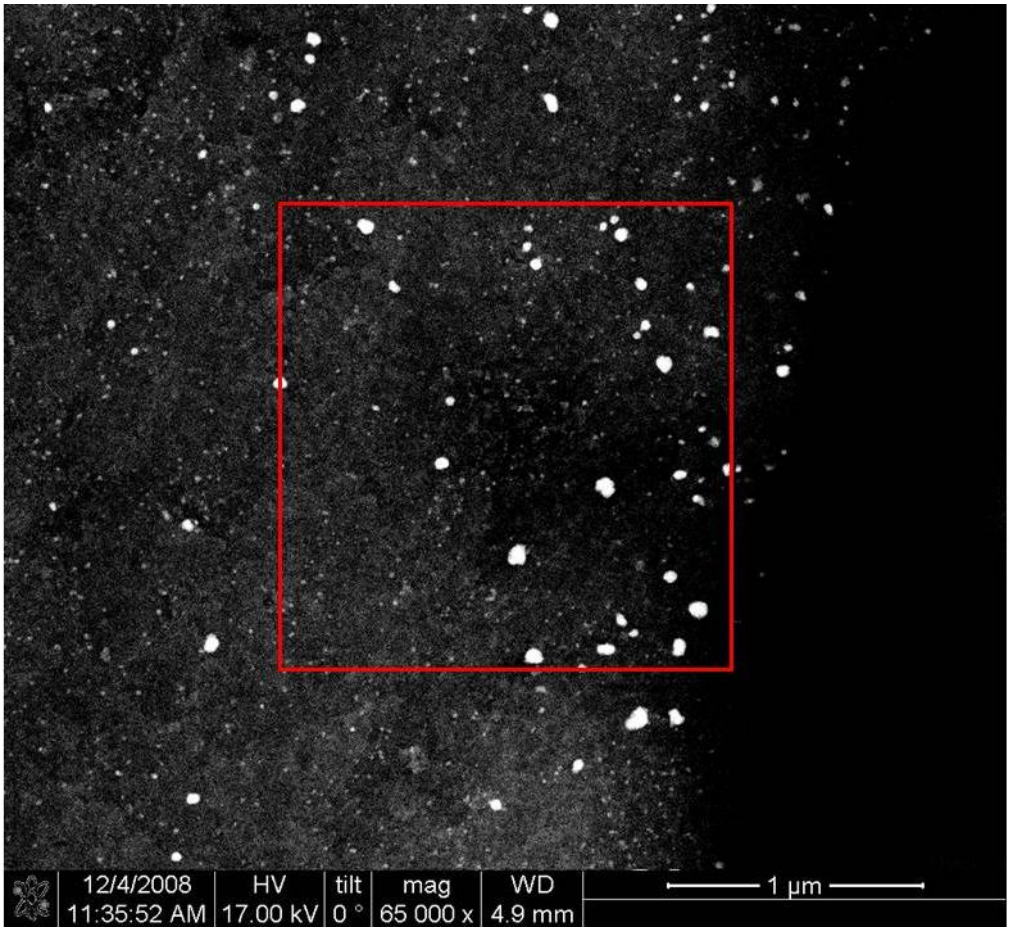

Figure D 3. FIB image of particle of lignite Fe-GAC by Mn/Fe.

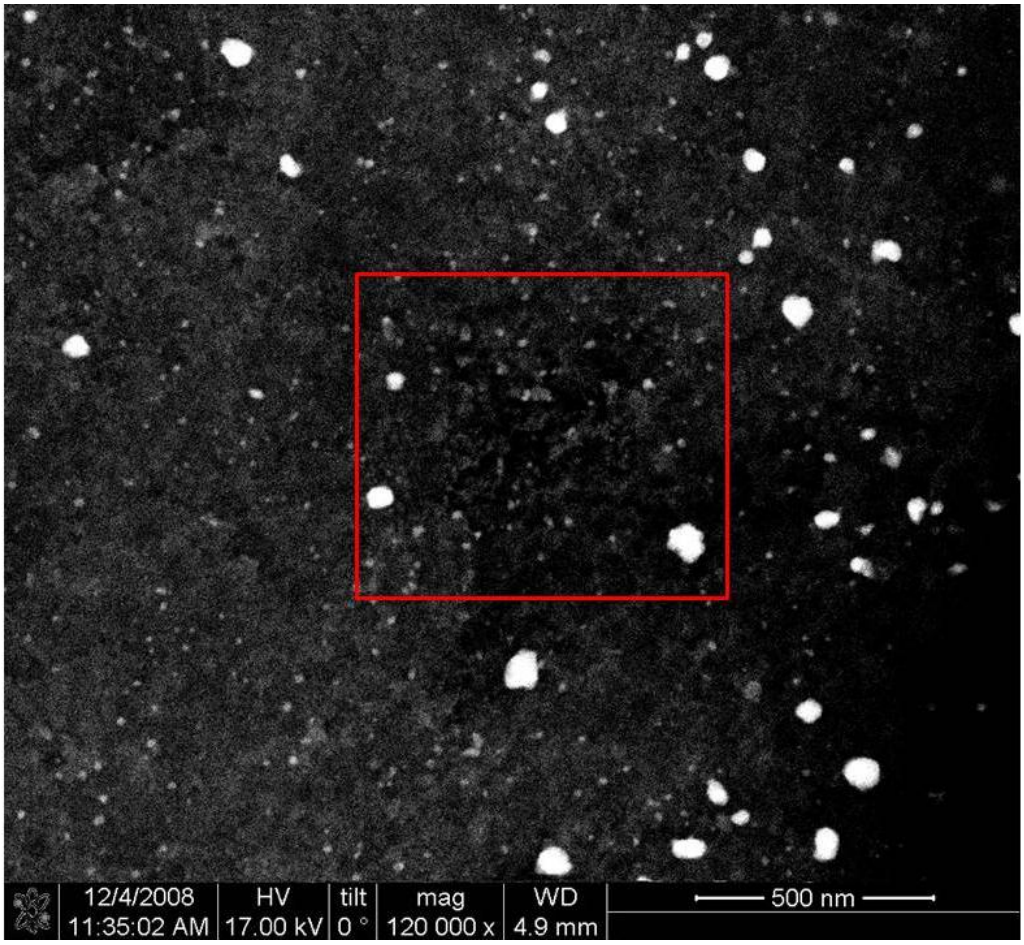

Figure D 4. FIB image of particle of lignite Fe-GAC by Mn/Fe.

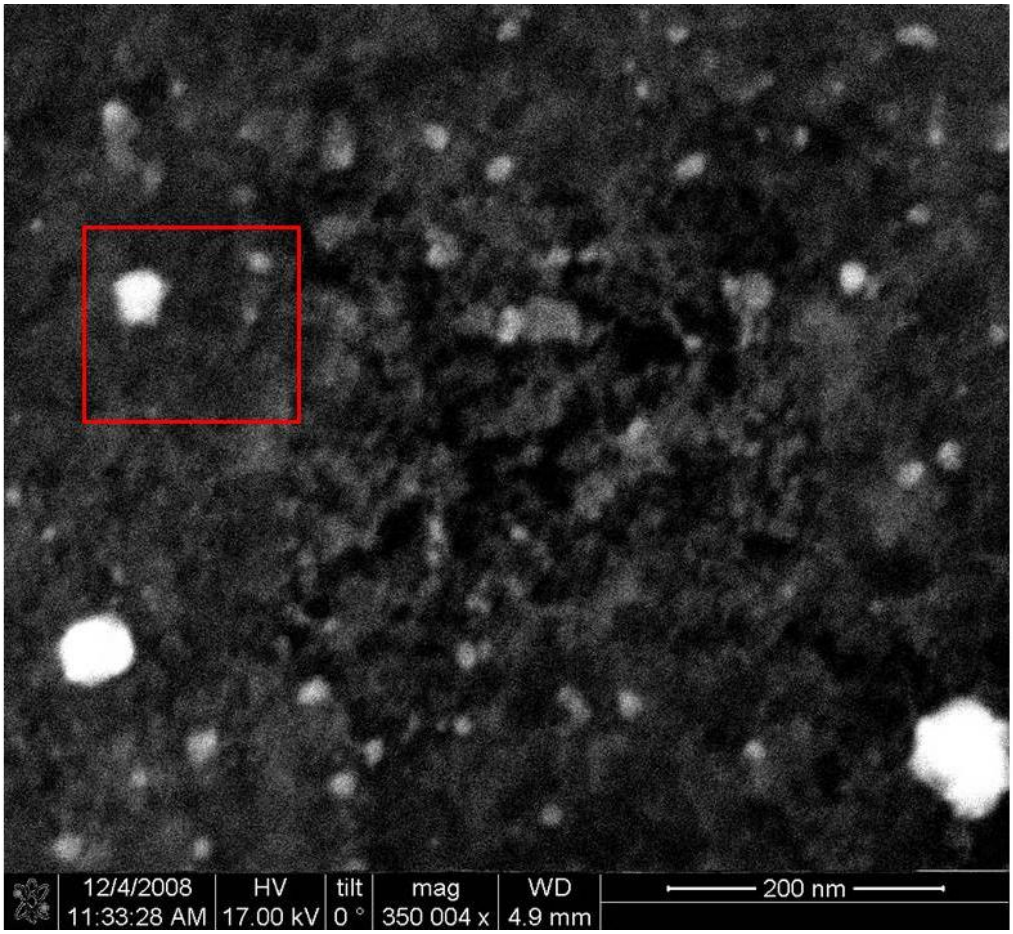

Figure D 5. FIB image of particle of lignite Fe-GAC by Mn/Fe.

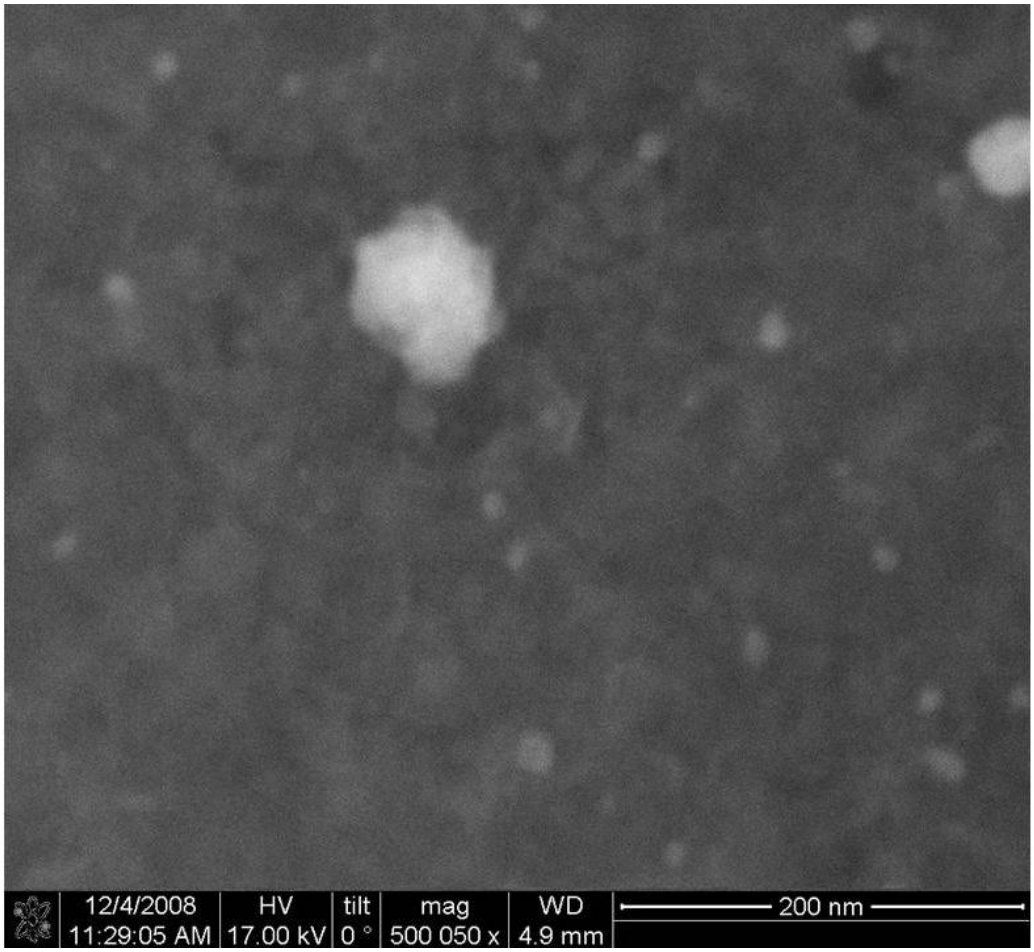

Figure D 6. FIB image of particle of lignite Fe-GAC from Mn/Fe.

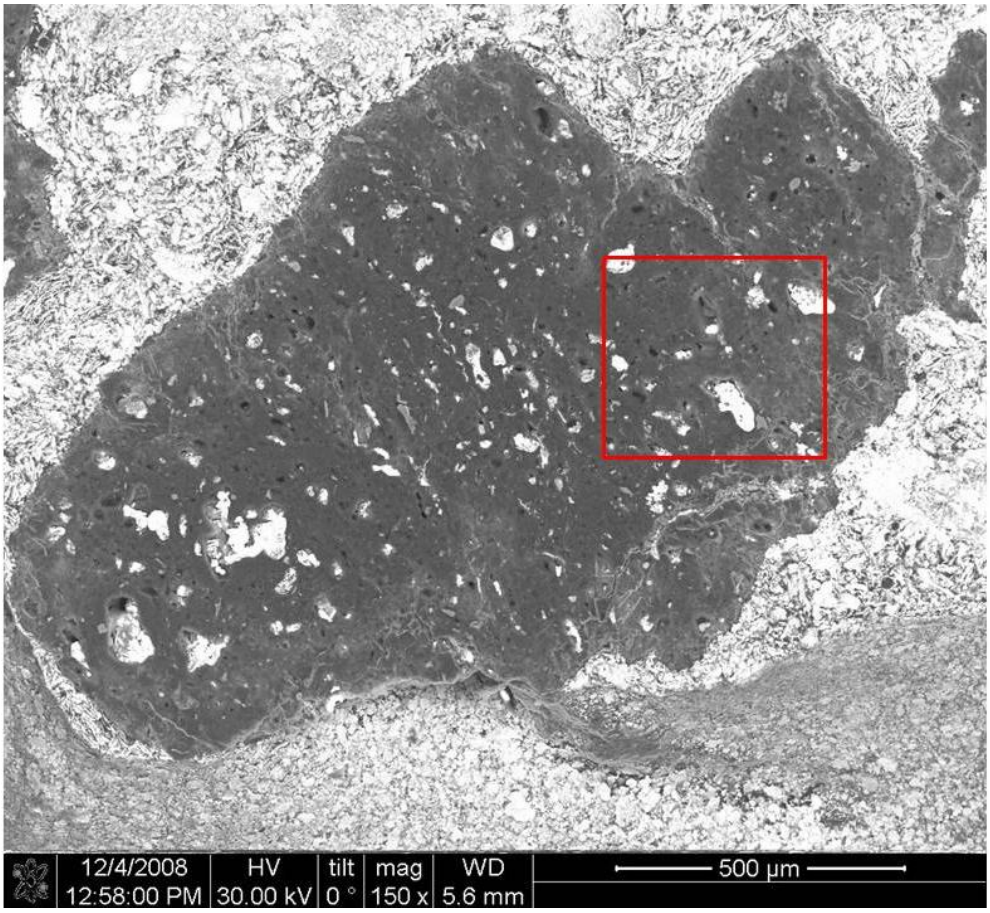

Figure D 7. FIB image of particle of bituminous Fe-GAC by Mn/Fe. Red square corresponds to approximate location of next image

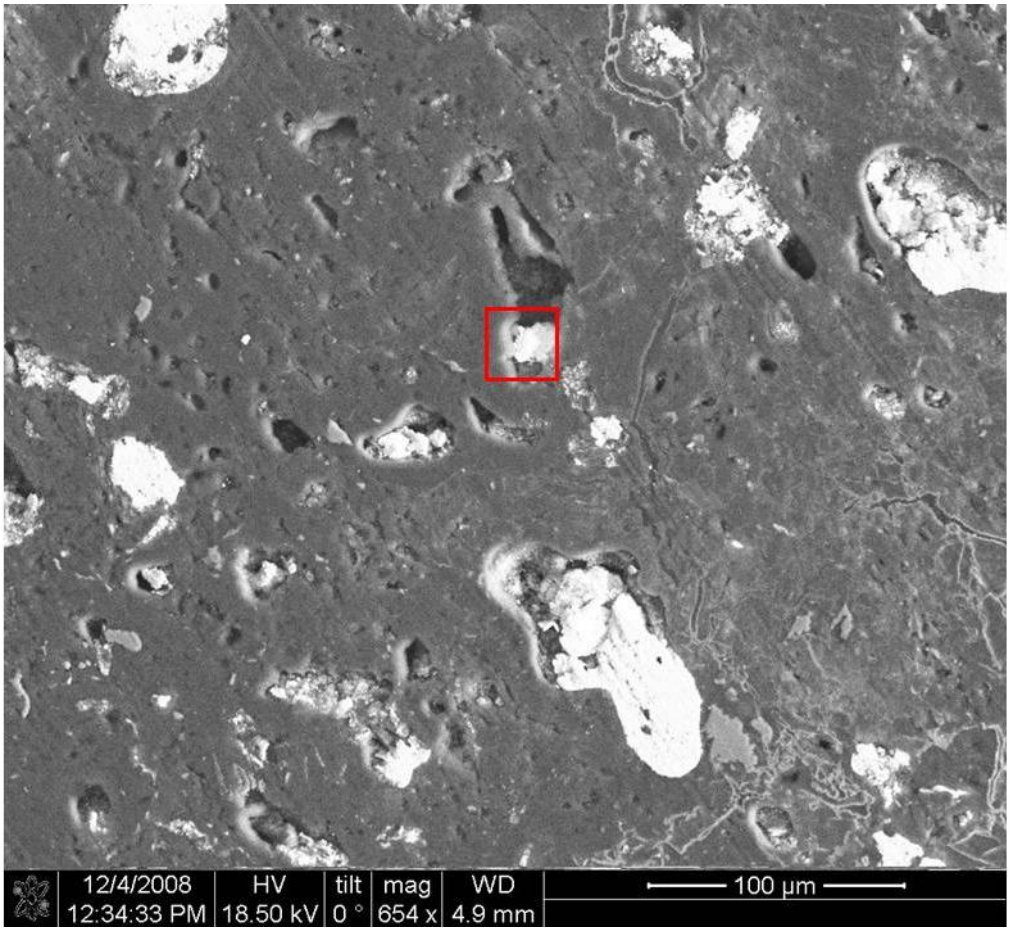

Figure D 8.FIB image of particle of bituminous Fe-GAC by Mn/Fe.

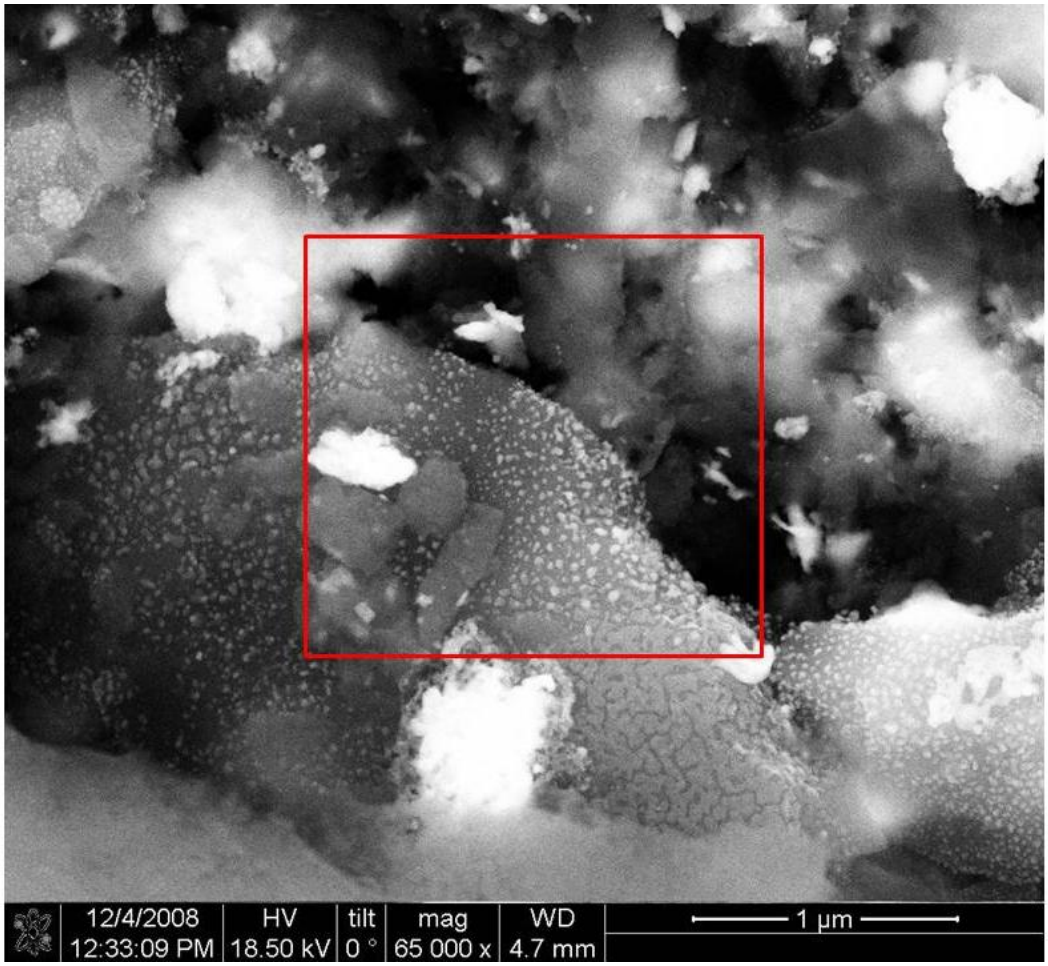

Figure D 9. FIB image of particle of bituminous Fe-GAC by Mn/Fe.

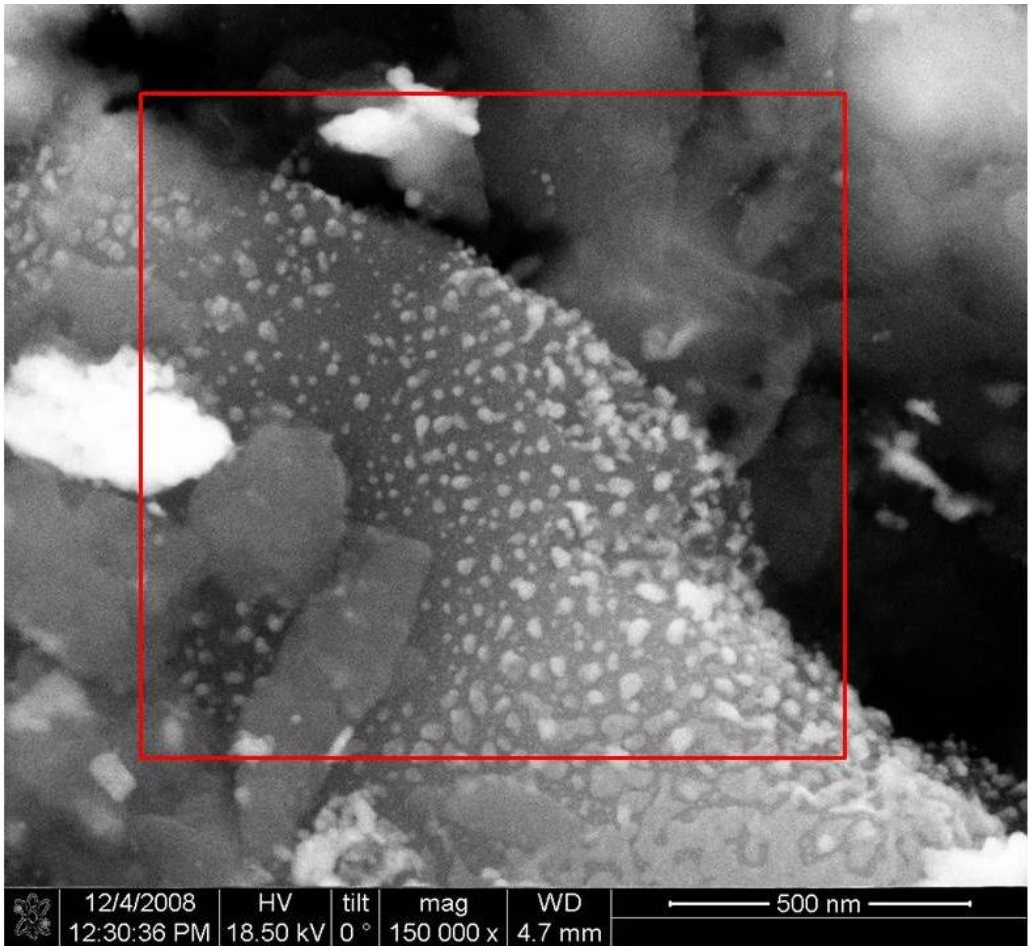

Figure D 10. FIB image of particle of bituminous Fe-GAC by Mn/Fe.

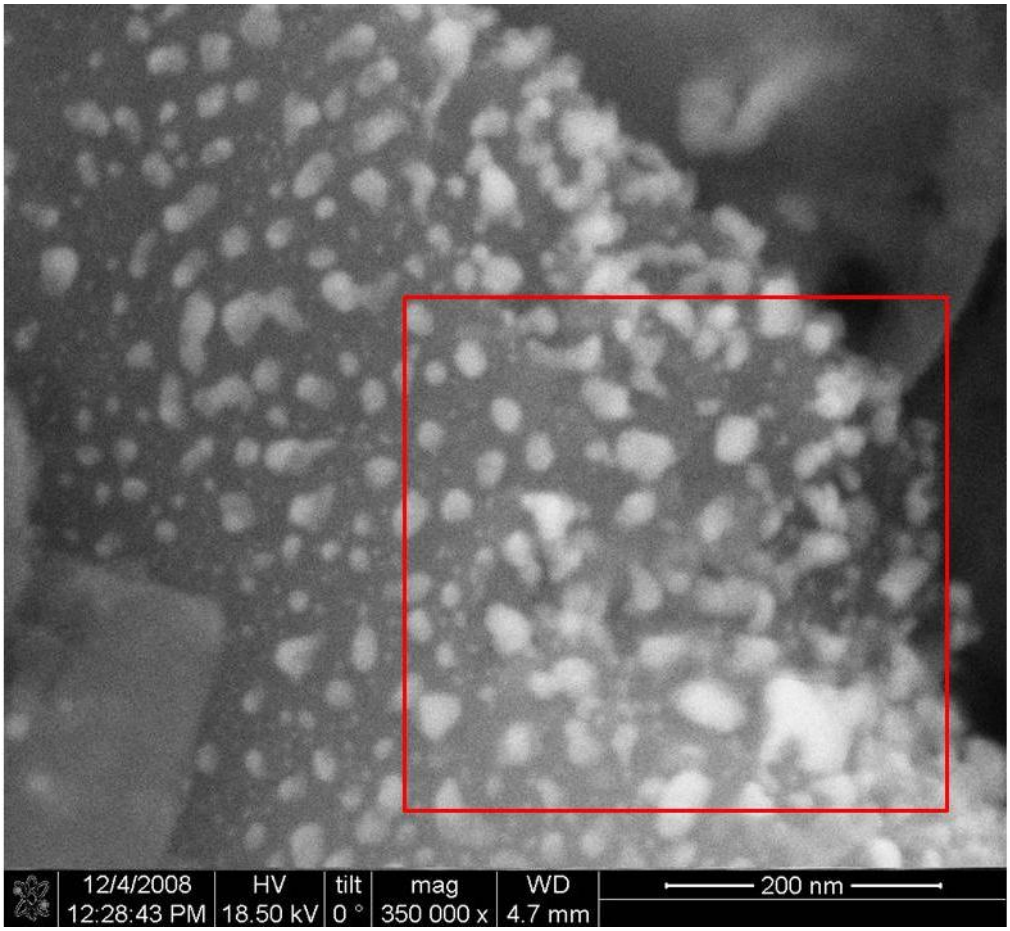

Figure D 11. FIB image of particle of bituminous Fe-GAC by Mn/Fe.

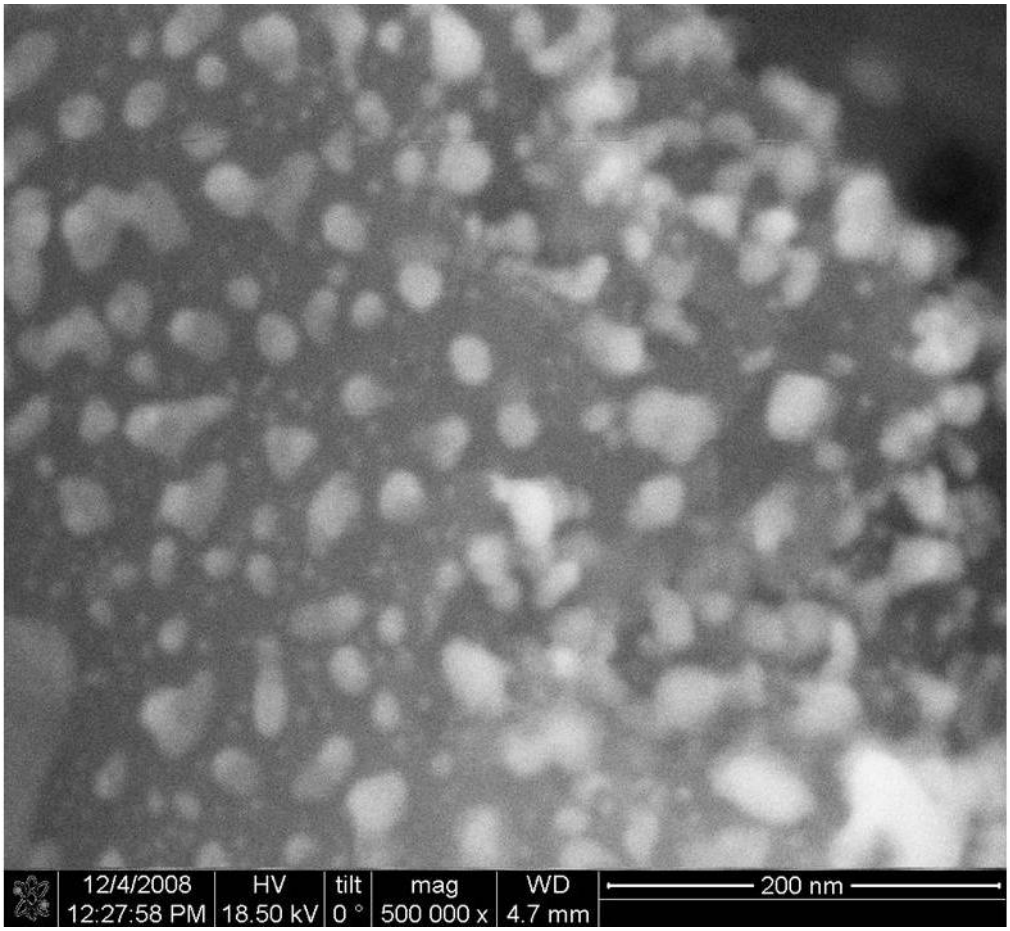

Figure D 12. FIB image of particle of bituminous Fe-GAC by Mn/Fe.

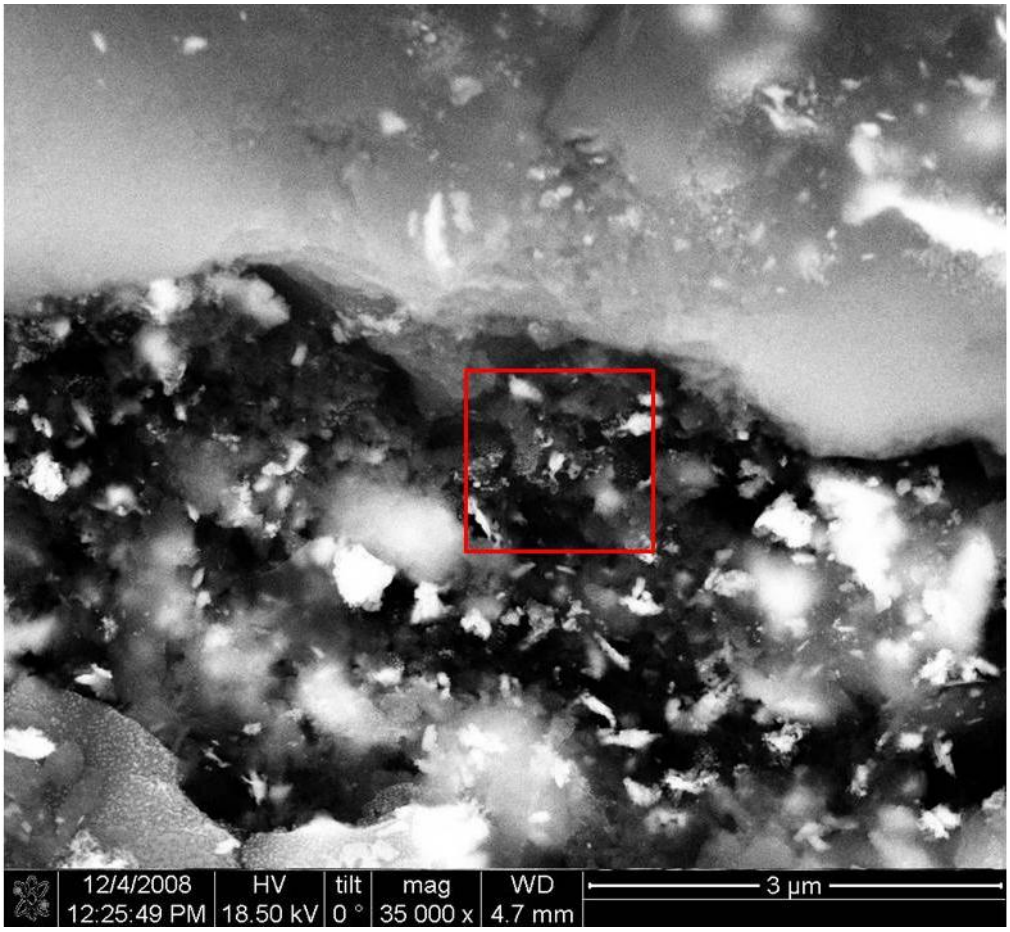

Figure D 13. FIB image of particle of bituminous Fe-GAC by Mn/Fe. Red square corresponds to approximate location of next image.

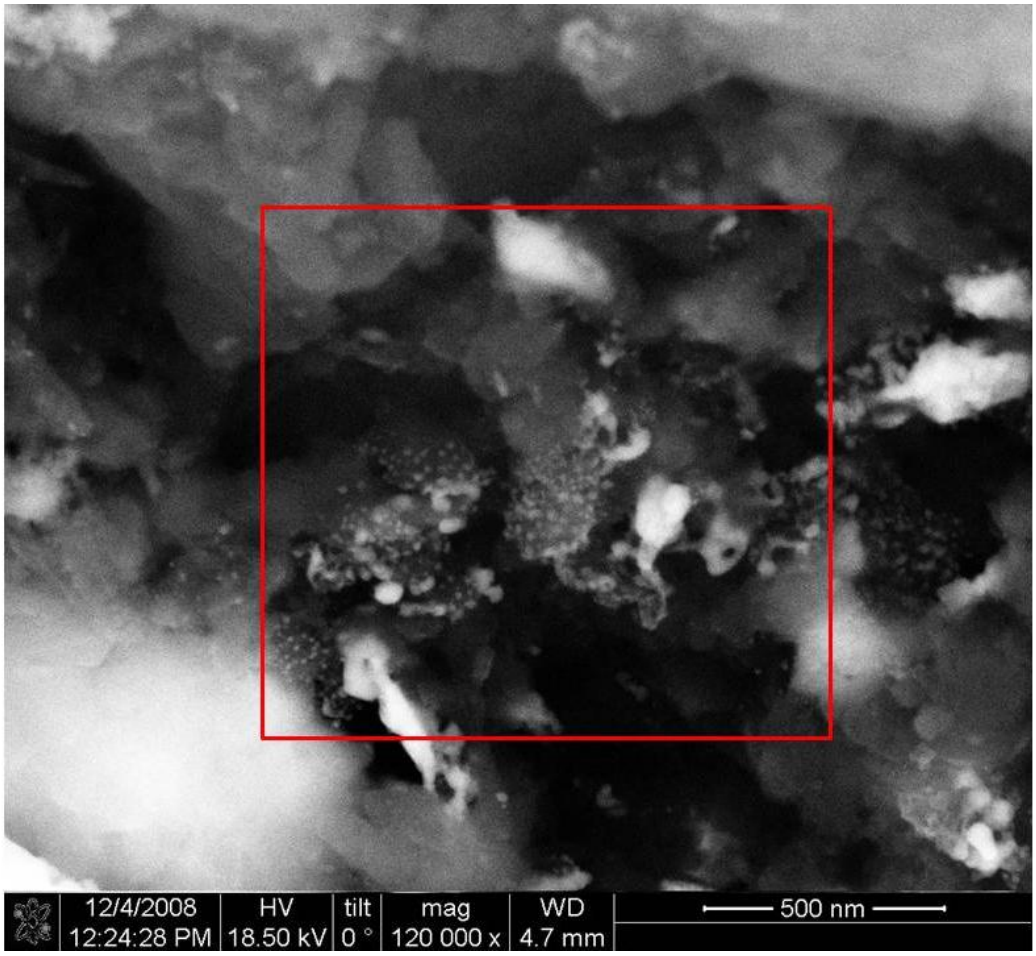

Figure D 14. FIB image of particle of bituminous Fe-GAC by Mn/Fe.

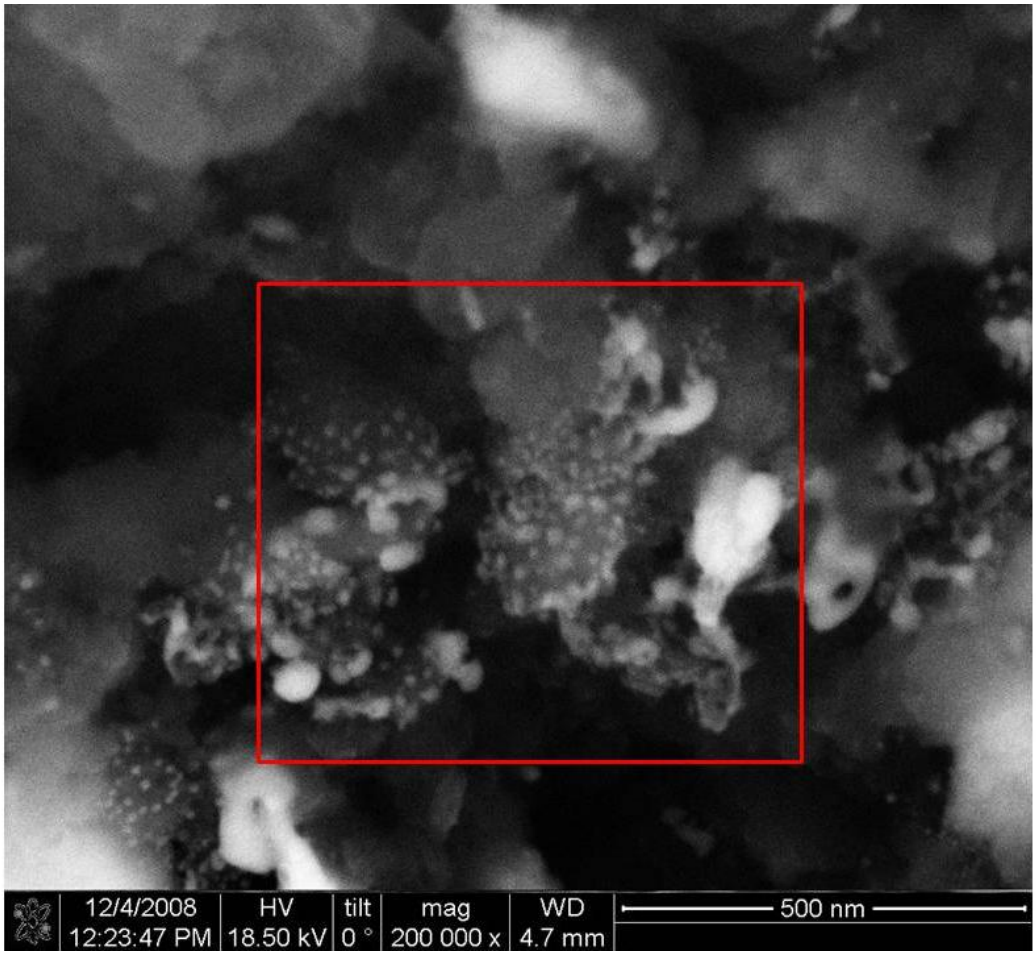

Figure D 15. FIB image of particle of bituminous Fe-GAC by Mn/Fe.

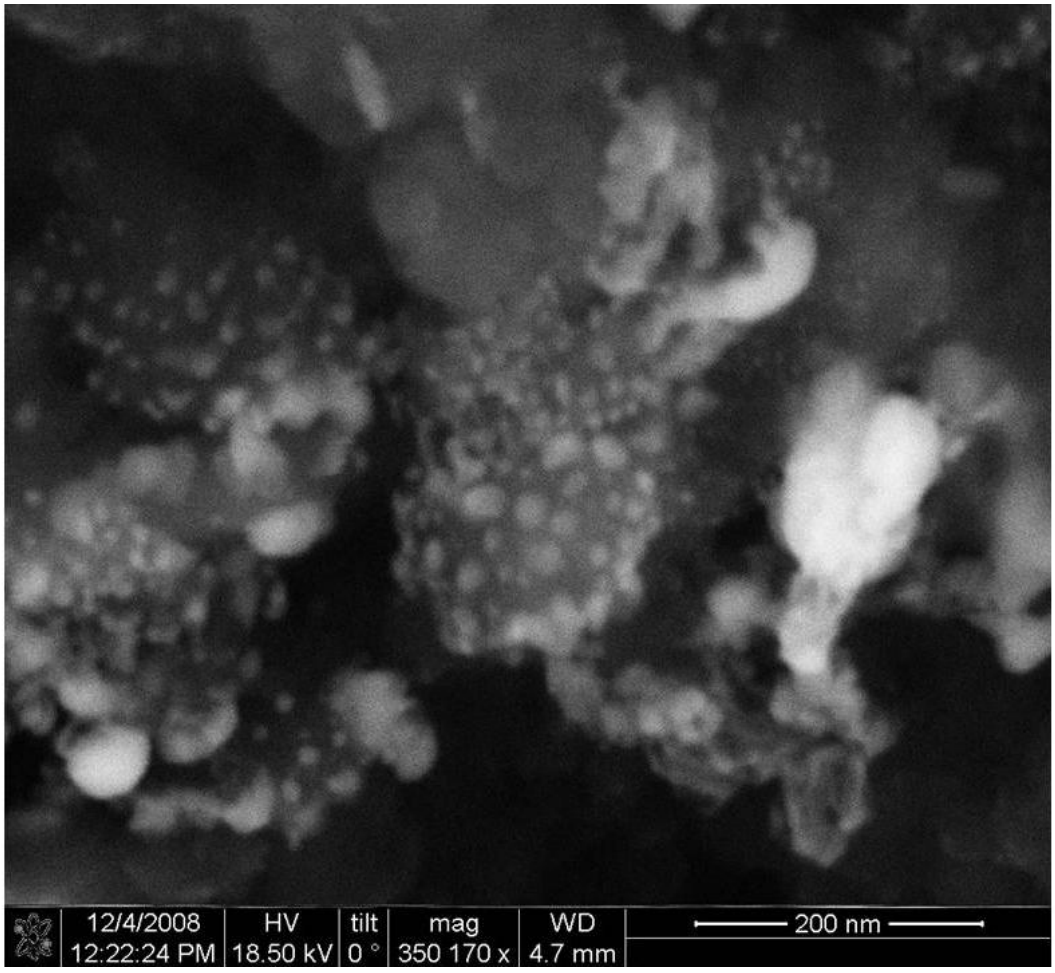

Figure D 16. FIB image of particle of bituminous Fe-GAC by Mn/Fe.

APPENDIX E

ARSENIC ADSORPTION ISOTHERM TABLES & CHARTS

Table E 1.

As adsorption data for virgin lignite GAC.

Virgin Lignite GAC % Fe < 0.25%				
Dry Mass	Volume	Dosage	Ce	q_e
g FeGAC	L	g_{FeGAC}/L	µg As/L	$\mu g_{As}/g_{FeGAC}$
0.1190	0.2770	0.4295	93.5	56.7
0.0563	0.2820	0.1996	85.6	161.4
0.0397	0.2790	0.1423	88.8	204.5
0.0195	0.2810	0.0692	100.0	258.4
0.0121	0.2790	0.0435	96.2	498.4
0.0031	0.2780	0.0110	89.9	2536
0.0569	0.2770	0.2053	87.9	146.0
0.0565	0.2770	0.2039	90.4	134.9
0.1190	0.2770	0.4295	93.5	56.7

Conditions: pH = 7.2 ± 0.1; 10 mM $NaHCO_3$; C_0(As) = 125 µg-As/L

Note: Virgin GACs did not exhibit any arsenic adsorption capacity and so Dose* and qe* were not calculated.

Table E 2.

As adsorption data for virgin bituminous GAC.

Virgin Bituminous GAC % Fe < 0.35%				
Dry Mass g FeGAC	Volume L	Dosage g_{FeGAC}/L	Ce µg As/L	q_e $\mu g_{As}/g_{FeGAC}$
0.1190	0.283	0.4204	87.9	71.3
0.0566	0.284	0.1996	83.8	170.4
0.0392	0.276	0.1421	106.5	80.2
0.0195	0.279	0.0699	97.3	293.7
0.0121	0.276	0.0440	89.9	635.9
0.0019	0.278	0.0070	96.9	3007
0.1196	0.278	0.4301	94.6	54.0
0.1191	0.279	0.4268	91.7	61.3
0.1190	0.283	0.4204	87.9	71.3

Conditions: pH = 7.2 ± 0.1; 10 mM $NaHCO_3$; C_0(As) = 125 µg-As/L

Note: Virgin GACs did not exhibit any arsenic adsorption capacity and so Dose* and qe* were not calculated.

Table E 3.

As adsorption data for lignite Fe-GAC Fe Only.

Lignite Fe-GAC Fe Only				% Fe = 5.46		
Dry Mass	Volume	Dosage	Ce	q_e	Dose*	q_e*
g FeGAC	L	g_{FeGAC}/L	µg As/L	$\mu g_{As}/g_{FeGAC}$	g_{Fe}/L	$\mu g_{As}/g_{Fe}$
0.0872	0.2740	0.3183	24.9	265.4	0.0174	4860
0.0391	0.2750	0.1420	44.8	454.6	0.0078	8327
0.0260	0.2780	0.0937	52.2	610.4	0.0051	11180
0.0155	0.2770	0.0558	67.7	746.6	0.0030	13674
0.0062	0.2750	0.0224	79.3	1338.4	0.0012	24513
0.0023	0.2770	0.0085	92.9	1936.2	0.0005	35462

Conditions: pH = 7.2 ± 0.1; 10 mM $NaHCO_3$; C_0(As) = 125 µg-As/L

Table E 4.

As adsorption data for Fe-GAC Fe Only at pH = 7.2 ± 0.1.

Bituminous Fe-GAC Fe Only				% Fe = 3.6		
Dry Mass	Volume	Dosage	Ce	q_e	Dose*	q_e*
g FeGAC	L	g_{FeGAC}/L	µg As/L	$\mu g_{As}/g_{FeGAC}$	g_{Fe}/L	$\mu g_{As}/g_{Fe}$
0.1188	0.278	0.4280	15.0	240.3	0.0152	6769
0.0561	0.278	0.2019	33.9	415.6	0.0072	11708
0.0200	0.279	0.0717	70.2	665.5	0.0025	18747
0.0123	0.277	0.0445	72.2	1025.7	0.0016	28894
0.0036	0.277	0.0132	100.2	1345.3	0.0005	37897
0.0396	0.278	0.1424	42.5	529.4	0.0051	14913

Conditions: pH = 7.2 ± 0.1; 10 mM $NaHCO_3$; C_0(As) = 125 µg-As/L

Table E 5.

As adsorption data for lignite Fe-GAC Mn/Fe.

Lignite Fe-GAC Mn/Fe				% Fe = 12.1		
Dry Mass	Volume	Dosage	Ce	q_e	Dose*	q_e*
g FeGAC	L	g_{FeGAC}/L	µg As/L	$µg_{As}/g_{FeGAC}$	g_{Fe}/L	$µg_{As}/g_{Fe}$
0.1188	0.2770	0.4289	22.3	222.7	0.0519	1839
0.0193	0.2800	0.0688	62.2	808.6	0.0083	6677
0.0133	0.2790	0.0476	76.7	865.9	0.0058	7150
0.0033	0.2770	0.0118	96.2	1829.3	0.0014	15105
0.0391	0.2800	0.1395	43.0	536.2	0.0169	4427

Conditions: pH = 7.2 ± 0.1; 10 mM $NaHCO_3$; C_0(As) = 125 µg-As/L

Table E 6.

As adsorption data for bituminous Fe-GAC Mn/Fe.

Bituminous Fe-GAC Mn/Fe				% Fe = 8.5		
Dry Mass	Volume	Dosage	Ce	q_e	Dose*	q_e*
g FeGAC	L	g_{FeGAC}/L	µg As/L	$µg_{As}/g_{FeGAC}$	g_{Fe}/L	$µg_{As}/g_{Fe}$
0.1200	0.278	0.4315	26.3	212.2	0.0368	2490
0.0563	0.277	0.2032	46.8	349.6	0.0173	4104
0.0390	0.277	0.1408	56.9	432.8	0.0120	5080
0.0198	0.279	0.0710	78.2	558.1	0.0061	6550
0.0117	0.279	0.0420	89.0	687.9	0.0036	8074
0.0566	0.278	0.2035	53.2	317.8	0.0173	3730
0.0567	0.276	0.2053	52.9	316.2	0.0175	3711

Conditions: pH = 7.2 ± 0.1; 10 mM $NaHCO_3$; C_0(As) = 125 µg-As/L

Table E 7.

As adsorption data for lignite Fe-GAC HCl/Mn/Fe.

Lignite Fe-GAC HCl/Mn/Fe				% Fe = 13.4		
Dry Mass	Volume	Dosage	Ce	q_e	Dose*	q_e*
g FeGAC	L	g_{FeGAC}/L	µg As/L	$µg_{As}/g_{FeGAC}$	g_{Fe}/L	$µg_{As}/g_{Fe}$
0.1204	0.2760	0.4362	9.2	249.7	0.0583	1867
0.0783	0.2810	0.2785	13.5	375.3	0.0372	2807
0.0430	0.2790	0.1543	34.7	540.4	0.0206	4042
0.0221	0.2780	0.0796	60.8	719.9	0.0106	5384
0.0159	0.2780	0.0572	65.5	919.6	0.0076	6878
0.0045	0.2815	0.0159	100.8	1090	0.0021	8154
0.0440	0.2770	0.1587	36.0	517.2	0.0212	3868
0.0416	0.2800	0.1484	34.0	566.6	0.0198	4238

Conditions: pH = 7.2 ± 0.1; 10 mM $NaHCO_3$; C_0(As) = 125 µg-As/L

Table E 8.

As adsorption data for bituminous Fe-GAC HCl/Mn/Fe.

Bituminous Fe-GAC HCl/Mn/Fe				% Fe = 9.2		
Dry Mass	Volume	Dosage	Ce	q_e	Dose*	q_e*
g FeGAC	L	g_{FeGAC}/L	µg As/L	$µg_{As}/g_{FeGAC}$	g_{Fe}/L	$µg_{As}/g_{Fe}$
0.1234	0.279	0.4430	16.1	230.2	0.0408	2499
0.0466	0.279	0.1673	46.6	427.6	0.0154	4642
0.0234	0.275	0.0851	73.2	527.3	0.0078	5726
0.0133	0.277	0.0481	81.0	770.7	0.0044	8369
0.0760	0.278	0.2739	33.4	309.0	0.0252	3355
0.0765	0.277	0.2762	29.7	320.1	0.0254	3475

Conditions: pH = 7.2 ± 0.1; 10 mM $NaHCO_3$; C_0(As) = 125 µg-As/L

:
Table E 9.

As adsorption isotherms for virgin lignite GAC.

Virgin Lignite GAC % Fe < 0.35				
Dry Mass	Volume	Dosage	Ce	q_e
g FeGAC	L	g_{FeGAC}/L	µg As/L	$\mu g_{As}/g_{FeGAC}$
0.1574	0.277	0.5682	82.5	52.7
0.0984	0.276	0.3567	98.1	40.2
0.0634	0.278	0.2280	97.3	66.4
0.0470	0.276	0.1703	98.1	84.0
0.0153	0.278	0.0551	101.9	190.6
0.0058	0.279	0.0209	97.9	694.4
0.0986	0.277	0.3561	100.0	35.0
0.1003	0.279	0.3596	99.2	36.6
0.1574	0.277	0.5682	82.5	52.7

Conditions: pH = 8.1 ± 0.1; 10 mM $NaHCO_3$; C_0(As) = 125 µg-As/L

Note: Virgin GACs did not exhibit any arsenic adsorption capacity and so Dose* and qe* were not calculated.

Table E 10.

As adsorption data for virgin bituminous GAC.

Virgin Bituminous GAC % Fe < 0.35%				
Dry Mass	Volume	Dosage	Ce	q_e
g FeGAC	L	g_{FeGAC}/L	µg As/L	$\mu g_{As}/g_{FeGAC}$
0.1425	0.2800	0.5088	63.1	96.9
0.1012	0.2790	0.3628	74.0	105.9
0.0823	0.2800	0.2939	75.6	125.3
0.0548	0.2770	0.1979	86.7	130.1
0.0217	0.2770	0.0785	97.5	190.5
0.0097	0.2780	0.0349	101.9	299.9
0.1431	0.2770	0.5168	77.3	68.0
0.1418	0.2775	0.5109	74.1	74.9
0.1425	0.2800	0.5088	63.1	96.9

Conditions: pH = 8.1 ± 0.1; 10 mM $NaHCO_3$; C_0(As) = 125 µg-As/L

Note: Virgin GACs did not exhibit any arsenic adsorption capacity and so Dose* and qe* were not calculated.

Table E 11.

As adsorption data for lignite Fe-GAC via Fe Only.

Lignite Fe-GAC Fe Only				%Fe = 5.46		
Dry Mass	Volume	Dosage	Ce	q_e	Dose*	q_e*
g FeGAC	L	g_{FeGAC}/L	µg As/L	$\mu g_{As}/g_{FeGAC}$	g_{Fe}/L	$\mu g_{As}/g_{Fe}$
0.0811	0.2760	0.2940	47.8	186.6	0.01605	3417
0.0623	0.2770	0.2247	53.0	220.9	0.01227	4046
0.0381	0.2790	0.1365	55.3	347.1	0.00745	6357
0.0196	0.2765	0.0708	60.4	596.7	0.00387	10928
0.0122	0.2770	0.0442	68.5	773.9	0.00241	14173
0.0382	0.2800	0.1363	54.9	350.3	0.00744	6417
0.0399	0.2810	0.1421	53.4	346.7	0.00776	6351

Conditions: pH = 8.1 ± 0.1; 10 mM $NaHCO_3$; C_0(As) = 125 µg-As/L

Table E 12.

As adsorption data for bituminous Fe-GAC Fe Only.

Bituminous Fe-GAC Fe Only				% Fe = 3.6		
Dry Mass	Volume	Dosage	Ce	q_e	Dose*	q_e*
g FeGAC	L	g_{FeGAC}/L	µg As/L	$µg_{As}/g_{FeGAC}$	g_{Fe}/L	$µg_{As}/g_{Fe}$
0.1384	0.2780	0.4978	2.9	200.4	0.0177	5645
0.0849	0.2780	0.3054	8.8	307.3	0.0108	8656
0.0559	0.2770	0.2020	22.2	398.1	0.0072	11214
0.0435	0.2770	0.1572	23.9	500.9	0.0056	14109
0.0086	0.2780	0.0308	70.7	1036.8	0.0011	29205
0.0553	0.2790	0.1980	19.6	419.2	0.0070	11807

Conditions: pH = 8.1 ± 0.1; 10 mM $NaHCO_3$; C_0(As) = 125 µg-As/L

Table E 13.

As adsorption data for lignite Fe-GAC Mn/Fe.

Lignite Fe-GAC Mn/Fe				% Fe = 12.1		
Dry Mass	Volume	Dosage	Ce	q_e	Dose*	q_e*
g FeGAC	L	g_{FeGAC}/L	µg As/L	$µg_{As}/g_{FeGAC}$	g_{Fe}/L	$µg_{As}/g_{Fe}$
0.1389	0.2770	0.5015	31.9	141.0	0.0607	1165
0.0816	0.2765	0.2951	44.5	196.9	0.0357	1626
0.0552	0.2805	0.1969	54.2	245.7	0.0239	2029
0.0382	0.2800	0.1365	60.8	306.0	0.0165	2527
0.0207	0.2785	0.0742	72.4	408.2	0.0090	3370
0.0134	0.2790	0.0479	76.3	549.5	0.0058	4538
0.0555	0.2800	0.1983	55.9	235.5	0.0240	1945
0.0556	0.2790	0.1993	51.8	254.8	0.0241	2104

Conditions: pH = 8.1 ± 0.1; 10 mM $NaHCO_3$; C_0(As) = 125 µg-As/L

Table E 14.

As adsorption data for bituminous Fe-GAC Mn/Fe.

Bituminous Fe-GAC Mn/Fe				% Fe = 8.5		
Dry Mass	Volume	Dosage	Ce	q_e	Dose*	q_e*
g FeGAC	L	g_{FeGAC}/L	µg As/L	$µg_{As}/g_{FeGAC}$	g_{Fe}/L	$µg_{As}/g_{Fe}$
0.1372	0.2780	0.4934	65.9	74.5	0.0420	874
0.0648	0.2770	0.2341	71.0	135.1	0.0199	1585
0.0422	0.2750	0.1533	78.6	156.5	0.0131	1837
0.0238	0.2765	0.0862	84.2	213.8	0.0073	2510
0.0134	0.2770	0.0485	88.4	293.5	0.0041	3444
0.0855	0.2795	0.3059	69.5	108.2	0.0261	1270
0.0845	0.2780	0.3041	68.6	112.1	0.0259	1315

Conditions: pH = 8.1 ± 0.1; 10 mM $NaHCO_3$; C_0(As) = 125 µg-As/L

Table E 15.

As adsorption data for lignite Fe-GAC HCl/Mn/Fe.

Lignite Fe-GAC HCl/Mn/Fe				% Fe = 13.4		
Dry Mass	Volume	Dosage	Ce	q_e	Dose*	q_e*
g FeGAC	L	g_{FeGAC}/L	µg As/L	$µg_{As}/g_{FeGAC}$	g_{Fe}/L	$µg_{As}/g_{Fe}$
0.1475	0.2780	0.5307	65.9	87.6	0.0710	656
0.0943	0.2780	0.3391	68.1	130.7	0.0453	978
0.0723	0.2775	0.2606	71.4	157.3	0.0348	1177
0.0425	0.2785	0.1525	75.3	243.1	0.0204	1818
0.0207	0.2795	0.0742	81.9	411.6	0.0099	3079
0.0099	0.2770	0.0359	83.0	817.9	0.0048	6117
0.0721	0.2800	0.2576	74.1	148.6	0.0344	1111

Conditions: pH = 8.1 ± 0.1; 10 mM $NaHCO_3$; C_0(As) = 125 µg-As/L

Table E 16.

As adsorption data for bituminous Fe-GAC HCl/Mn/Fe.

Bituminous Fe-GAC HCl/Mn/Fe				% Fe = 9.2		
Dry Mass	Volume	Dosage	Ce	q_e	Dose*	q_e*
g FeGAC	L	g_{FeGAC}/L	µg As/L	$µg_{As}/g_{FeGAC}$	g_{Fe}/L	$µg_{As}/g_{Fe}$
0.1459	0.2770	0.5267	77.83	65.67	0.04851	713
0.1073	0.2780	0.3859	81.41	80.37	0.03554	873
0.0685	0.2750	0.2492	85.02	109.93	0.02296	1194
0.0289	0.2790	0.1034	94.39	174.35	0.00953	1893
0.0135	0.2775	0.0487	100.73	239.89	0.00449	2605
0.0074	0.2770	0.0266	102.45	374.08	0.00245	4062
0.0316	0.2800	0.1130	95.98	145.53	0.01041	1580

Conditions: pH = 8.1 ± 0.1; 10 mM $NaHCO_3$; C_0(As) = 125 µg-As/L

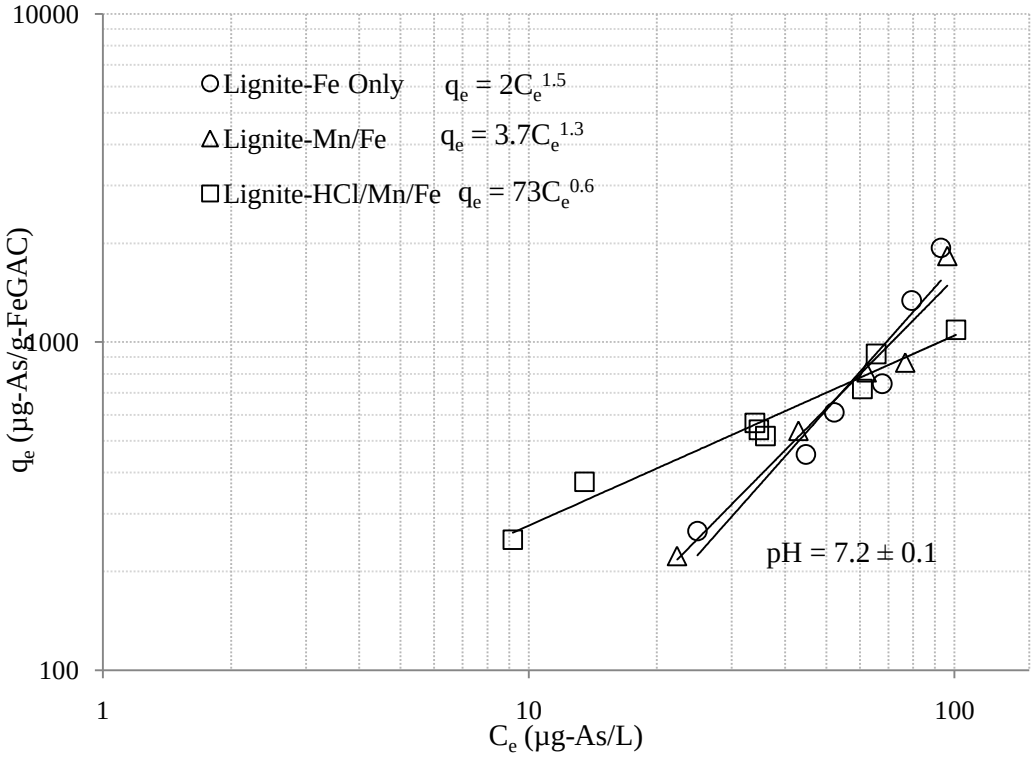

Figure E 1. Arsenic adsorption isotherms for lignite Fe-GAC.

Conditions: pH = 7.2 ± 0.1, 10 mM $NaHCO_3$, C_0 = 125 µg-As/L.

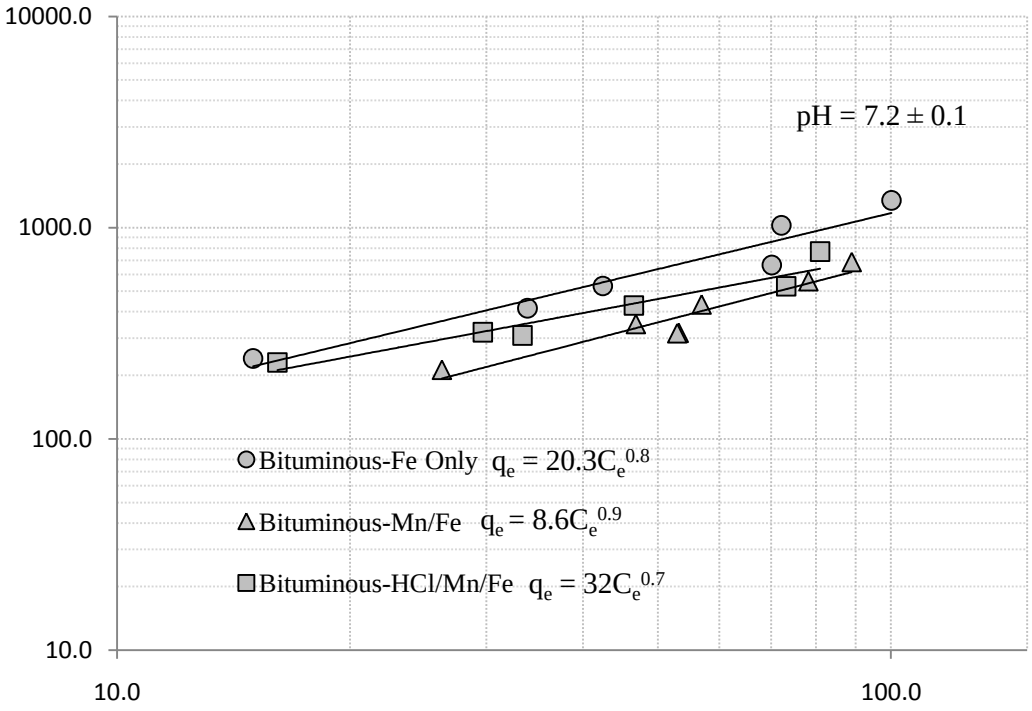

Figure E 2. Arsenic adsorption isotherms for bituminous Fe-GAC.

Conditions: pH = 7.2 ± 0.1, 10 mM $NaHCO_3$, C_0 = 125 µg-As/L.

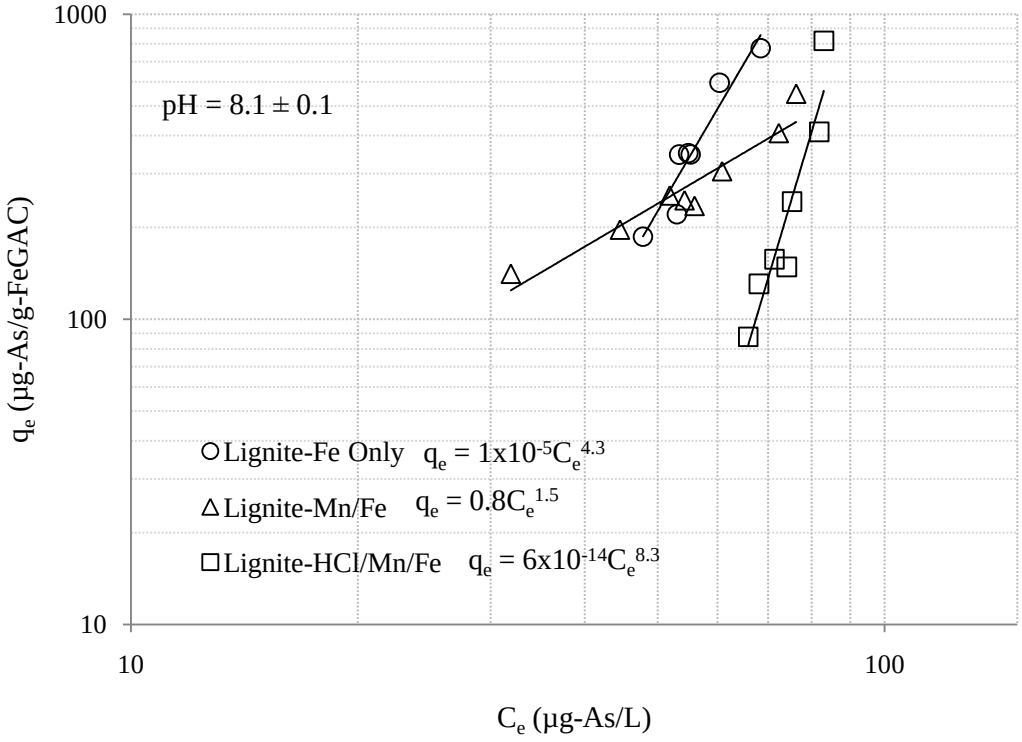

Figure E 3. Arsenic adsorption isotherms for lignite Fe-GAC.

Conditions: pH = 8.1 ± 0.1, 10 mM $NaHCO_3$, C_0 = 125 µg-As/L.

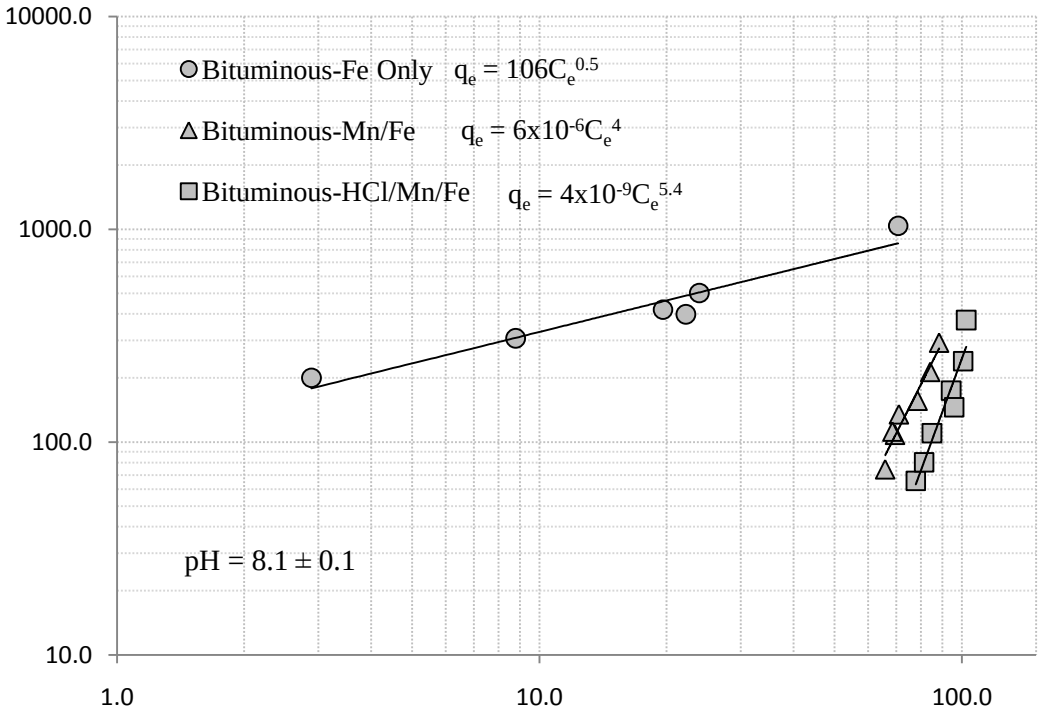

Figure E 4. Arsenic adsorption isotherms for bituminous Fe-GAC.

Conditions: pH = 8.1 ± 0.1, 10 mM $NaHCO_3$, C_0 = 125 µg-As/L.

APPENDIX F

TCE ADSORPTION ISOTHERM DATA & CHARTS

Table F 1.

TCE adsorption isotherm data for virgin GAC.

Virgin (Untreated) GAC					
Lignite GAC			Bituminous GAC		
Dose D (g_{GAC}/L)	C_e (mg_{TCE}/L)	q_e (mg_{TCE}/g_{GAC})	Dose D (g_{GAC}/L)	C_e (mg_{TCE}/L)	q_e (mg_{TCE}/g_{GAC})
0.4295	0.61	10.3	0.4204	0.43	11.0
0.1423	1.82	22.6	0.1421	1.25	26.7
0.0435	3.47	35.8	0.0699	2.67	33.7
0.0110	4.32	64.9	0.0440	3.31	39.1
0.2053	1.33	18.0	0.4268	0.87	9.8

Conditions: 10 mM $NaHCO_3$, C_0(TCE) ≈ 6 mg-TCE/L, pH = 7.2 ± 0.1

Table F 2.

TCE adsorption isotherm data for Fe-GAC Fe Only.

Fe Only					
Lignite Fe-GAC			Bituminous Fe-GAC		
Dose D (g_{GAC}/L)	C_e (mg_{TCE}/L)	q_e (mg_{TCE}/g_{GAC})	Dose D (g_{GAC}/L)	C_e (mg_{TCE}/L)	q_e (mg_{TCE}/g_{GAC})
0.4314	0.53	13.1	0.2019	0.31	29.2
0.0479	2.51	77.2	0.1436	0.25	41.4
0.0702	1.69	64.2	0.0717	0.67	77.2
0.0723	1.54	64.4	0.0445	2.91	74.0
			0.0132	2.96	246.6

Conditions: 10 mM $NaHCO_3$, C_0(TCE) ≈ 6 mg-TCE/L, pH = 7.2 ± 0.1

Table F 3.

TCE adsorption isotherm data for Fe-GAC Mn/Fe.

Mn/Fe					
Lignite Fe-GAC			Bituminous Fe-GAC		
Dose D (g_{GAC}/L)	C_e (mg_{TCE}/L)	q_e (mg_{TCE}/g_{GAC})	Dose D (g_{GAC}/L)	C_e (mg_{TCE}/L)	q_e (mg_{TCE}/g_{GAC})
0.4289	0.74	12.7	0.4315	1.60	10.7
0.2009	1.51	23.4	0.2032	2.38	18.8
0.0688	3.16	44.3	0.1408	3.54	40.8
0.0476	3.21	62.9	0.0710	2.93	31.1
0.1410	1.47	33.6	0.2053	2.52	18.0

Conditions: 10 mM $NaHCO_3$, C_0(TCE) ≈ 6 mg-TCE/L, pH = 7.2 ± 0.1

Table F 4.

TCE adsorption isotherm data for Fe-GAC HCl/Mn/Fe.

HCl/Mn/Fe					
Lignite Fe-GAC			Bituminous Fe-GAC		
Dose D (g_{GAC}/L)	C_e (mg_{TCE}/L)	q_e (mg_{TCE}/g_{GAC})	Dose D (g_{GAC}/L)	C_e (mg_{TCE}/L)	q_e (mg_{TCE}/g_{GAC})
0.4362	2.61	5.5	0.4430	1.61	7.7
0.0796	3.06	24.8	0.2778	2.39	9.5
0.0572	3.53	26.3	0.1673	3.01	12.1
0.0159	3.97	67.1	0.0851	3.69	15.8
0.1587	3.47	9.8	0.0481	4.03	20.9
0.1484	3.47	10.5			

Conditions: 10 mM $NaHCO_3$, C_0(TCE) ≈ 6 mg-TCE/L, pH = 7.2 ± 0.1

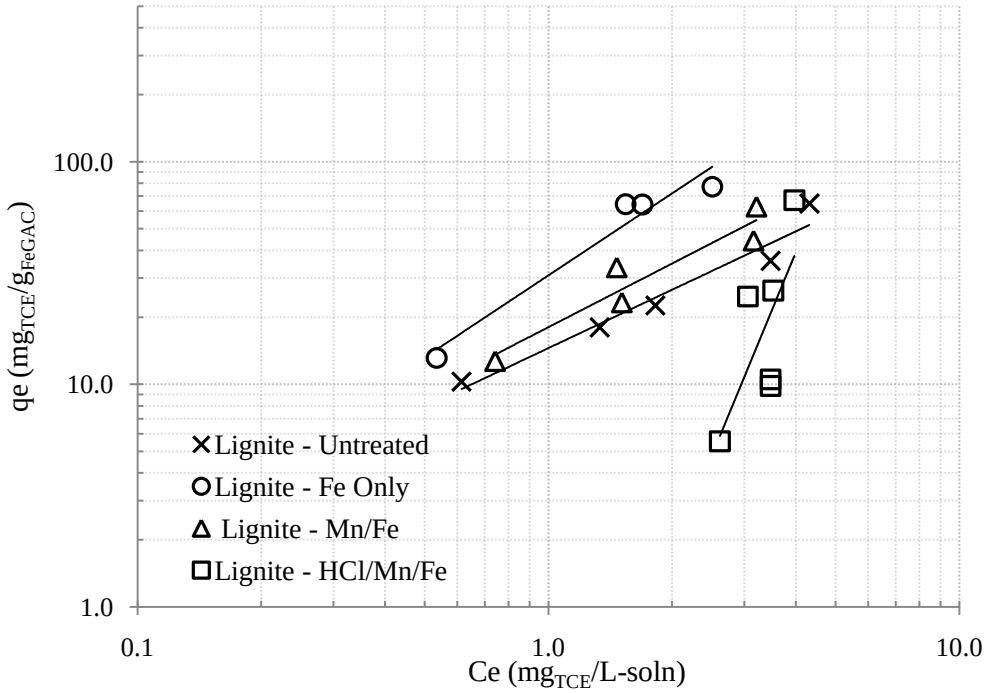

Figure F 1. TCE adsorption isotherms for lignite virgin and Fe-GAC

Conditions: 10 mM $NaHCO_3$, C_0(TCE) ≈ 6 mg-TCE/L, pH = 7.2 ± 0.1

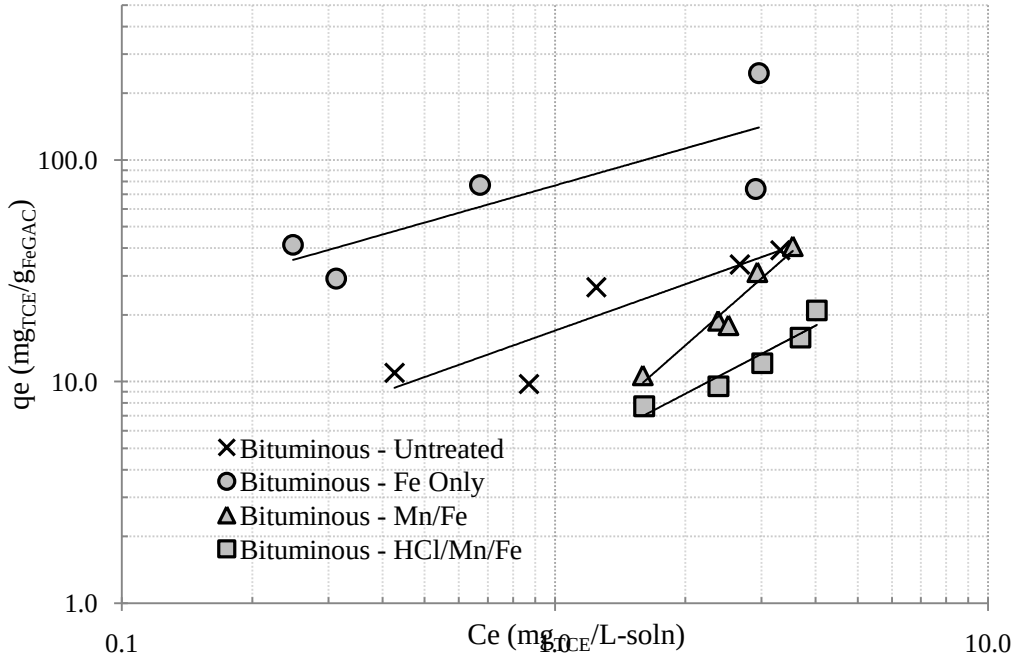

Figure F 2. TCE adsorption isotherm data for bituminous virgin and Fe-GAC.

Conditions: 10 mM $NaHCO_3$, C_0(TCE) ≈ 6 mg-TCE/L, pH = 7.2 ± 0.1